CHEMICAL AND MICROBIAL CONTROL OF PYRITE WEATHERING AND ITS IMPLICATIONS TO ARSENIC MOBILITY AND SULFUR AND IRON GEOCHEMISTRY

by

WENYI ZHU

A Dissertation submitted to the

Graduate School-New Brunswick

Rutgers, The State University of New Jersey

in partial fulfillment of the requirements

for the degree of

Doctor of Philosophy

Graduate Program in Environmental Sciences

written under the direction of

Dr. John R. Reinfelder

and approved by

_____

_____

_____

_____

New Brunswick, New Jersey

[January, 2010]

ABSTRACT OF THE DISSERTATION

Chemical and microbial control of pyrite weathering and its implications to arsenic mobility and sulfur and iron geochemistry

By WENYI ZHU

Dissertation Director
Dr. John R. Reinfelder

Controls on pyrite deposition and weathering were investigated in Newark Basin (Lockatong formation) black shale. Inorganic sulfur species including pyritic S and acid volatile S were quantified in early, middle, and late Lockatong formation black shale samples obtained from the Newark Basin rock core collection. Pyritic S accounted for more than 50% of total S in Lockatong black shale and was strongly correlated to total S, yet no correlation was found between acid volatile S and total S. An inverse relationship was identified between pyritic S and acid volatile S at various depths in the formation which may indicate their redox potential-controlled interconversion. Further analysis of the redox potential index, Th/U ratio, showed that redox potential was one of the controlling factors for the deposition of the reduced sulfur species in the Newark Basin sedimentary environments.

Trace metal enrichment factors showed that As and Mo were two highly enriched elements in Lockatong formation black shale. Correlation analyses show that As was closely linked to pyritic S and Mo was associated with organic matter in Lockatong black shale. The hypothesized mobilization of arsenic from pyritic black shale by a sulfide-arsenide exchange and oxidation reaction was tested with FeAsS, homogenized Lockatong formation black shale and Lockatong formation black shale pyrite incubated under oxic, hypoxic and anoxic conditions. Incubation results showed that sulfide increased arsenic mobilization to the dissolved phase from all three

solids under oxic and hypoxic, but not anoxic conditions. Moreover, XANES results show that arsenic in Newark Basin black shale pyrite has the same oxidation state as that in FeAsS (-1) and thus extend the sulfide-arsenide exchange mechanism of arsenic mobilization to sedimentary rock, black shale pyrite. This process will be most important to arsenic mobilization in aquifers where pyrite is exposed to a supply of sulfide from zones of anoxic groundwater which supports sulfate reducing bacteria and oxic groundwater or other oxidants..

The direct role of microorganisms in pyrite weathering in Newark Basin black shale was examined through microbial colonization experiments. Thick biofilms were observed on the surface of pyrite bearing, polished black shale thick sections during their incubation in a subsurface groundwater well and the microbial community structure of the colonized microbes was analyzed. Colonizing microbes preferentially attached to pyrite rather than the shale matrix and the co-occurrence of bacteria-shaped pits and secondary iron minerals on pyrite were observed. 16S rDNA sequence analysis of pyrite and arsenopyrite biofilm communities indicated that most of the mineral colonizing microorganisms were members of the Fe(III)-reducing Geobacteraceae (δ-proteobacteria). Other sequences showed high similarity (>99%) with species in the β and ε-proteobacteria that are able to oxidize iron or sulfur. These results indicate that microbes may play a critical role in the transformation of iron sulfides and their secondary minerals such as iron oxides, as well as the mobilization of trace elements from such minerals in slightly acidic black shale aquifers.

Acknowledgement

Attending graduate school has been one of the most invaluable experiences to me. Looking back, it was quite a long and tough journey. However, along the road, I have not only achieved my academic goals, but also learned something beyond knowledge, which I can never acquire from anywhere else.

These achievements will be impossible for me without the advising and support from my advisor, Dr. John Reinfelder, and my committee members, Dr. Young, Dr. Yee and Dr. Serfes, as well as so many friends and staffs across the department of environmental science at Rutgers. I want to give my most sincere thanks to my advisor, Dr. Reinfelder, who directed on my research projects, helped me with every detail of my experiments, and assisted me to resolve all kinds of problems I faced during the process. Without his patience, support and encouragement, the journey of achieving my goals would be much harder and even become impossible. My committee members also gave me many valuable suggestions and comments and I was inspired by their advices and benefit from their kind support.

I would also like to thank all the friends and staffs in the department of environmental science and across Rutgers University. They helped me to conquer the difficulties when I first came to this unfamiliar environment and later assisted me with so many things, both in academia and life. Special thanks to Songyan Du and Fang Liu, who treated me like their own sisters --- the graduate journey would be tough and boring without you guys!

Last, but definitely not the least, I would like to thank my parents. They are far away from me, but I know they stand behind me all the time. Without them, it is impossible for me to accomplish this, or anything. They taught me to dream and supported me unconditionally to achieve my dreams. And I will never let my dreams go.

Dedication

To my loving parents, Heping Wang and Weili Zhu

Table of Contents

Abstract ----------ii

Acknowledgements ----------iv

Dedication ----------vi

Table of Contents ----------vii

List of Tables ----------x

List of Illustrations ----------xi

CHAPTER

I. INTRODUCTION----------1
1.1 The Biogeochemistry of Iron, Sulfur and Trace elements in the Environment-1
1.2 Research Objectives----------6
1.3 Dissertation Overview----------7
References----------8

II. DEPOSITIONAL ENVIRONMENT AND WEATHERING PROXIES OF PYRITE IN NEWARK BASIN BLACK SHALE ----------11
Abstract----------11
2.1 Introduction----------13
2.2 Methodology----------16
Site description and whole rock analysis ----------17
Sulfur speciation----------17
2.3 Results and Discussion----------18
Whole rock analysis of the Lockatong formation shale----------18
Sulfur speciation of black shale----------19
Evaluation of depositional conditions with the Th/U redox index and its relation to sulfur species' depth profiles----------21
Trace metal enrichment factors in the Lockatong formation black and red shale----------22
As and Mo as Pyrite and Organic Carbon Proxies in Lockatong Formation ----------25
The release of As and Mo into groundwater from sedimentary rocks------28
2.4 Conclusion----------29
References----------43

III. SULFIDE-DRIVEN ARSENIC MOBILIZATION FROM ARSENOPYRITE AND BLACK SHALE PYRITE----------49

Abstract----------49
3.1 Introduction----------51
3.2 Materials and Methods----------54
Materials ----------54
Abiotic arsenic mobilization experiments---------- 54
Biological arsenic mobilization from black shale under sulfate reducing conditions----------56
Analytical techniques----------56
3.3 Results----------58
Sulfide-driven arsenic mobilization from arsenopyrite ----------58
Sulfide-driven arsenic mobilization from homogenized black shale and isolated black shale pyrite----------59
XANES spectroscopy of arsenic in black shale pyrite----------60
Biological arsenic mobilization from homogenized black shale under sulfate reducing conditions----------60
3.4 Discussion----------61
Sulfide-driven arsenic mobilization from arsenopyrite and pyritic black shale ----------61
Implications for the environment----------64
References----------73

IV. MICROBIAL COLONIZATION OF IRON SULFIDE SUBSTRATE IN SUBSURFACE ENVIRONMENT----------78
Abstract----------78
4.1 Introduction ----------83
4.2 Methodology ----------83
Site description ----------83
Sample deployment----------84
DAPI staining----------85
Scanning electron microscopy and Energy Dispersive Spectroscopy85
Enrichment of the Biofilm Microorganisms----------86
DNA extraction and PCR----------87
Denaturing Gradient Gel Electrophoresis (DGGE) ----------87
DNA sequencing results analysis----------88
4.3 Results----------88
DAPI staining----------88
Scanning Electron Microscopy----------89
Energy Dispersive Spectroscopy----------89
Molecular study of attached microbes----------89
DGGE----------90
16S rDNA sequencing results and phylogenetic tree construction------90
4.4 Discussion----------91
4.5 Conclusion and implications----------96
References----------111

V. SUMMARY AND CONCLUSIONS----------116

5.1 Summary----------116
5.2 Conclusions----------119
5.3 Suggested future researches----------120
References----------123

APPENDIX

APPENDIX I----------124
APPENDIX II----------133
APPENDIX III----------135

CURRICULUM VITA----------136

Lists of Tables

CHAPTER IV

1. Groundwater chemistry of NAWC well 33BR----------99

2. The phylogenetic position of each band excised from DGGE----------109

3. Bacteria detected from biofilms attached to pyrite, arsenopyrite minerals and quartz sand in the subsurface well----------110

List of Illustrations

CHAPTER II

1. Lithology logs from the cores from the Newark Basin Coring Project: the Nursery---31

2. Apparatus setting of pyritic sulfur and acid volatile sulfur----------32

3. Relationship between pyritic sulfur and total sulfur in various sedimentary rocks-----33

4. The depth profile of total sulfur, pyritic sulfur and acid-volatile sulfur in Newark Basin Lockatong formation----------34

5. The relationship between redox index Th/U and pyrite and AVS amount in shale-----36

6. Enrichment factors for trace elements in red and black shale of Newark Basin Lockatong formation----------37

7. Arsenic versus pyritic sulfur in Lockatong formation black shale----------38

8. Mo normalized by Al vs. organic carbon content in Lockatong formation black shale----------39

9. As versus Mo concentrations in Lockatong formation black shale----------40

10. The hypothesized As and Mo depositional mechanisms in the anoxic lake bottom of Newark Basin----------41

11. Mo versus As in Passaic formation groundwater, data from Serfes PhD dissertation (Serfes, 2005) ----------42

CHAPTER III

1. Mobilization kinetics of total arsenic from arsenopyrite incubated at pH 8 under oxic, hypoxic, and anoxic conditions with or without 1 mM sulfide ----------67

2. Mobilization kinetics of total arsenic and arsenite from arsenopyrite under oxic and hypoxic conditions with or without 1 mM sulfide ----------68

3. Mobilization kinetics of total arsenic from homogenized Newark Basin black shale under oxic and hypoxic conditions with or without 1 mM sulfide ----------69

4. Mobilization kinetics of total arsenic from isolated Newark Basin black shale pyrite under oxic and hypoxic conditions with or without 1 mM sulfide ----------70

5. Arsenic K-edge x-ray absorption-near edge structure (XANES) for the As(III) oxide, sodium arsenite ($NaAsO_2$), the As(II) sulfide, realgar (AsS), the As(-I) iron sulfide, arsenopyrite (FeAsS), and arsenian pyrite isolated from Newark Basin (Lockatong formation) black shale ----------71

6. Arsenic mobilization from homogenized Newark Basin black shale incubated under biologically active, sulfate reducing and sterile conditions ----------72

CHAPTER IV

1. Geological map of New Jersey http://www.state.nj.us/dep/njgs/ ----------100

2. Air view of the Naval air warfare center. Red circle indicated the sampling and deploy well----------101

3. Apparatus of sample deployment to the Naval air warfare center well----------102

4. Experimental design of the investigation regarding microbial colonization on the pyritic black shale----------103

5. Comparison among DAPI Staining of black shale thick sections with square pyrite grains shown with red fluorescence----------104

6. DAPI staining of microorganisms colonized on black shale thick sections----------105

7. Scanning electron microscopy observation of biofilm–cells were embedded within EPS and more associated with pyrite than shale matrix----------106

8. SEM image of the exopolymers from *G. ferruginea* on the black shale thick section incubated in groundwater----------107

9. DGGE (30% to 80%, 55V, 16h) profile of PCR amplified 16*S* rDNA gene products----------108

CHAPTER V

1. The subsurface iron and sulfur geochemistry----------116

CHAPTER 1

INTRODUCTION

1.1 The Biogeochemistry of Iron, Sulfur and Trace elements in the Environment

Besides hydrothermal and igneous processes, the introduction of iron to the environment may begin with the weathering of iron containing minerals from rock, soil and sediments. Pyrite (FeS_2) is one of the most abundant minerals containing iron and sulfur in the earth's crust and was found by humans since antiquity. It is a pale brass yellow mineral with a density of 5.01 g/cm^3 and a hardness of 6.5, and often contains impurities such as gold, silver and arsenic. Most pyrite is disseminated in sedimentary rock and sediments, particularly organic carbon rich black shales and coastal marine sediments. In the ocean, pyrite is prevalent at mid-ocean ridges (Edwards, 2004). One of the most important weathering processes for iron mobilization is pyrite oxidation. When pyritic rocks are exposed to subsurface or surface water, the chemical and microbial oxidation of pyrite can release iron and sulfur from solid phases and produce a large amount of acid, sometimes may lead to acid mine drainage (or acid rock drainage). The generated acid may enter adjacent aquifers and cause further rock weathering. The oxidation of pyrite can be achieved by reaction with either oxygen or ferric iron. The overall reactions are

$$FeS_2+15/4\ O_2+1/2H_2O \rightarrow Fe^{3+}+2SO_4^{2-}+H^+ \quad (1)$$

$$FeS_2+14Fe^{3+}+8H_2O \rightarrow 15Fe^{2+}+2SO_4^{2-}+16H^+ \quad (2)$$

Equation (1) usually occurs in acidic environments, where acidophilic microbes such as *Thiobacillus ferrooxidans* catalyze the oxidation process with oxygen. Under anoxic condition, equation (2) may be more predominant. For the complete redox reaction, 15 electrons (1 for Fe and 14 for S) are transferred. However, it is only possible to donate or accept one or two electrons at each step in nature. Thus, intermediate sulfur compounds are expected to occur during pyrite oxidation. This process is described as the "thiosulfate pathway" (Luther and George, 1987; Moses et al., 1987; Schippers and Jorgensen, 2001). The intermediate sulfur compounds in this process of pyrite oxidation are then either oxidized chemically by ferric iron or biologically by sulfur oxidizing microorganisms to sulfate (McGuire et al., 2001; Schippers and Sand, 1999). As a major ion in most groundwater systems, sulfate can be converted to sulfide by bacterial sulfate reduction when coupled with organic matter under anoxic conditions. Ferric ion produced by the oxidation of solid or aqueous phase Fe (II) with oxygen can be precipitated and thereby immobilized as hydroxide, oxide, phosphate or sulfate, or, if bound to soluble organic ligands, will be converted to soluble complexes and dispersed from its source.

In natural environments, pyrite weathering is indisputably involved with or even controlled by biological activities. It has been discovered that chemolithotrophic microorganisms are able to harness energy from the weathering of sulfides via various redox reactions with the reduced chemical species in sulfides (Edwards, 2004; McCollom, 2000). Among them, mesophiles such as *Thiobacillus ferrooxidans, Leptospirillum ferrooxidans* and *Thiobacillus thiooxidans,* thermophiles such as *Thiobacillus caldus, Metallosphaera sedula, Acidianus brierleyi* and *Sulfolobus acidocaldarius* were the most

commonly identified microbes in the process of pyrite oxidation (Ehrlich, 2002). There have been abundant research concerning the biological control of pyrite oxidation at low pH conditions, such as in the bioleaching industry or acid mine drainage environment (Bond and Banfield, 2001; Edwards et al., 2000; Edwards et al., 1999; Meyer et al., 1999). With high acidity, microorganisms such as *Thiobacillus ferrooxidans* play a crucial role in oxidation of mineral sulfides via "direct" (attach to mineral surface and dissolve sulfides without a soluble electron shuttle) or "indirect" (not attach to mineral surface and oxidize the metal sulfide via Fe(II)/Fe(III) shuttle) pathways (Rodriguez et al., 2003a; Rodriguez et al., 2003b; Schippers and Sand, 1999). However, compared with the extensive studies under extremely acidic condition, the weathering of pyrite at slightly acidic to neutral pH is much less examined and the microbial consortia that utilize the mineral substrates are not well described and characterized.

Microbial activities can also mobilize Fe (III) from solid phases. In the anoxic zone, Fe (III) oxides are readily reduced at pH >4.0 and may function as a terminal electron acceptor for iron reducing microorganisms. Equation (3) indicates the reduction of Fe (III) coupled with organic matter oxidation.

$$FeOOH + 1/4CH_2O + 2H^+ \rightarrow Fe^{2+} + 1/4CO_2 + 7/4H_2O \qquad (3)$$

Microbial iron respiration may also be coupled with hydrogen or S(0) oxidation and iron reduction linked to in the oxygen depleted environment (Chapelle and Lovley, 1992; Lovley, 1995; Lovley, 1997). Diverse species throughout the Archaea and Bacteria

domains may be involved in this process. Pure cultures of thermophilic and hyperthermophilic archaea and bacteria capable for Fe reduction have been obtained from extreme environments such as deep subsurface (Lovley et al., 2004; Slobodkin et al, 1999). At circumneutral pH, family Geobacteraceae from ε-proteobacteria, *Shewanella putrefaciens* from γ-proteobacteria together with other ferric iron respirers have been well characterized for their iron reduction functions in the terrestrial and subsurface environment (Ehrlich, 2002; Lovley, 2001). In addition, some microbes that belong to β-proteobacteria and *Geothrix fermentans* from Acidobacteria might also be responsible for iron reduction in sediments and aquifers (Coates et al., 1999; Cummings et al., 1999; Weber et al., 2006). Moreover, various fermentative microorganisms may also contribute to the process, yet, they are considered to play a minor role in iron geochemical cycling compare to respiratory iron reducers (Lovley et al, 1986; Weber et al., 2006).

Ferrous iron produced by microbial Fe (III) reduction may react with dissolved sulfide in the anoxic environment, form iron sulfides including iron monosulfide and pyrite, and be formed and deposited in sediments which ultimately can became sedimentary rock. Iron monosulfide functions as the precursor for pyrite formation, in which a redox reaction may take place between the iron monosulfide (such as mackinawite) and an oxidant through sulfur gain or iron loss pathways to generate pyrite. The reservoir of reducing equivalents thus formed can provide electrons for both chemical and biological processes. The burial of pyrite in sedimentary environments is closely linked to several geochemical cycles. For example, the Phanerozoic oxygen level is kept nearly constant by the balance between the organic carbon and pyrite reservoirs

(such as black shales) and carbonate and sulfate reservoirs on earth (Berner, 1999; Petsch, 2003).

Besides oxygen, the biogeochemical cycles of various trace elements are also associated to iron and sulfur geochemistry in the environment. Trace elements such as As, Mo, Co, Cu, Re may be precipitated with sulfides, incorporated into pyrite and/or fixed with organic matter. By studying the enrichment of these trace elements in sedimentary rocks, we may gain insights about their distribution and possible mobilization mechanisms. Upon exposure of the sediments or sedimentary rocks to oxic conditions and water, weathering of iron sulfide may be initiated. The release of incorporated trace metals during iron oxidation-reduction processes depends on their chemical associations in the solid phase as well as the ambient geochemical environment. The progressive weathering of the New Albany Shale in Kentucky lead to the release of elements during sulfide and organic matter oxidation and trace element mobilization was differentiated based on their associations with the original minerals (Tuttle et al., 2009). One of the concerns regarding trace element mobilization is that dissolved elements may cause adverse environmental effects upon release to top soils and surface/subsurface waters. Indeed, compared to pure pyrite, pyrite with substantial concentrations of trace elements may be even more prone to weathering (Lehner et al., 2007; Savage et al., 2000). Since pyrite is considered one of the most important natural sources of arsenic in the environment, there is concern about the environmental damage associated with its oxidation (Ahmed et al., 2004; Lowers et al., 2007; Peters and Burkert, 2008). Other trace metals, such as Cd, Mo and U, have also been shown to be easily released from black

shale (Lavergren et al., 2009). The mobilization of heavy metals may lead to higher incidence of endemic diseases as well (Peng et al., 2004).

The Newark Basin is a sediment filled rift basin located mostly in New Jersey, but also stretching into south-eastern Pennsylvania and southern New York. The Lockatong Formation is one of the fundamental lithological divisions of the Newark basin along with the Stockton and Passaic Formations. The Lockatong Formation is mostly composed by black (organic rich), gray and red mudstone, siltstone and shale (Olsen, 1996; Serfes, 2005). Black shale is recognized as a fine-grained laminated sedimentary rock rich in organic carbon and pyrite. It also hosts various trace elements including Ag, As, Au, Cu, Hg, Mo, Ni, Pb, Re, Sb, U,V, Zn (Pratt and Davis 1992; Tuttle et al. 2003; Peng et al. 2004). The Newark Basin is of great interest and importance as it contains significant aquifers in the NJ and PA area. Moreover, high arsenic occurrence has been identified in 15 to 30% of the sampled water supply wells (Serfes, 2005).

1.2 Research Objectives

The objectives of this research were to advance our knowledge of the depositional environment of pyrite and the trace elements distribution patterns in the Newark Basin Lockatong Formation shales, especially for arsenic. Further, in order to understand the controls of trace element (arsenic) mobilization from solid phases, chemical and biological studies were performed and possible mechanisms were proposed.

The iron and sulfur biogeochemical processes involved with the mobilization were also studied and discussed, and several perspectives were then presented.

1.3 Dissertation Overview

Three research chapters are presented in this dissertation.

The first research chapter presents the results of an investigation of the pyrite depositional environment in Newark Basin Lockatong formation black shale and the local trace elemental distribution. The first part of this chapter focused on pyrite and acid volatile sulfide quantification in Lockatong formation black shale, together with the redox index Th/U, pyrite depositional environment was investigated; while in the second part, attention is given to the highly enriched trace metals and their chemical associations in black shale, and possible mobilization patterns.

The second research chapter examined the arsenic mobilization mechanisms from pyritic rich solid phases such as arsenopyrite, arsenian pyrite as well as the pyritic black shale collected from Newark Basin Lockatong formation. It was concluded that the arsenic release from the solid phase can take place in a hypoxic environment in the presence of dissolved sulfide. This observation will be most important at oxic-anoxic interfaces of groundwater.

The last research chapter focused on the investigation of the biofilm that formed on the pyrite surface in the Newark Basin subsurface groundwater, as to study the microbial activities associated with trace element mobilization. The involvement of microbes in the subsurface iron cycling at slightly acidic to neutral pH, e.g., the oxidation of iron sulfides and the reduction of iron hydroxide, was also examined and discussed.

References

Ahmed K. M., Bhattacharya P., Hasan M. A., Akhter S. H., Alam S. M. M., Bhuyian M. A. H., Imam M. B., Khan A. A. and Sracek O. (2004) Arsenic enrichment in groundwater of the alluvial aquifers in Bangladesh: an overview. *Appl. Geochem.* **19**, 181-200.

Berner R. A. (1999) Atmospheric oxygen over Phanerozoic time. *Proc Natl Acad Sci U S A.* **96**(20), 10955-10957.

Bond P. L. and Banfield J. F. (2001) Design and performance of rRNA targeted oligonucleotide probes for in situ detection and phylogenetic identification of microorganisms inhabiting acid mine drainage environments. *Microbial Ecology* **41**(2), 149-161.

Edwards K. J., Goebel B. M., and Rodgers T. M., et al. (1999) Geomicrobiology of Pyrite (FeS2) Dissolution: Case Study at Iron Mountain, California. *Geomicrobiology Journal* 16, 155-179.

Edwards K. J. (2004) Formation and degradation of seafloor hydrothermal sulfide deposits. *Sulfur Biogeochemistry: Past and Present* **379**(0), 83-96.

Edwards K. J., Bond P. L., and Banfield J. F. (2000) Characteristics of attachment and growth of Thiobacillus caldus on sulphide minerals: a chemotactic response to sulphur minerals? *Environmental Microbiology* **2**(3), 324-332.

Ehrlich H. L. (2002) 15. Geomicrobiology of Iron. In *Geomicrobiology*. Marcel Dekker, Inc.

Emerson D. and Moyer C. L. (2002) Neutrophilic Fe-Oxidizing bacteria are abundant at the Loihi Seamount hydrothermal vents and play a major role in Fe oxide deposition. *Applied and Environmental Microbiology* **68**(6), 3085-3093.

Lehner S., Savage K., Ciobanu M., and Cliffel D. E. (2007) The effect of As, Co, and Ni impurities on pyrite oxidation kinetics: An electrochemical study of synthetic pyrite. *Geochi.et. Cosmo. Acta* **71**(10), 2491-2509.

Lovley, D. R. & Phillips, E. J. P. Organic matter mineralization with reduction of ferric iron in anaerobic sediments. Appl. Environ. Microbiol. 51, 683–689 (1986).

Lovley D. R. (1995) Microbial Reduction of Iron, Manganese, and Other Metals. *Advances in Agronomy, Vol 54* 54, 175-231.

Lovley D. R. (1997) Microbial Fe(III) reduction in subsurface environments. *Fems Microbiology Reviews* 20(3-4), 305-313.

Lovley D. R. (2001) Reduction of iron and humics in subsurface environments. In *Subsurface Microbiology and Biogeochemistry* (ed. J. K. Fredrickson and M. Fletcher), pp. 193-217. Wiley-Liss, Inc.

Lovley D. R., Holmes D. E., Nevin K. P., and Poole. (2004) Dissimilatory Fe(III) and Mn(IV) Reduction. In *Advances in Microbial Physiology*, Vol. Volume 49, pp. 219-286. Academic Press.

Lowers H. A., Breit G. N., Foster A. L., Whitney J., Yount J., Uddin M. N. and Muneem A. A. (2007) Arsenic incorporation into authigenic pyrite, Bengal Basin sediment, Bangladesh. *Geochim. Cosmochim. Acta* **71**, 2699-2717.

Luther I. and George W. (1987) Pyrite oxidation and reduction: Molecular orbital theory considerations. *Geochimica et Cosmochimica Acta* **51**(12), 3193-3199.

McGuire M. M., Edwards K. J., Banfield J. F., and Hamers R. J. (2001) Kinetics, surface chemistry, and structural evolution of microbially mediated sulfide mineral dissolution. *Geochimica et Cosmochimica Acta* **65**(8), 1243-1258.

Meyer G., Waschkies C., and Huttl R. F. (1999) Investigations on pyrite oxidation in mine spoils of the Lusatian lignite mining district. *Plant and Soil* **213**(1-2), 137-147.

Moses C. O., Kirk Nordstrom D., Herman J. S., and Mills A. L. (1987) Aqueous pyrite oxidation by dissolved oxygen and by ferric iron. *Geochimica et Cosmochimica Acta* **51**(6), 1561-1571.

McCollom T. M. (2000) Geochemical constraints on primary productivity in submarine hydrothermal vent plumes. *Deep Sea Research Part I: Oceanographic Research Papers* 47(1), 85-101.

Olsen P. E., Kent D. V., Cornet B., Witte W. K., and Schlische R. W. (1996) High resolution stratigraphy of the Newark Rift Basin (early Mesozoic, eastern North America) (vol 108, pg 40,1996). *Geological Society of America Bulletin* **108**(7), 912-912.

Peng, B., Z. Song, et al. (2004). "Release of heavy metals during weathering of the Lower Cambrian Black Shales in western Hunan, China." Environmental Geology **45**: 1137-1147.

Peng B., Piestrzynski A., Pieczonka J., Xiao M., Wang Y. Z., Xie S. R., Tang X. Y., Yu C. X., and Song Z. (2007) Mineralogical and geochemical constraints on environmental impacts from waste rock at Taojiang Mn-ore deposit, central Hunan, China. *Environmental Geology* **52**(7), 1277-1296.

Petsch S. T. (2003) Ch.11: The Global Oxygen Cycle. In *Treatise on Geochemistry* Vol. 8 (ed. H. D. Holland and K. K. Turekian), pp. 515-556. Elsevier Science.

Rodriguez Y., Ballester A., Blazquez M. L., Gonzalez F., and Munoz J. A. (2003a) New information on the pyrite bioleaching mechanism at low and high temperature. *Hydrometallurgy* **71**(1-2), 37-46.

Rodriguez Y., Ballester A., Blizquez M. L., Gonzilez F., and Muioz J. A. (2003b) Study of Bacterial Attachment During the Bioleaching of Pyrite, Chalcopyrite, and Sphalerite. *Geomicrobiology Journal* **20**(2), 131.

Peters S. C. and Burkert L. (2008) The occurrence and geochemistry of arsenic in groundwaters of the Newark basin of Pennsylvania. *Appl. Geochem.* **23**, 85-98.

Pratt, L. M. and C. L. Davis (1992). Intertwined fates of metals, sulfur and organic carbon in black shales. Geochemistry of organic matter in sediments and sedimentary rocks. **27:** 1-27.

Savage K. S., Tinglea T. N., O'Day P. A., Waychunas G. A. and Bird D. K. (2000) Arsenic speciation in pyrite and secondary weathering phases, Mother Lode Gold District, Tuolumne County,California. *Appl. Geochem.* **15**, 1219-1244.

Schippers A. and Jorgensen B. B. (2001) Oxidation of pyrite and iron sulfide by manganese dioxide in marine sediments. *Geochimica et Cosmochimica Acta* **65**(6), 915-922.

Schippers A. and Sand W. (1999) Bacterial Leaching of Metal Sulfides Proceeds by Two Indirect Mechanisms via Thiosulfate or via Polysulfides and Sulfur. *Appl. Environ. Microbiol.* **65**(1), 319-321.

Slobodkin A., Jeanthon C., L'Haridon S. , Nazina T., and Miroshnichenko M., Dissimilatory reduction of Fe(III) by thermophilic bacteria and archaea in deep subsurface petroleum reservoirs in Western Siberia. *Curr Microbiol* **39** (1999), pp. 99–102.

Tuttle, M. L., G. N. Breit, et al. (2003). Geochemical Data from New Albany Shale, Kentucky: A Study in Metal Mobility During Weathering of Black Shales, USGS.

Tuttle M. L. W., Breit G. N., and Goldhaber M. B. (2009) Weathering of the new albany shale, kentucky: II. redistribution of minor and trace elements. *Applied Geochemistry*. **24** (8), 1549-1564

Weber KA, Achenbach LA, Coates JD. Microorganisms pumping iron: anaerobic microbial iron oxidation and reduction. *Nature reviews. Microbiology* 2006 Oct; 4(10):752-64

CHAPTER 2

DEPOSITIONAL ENVIRONMENT AND WEATHERING PROXIES OF PYRITE IN NEWARK BASIN BLACK SHALE

Abstract

The sedimentary depositional environment of Newark Basin black shale was investigated. Inorganic sulfur species including pyritic sulfur (S(-I)) and acid volatile sulfur (S(-II)) were quantified in black shale of the Lockatong Formation and the analytical results showed that pyrite was the most abundant source of total sulfur (more than 50%). Pyritic S abundance was also strongly correlated to total sulfur, however, no correlation was found between acid volatile sulfur and total sulfur. An inverse relationship was identified between pyritic sulfur and acid volatile sulfur at different depths. Inverse relationships between Th/U, which is proportional to redox potential, and pyritic S and positive correlations between Th/U and acid volatile S were observed at various depths in the Lockatong formation. Under strongly anoxic conditions indicated by low Th/U ratios (<2), the generation of abundant H_2S may have resulted in the conversion of AVS to pyrite. By contrast, under less strongly anoxic conditions indicated by higher Th/U, the production of H_2S may have been limited and the consumption of AVS in pyrite formation restricted.

Attention was also given to the distribution pattern of trace metal enrichment in the Lockatong formation shales. Trace metal enrichment factors were analyzed and arsenic and molybdenum were two highly enriched elements observed in the black shale.

Further analysis showed that the arsenic content was closely linked to pyrite and molybdenum was associated with organic matter. Knowledge about the binding phases of these trace elements in black shale may be useful in the evaluation of their mobilization patterns to the aqueous phase in black shale aquifers. It was observed that the concentrations of arsenic and molybdenum were positively correlated in Lockatong formation black shale. Positive correlation between these two trace elements in Newark Basin (Passaic formation) groundwater, but not Newark Basin (Lockatong formation) red shale suggests that black shale may be the ultimate source of As and Mo to groundwater in the Newark Basin.

2.1 Introduction

The formation and weathering of pyrite are very important processes for the geochemical cycles of iron, sulfur, atmospheric oxygen and carbon (Berner and Canfield, 1989; Schoonen, 2004). The formation of pyrite in marine and freshwater sediments not only fixes iron and sulfur, but also partly controls atmospheric oxygen level. Reduced sulfur in pyrite is produced by bacterial sulfate reduction in which organic matter is oxidized and sulfate is reduced to sulfide without consumption of O_2; this process resupplies oxidized carbon to the ocean and atmosphere system where it may be reduced in oxygenic photosynthesis. In effect, the formation of pyrite derived from bacterial sulfate reduction (BSR) in sediments results in a net release of O_2 to the atmosphere (Petsch, 2003). Conversely, the oxidative weathering of pyrite consumes oxygen and lowers the atmospheric oxygen level (Berner and Canfield, 1989). Thus, it is thought that the Phanerozoic oxygen level was kept nearly constant by the balance between oxidized and reduced sulfur and carbon reservoirs on Earth (Berner, 1999; Petsch, 2003).

The formation of pyrite mostly occurs in marine coastal environments, but also in aquifers, lakes, swamps, soils and waste ponds (Schoonen, 2004). The mechanism of pyrite formation in the natural environment is controversial and remains an active research area. Direct precipitation of pyrite is greatly inhibited because of the difficulty of direct nucleation of pyrite in solution (Schoonen and Barnes, 1991a). Thus, the formation process is generally considered to be a redox reaction between iron monosulfide precursor (such as mackinawite) and an oxidant such as zero valence sulfur (Berner,

1970), the hydrogen in H_2S (Rickard and Luther, 1997) or adsorbed polysulfides (Benning et al., 2000; Schoonen and Barnes, 1991b) through a sulfide gain pathway, or with oxidants such as oxygen (Wilkin and Barnes, 1996) or manganese oxides through iron loss pathways. Nevertheless, greigite (Fe_3S_4) has been implicated and further confirmed to be involved with the formation of pyrite as the intermediate product under anoxic condition (Hunger and Benning, 2007; Wilkin and Barnes, 1996). Although most of the conversion studies of iron monosulfide to pyrite are designed and performed abiotically, microorganisms also play a role in the formation of pyrite (Schoonen, 2004). By coupling with organic matter, sulfate reducing bacteria (SRB) can produce hydrogen sulfide which may be sequestered as pyrite with dissolved iron. Moreover, the sulfate reducing bacteria may also transform and incorporate organic sulfur compounds into the FeS precursors and lead to pyrite formation on the outside of their cells (Donald and Southam, 1999). Sulfur-disproportionating bacteria can also accelerate pyrite formation by adding zero valence sulfur and by reacting H_2S with FeS (Canfield et al., 1998).

Besides pyrite, there are also other reduced inorganic sulfur species that are important components of the total sulfur mass balance in sedimentary rocks, such as acid volatile sulfides (AVS) and elemental sulfur. AVS are reduced inorganic sulfides that react with HCl to produce H_2S and are usually in the forms of amorphous FeS and poorly ordered mackinawite in modern sediments or ancient sedimentary rocks (Rickard and Morse, 2005). Acid volatile sulfides, iron disulfides and elemental sulfur altogether are often analyzed as total reduced inorganic sulfides. The difference between the total reduced sulfides and acid volatile sulfides provide an estimation of elemental sulfur and

iron disulfides including pyrite and marcasite (Morse and Cornwell, 1987; Morse et al., 1987). The coexistence of AVS and pyrite has been observed in various sedimentary environments. Typically, the fraction of sulfur present as AVS is much smaller than that of pyrite in sediments or sedimentary rocks (Rickard and Morse, 2005). Within the depth profile of sediments, it is usually observed that AVS to pyritic S ratio decreases because of the conversion of metastable iron monosulfides and greigite to pyrite (Burton et al., 2006; Goldhaber, 2003; Rickard and Morse, 2005; Yin et al., 2008). However, the proportions of AVS and pyritic sulfur vary widely among different sediments and environments (Rickard and Morse, 2005).

The weathering of pyrite not only because it is linked to the global Fe, S and O cycles, but also because other metals enriched in pyrite may be mobilized, and possibly leading to adverse environmental effects. For example, the progressive weathering of the New Albany Shale in Kentucky lead to the release of various trace elements during sulfide and organic-matter oxidation and this mobilization of trace elements was differentiated based on their associations with the original minerals (Tuttle et al., 2009). Studies have shown that Cd, Mo, U are very easily released from black shale (Lavergren et al., 2009). Pyrite is also considered as the ultimate source for arsenic released to aquatic environments (Ahmed et al., 2004; Lowers et al., 2007; Peters and Burkert, 2008).

Black shale is recognized as the fine-grained laminated sedimentary rocks rich in organic carbon. One of the most important reservoirs of pyrite on earth is black shale. The average black shale contains 3% of organic carbon by weight (Raiswell and Berner ,

1986). In addition to pyrite, black shale also hosts various elements including Ag, As, Au, Cu, Hg, Mo, Ni, Pb, Re, U, V, Sb and Zn (Pratt and Davis 1992; Tuttle et al. 2003; Peng et al. 2004). Many black shale containing formations remain in the subsurface and weather through contact with groundwater. As productive aquifers, their formations are also sources of drinking water and their weathering can cause serious consequences to the local environment. The goal of this study was to quantify pyrite and other forms of S in Newark Basin black shale as well as the incorporation of trace metals in pyrite or other solid phases to shed light on trace metal mobilization patterns upon weathering.

2.2 Methodology

Site description and whole rock analysis

The depositional environments of the Newark Basin ranged from the deep anoxic lakes with organic carbon-rich detrital sediments to oxic shallow and playa lakes (Serfes, 2005). In the Newark Basin, pyrite-rich black shale was formed from sediments deposited mostly during the Upper Triassic (~225 to 200 Ma) in the Passaic and Lockatong formations. The Lockatong formation in the Newark Basin is mostly composed of black (organic carbon-rich), gray and red mudstone, siltstone and shale (Serfes, 2005).Samples for this study were taken from top, middle and lower parts of the Lockatong formation at core depth of 522 to 564 ft, 1539 to 1589 ft, and 2986 to 3002 ft for elemental analysis which dated around (~223 to 218 Ma) (Fig. 2.1). A total of 20 samples were cut including nine black, two grey, and nine red shale samples. The whole rock analysis was

performed by ALS Chemex Labs Inc., Sparks, NV. They prepared samples by coarse crushing the rock until 70% <2 mm, then splitting and pulverizing to 85% passing through 75 um with four acid digestion (nitric acid (HNO_3), HNO_3/hydrochloric acid (HCl), aqua regia and HNO_3/hydrofluoric acid (HF)) in the end. The samples were undergone various elemental analysis with analytical instruments. More details can be found online in the service protocol provided by ALS chemex labs (http://www.alsglobal.com/).

Sulfur speciation

Subsamples of Lockatong black shale were analyzed for pyritic sulfur, acid volatile sulfur and elemental sulfur at Rutgers. Small samples of pulverized black shale (0.5 -1g) were added into a three-port glass reaction vessel. Before the extraction of pyritic sulfur, all samples were pretreated with acetone to remove any elemental sulfur that may exist on the surface of material. Then, each black shale sample was split into 2 parts. One part was treated with concentrated HCl to analyze for AVS (acid volatile sulfur) and the other part underwent chromium-reduction to determine pyritic sulfur content.

Elemental sulfur was determined by acetone extraction. Small samples of pulverized rock (0.5-1g) were soaked in 10 ml acetone overnight. The extraction flasks were placed in a rotary shaker and covered with Parafilm. Analysis of elemental sulfur followed the method developed by Bartlett and Skoog (Bartlett and Skoog, 1954).

Acid volatile sulfide (AVS) was examined by adding 10 ml of 12 N HCl to the reaction vessel. The system was flushed with N_2 and heat applied after 10 minutes. Contents of the flask were then boiled for 5 minutes and later kept at below boiling point for 45 minutes. Zn acetate was used as a trap for absorbing H_2S. H_2S was trapped by Zn Acetate solution and analyzed using the methylene blue method (Cline, 1969; Popa and Kinkle, 2000). The sulfur content in H_2S was calculated back as sulfur in acid volatile sulfur.

Chromium reducible sulfur (pyritic sulfur, acid volatile sulfur and elemental sulfur) was determined by passing 1 M $CrCl_3$ through 2% acidified $HgNO_3$ amalgamated Zn which was pretreated with 0.5 M HCl, thereby reducing Cr^{3+} to Cr^{2+} (Canfield et al., 1986)). The system was flushed with N_2 for 20 minutes and then 10 ml of reduced chromium solution was introduced to the reaction vessel along with 10 ml of 12 N HCl. Heat was applied after 10 min and the flask kept boiling for about 1 hour. H_2S was also trapped by Zn Acetate solution and analyzed using the methylene blue method. The sulfur content in H_2S was calculated back as sulfur in pyrite. Figure 2.2 showed the apparatus setting of extracting pyritic sulfur and acid volatile sulfur from the pyritic black shale.

2.3 Results and Discussion

Whole rock analysis of the Lockatong formation shale

Whole rock analysis of both black and red shale from the Lockatong formation

gives us information about the elemental composition of the Newark Basin sedimentary rock aquifer. Black shale and red shale have a different general chemical composition due to the different depositional oxygenation environment in which they formed. Analytical results for elemental concentrations are presented in Appendix I.

Sulfur speciation of black shale

Pyritic sulfur, acid volatile sulfur (AVS) and elemental sulfur were quantified in black shale from upper (depth around 550 ft), middle (depth around 1550 ft) and lower sections (depth around 3000 ft) of the Lockatong formation. Pyritic sulfur was the most abundant form of inorganic reduced sulfur in the black shale and was highly correlated to total sulfur with R^2=0.97 ($p < 1\times10^{-7}$) (Fig 2.3 a). The average concentration of pyritic S in black shale in this study was 2039 ppm which ranged from 16.9 to 6289 ppm at all depths. The close correlation between pyritic sulfur and total sulfur in Newark Basin black shale was not a unique observation (Fig. 2.3 b, c, d). Highly positive associations between pyritic and total sulfur were also reported elsewhere. For example, in Upper Sinian and Lower Cambrian black shale in Southwest China, total sulfur and pyritic sulfur were highly correlated, R^2=0.96 (Fig 2.3 b)(Wu et al., 1999). A similar trend was also observed in Mediterranean Sea basin sediments (Fig 2.3 c) (Henneke et al., 1997). Moreover, the New Albany shale from eastern Kentucky indicated an extremely tight relationship between total sulfide and total sulfur as well (Fig 2.3 d) (Tuttle et al., 2003).

AVS content in Lockatong black shale was much lower than that of pyritic sulfur. The average AVS amount in black shale was about 56 ppm, but AVS ranged from 13.6 to

293 ppm throughout all depths. Yet, the abundance of AVS did not show strong correlation to the amount of total sulfur or pyritic sulfur in the black shales. The concentrations of pyritic sulfur and acid volatile sulfur in all black shale and some red shale are presented in Appendix I.Elemental sulfur was below detection in all Lockatong shale samples.

In addition to reduced inorganic sulfur, black shale may contain sulfate and organic sulfur. Organic sulfur is a more important component of black shale sulfur than sulfate.For example, black shale often has high concentrations of organic sulfur (ranges from 17% to 71% with an average of 42% in total S in Lower Cambrian black shales from Southwest China) (Wu et al, 1999; Lei et al, 2001), but low levels of sulfate (Lei et al, 2001; Arndt et al, 2006). This may be attributed to the anoxic environments in which black shale is deposited where much of the sulfate may have undergone reduction. Nevertheless, the amount of organic S and sulfate in the Newark Basin Lockatong Formation black shale were not measured in the present study since they are not directly linked to the formation and weathering of pyrite .

At a core depth in the Lockatong formation of around 550 and 1550 ft, pyritic sulfur had a similar profile to total sulfur (Fig 2.4 a, d), but its profile was opposite to that of AVS (Fig 2.4 c, f). In the lower Lockatong (around 3000 ft) only two samples were identified as black shale, so profiles were not plotted. The inverse correlation between AVS and pyrite profiles may be explained by their redox inter-conversion. The formation of pyrite in sediments is usually through the precursor of iron monosulfide, a major

component of acid volatile sulfur (AVS) (Rickard and Morse, 2005). Their conversion may occur as FeS is consumed and pyrite forms, with the addition of sulfur or loss of iron, resulting in increasing pyritic S to AVS ratios with time as pyrite is the thermodynamically favored species of sulfide (Burton et al., 2006). Thus, the consumption of iron monosulfide will lead to the accumulation of pyrite in the sedimentary environment and cause their inverse correlation.

Evaluation of pyrite depositional conditions with the Th/U redox index

The Th/U ratio in sedimentary rocks can be used as an indicator of the redox conditions of paleo-depositional environments (Jones and Manning, 1994). These two elements tend to exhibit similar geochemical characteristics except under oxidizing conditions. Thorium remains insoluble Th^{4+} under all redox conditions in the environment, but uranium is only soluble under oxidizing conditions as uranyl cation $(UO_2)^{2+}$. Under strongly reducing conditions, U is transformed to the immobile UO_2 and it may be enriched in the solid phase (Guo et al., 2007). Thus, the more anoxic redox condition will lead to a lower Th/U ratio. The average shale has a Th/U ratio of 3.8 in the upper continental crust (Taylor and Mclenna, 1985). The range of Th/U ratios for black shale is 3.9±2.9 and for red shale is 7.1±2.0 in present study.

At a core depth of 550, the Th/U profile showed opposite trends compared with total S and pyritic S, yet was almost identical to that of AVS (Fig. 2.4 a, b, c). A similar,

but more noisy relationship among total sulfur/pyritic sulfur, AVS and Th/U was observed at depth around 1550 ft (Fig. 2.4 d, e, f).

According to Th/U data, Newark Basin sedimentary shale experienced different redox conditions during deposition through time. The inverse correlation between Th/U and pyrite was observed with low Th/U value indicating anoxic condition corresponded to high pyrite content at the same depth and vice versa (Fig. 2.4 b and c). On the other hand, low Th/U indicating anoxic condition corresponded to low AVS at the same depth and vice versa (Fig. 2.4 e and f). The relationships between them can be simply illustrated in Fig. 2.5. Under strongly anoxic conditions, indicted by low Th/U ratios (<2), the generation of abundant H_2S could result in the conversion of AVS to pyrite and thus the consumption of AVS and accumulation of pyritic S (equation 1) (Rickard and Morse, 2005).

$$FeS + H_2S \rightarrow FeS_2 + H_2\uparrow \quad (1)$$

On the other hand, under less strongly anoxic conditions, indicated by higher Th/U ratios, production of H_2S and the consumption of AVS may be limited and AVS can accumulate.

Trace metal enrichment factors in Lockatong formation black and red shale

Lockatong formation black shale and red shale were formed under different oxygenation conditions; black shale formed in an oxygen-deficient environment while red shale formed under oxic conditions. Organic carbon-rich black shale can contain pyrite while red shale hosts hematite (Fe_2O_3). Redox conditions of the depositional environment likely had a great impact on the enrichment or scavenging of specific trace elements by Lockatong formation shale. Other factors such as organic matter type, sediment accumulation rates, and diagenetic and later mineralization processes as well as the availability of trace elements may also be important in affecting the association between the elements and shales (Pratt and Davis, 1992). The whole rock analysis indicated different levels of trace elemental enrichment or depletion in the black and red shale. Enrichment factors (EF) were calculated by normalizing each trace element to Al and comparing these ratios to those of upper continental shale (McLennan, 2001).

$$EF = (Element/Al)_{sample\ or\ Lockatong\ formation}/(Element/Al)_{average\ shale}$$

Based on EF values, the magnitude of each trace element enrichment or depletion differed in red shale and black shale (Fig. 2.6). Sediments and sedimentary rocks may function as sinks for trace elements at the time of anoxic conditions. For example, in black shale, Mo showed a much higher enrichment factor (6.2) than in red shale (0.16). As one of the redox potential controlled metalloids, arsenic was enriched in black shale yet much less enriched in red shale. Other metals such as U and V, with higher enrichment factors of 1.4 and 1.1 in black shale and lower values of 0.45 and 0.83 in red shale, respectively, indicate their redox sensitive nature. For other elements, such as Ba,

Co, Cu, Pb and Zn, no apparent enrichments were detected in either shale. Ni, Cr and Mn showed depletion and Se showed enrichment in both shales. However, the enrichment factor for Cs is higher in red shale than black shale.

Since the Lockatong formation shales analyzed in this study were not weathered, enrichment factors may show the original incorporation of trace metals in the depositional and/or diagenetic environments. Organic carbon (OC) and pyrite represent two major sites in black shale for the concentration of trace elements that are present in low abundance in red shale. The average OC is 0.4% in the black shale while the red shale has an average value of 0.04%. More than 50% of the sulfur existed as pyritic sulfur in the black shale (except in 1 out of the 11 samples) while only 7 to 8% of sulfur was identified as pyrite in the two red shale samples analyzed (see Appendix I). The enrichment of specific trace elements in Lockatong shale showed distinct patterns. For example, arsenic was reported to be incorporated in pyrite or adsorbed by metal oxides (Lowers et al., 2007; Thornburg and Sahai et al, 2004; Savage et al, 2000),In the present study, both black and red shale indicated enrichment of arsenic with the EF of the former more than 7 times higher than the latter. The enrichment of arsenic in black shale may be due to its incorporation in pyrite while the enrichment in red shale may be related to the adsorption of arsenic to metal oxides such as Fe_2O_3 and Al_2O_3. On the other hand, the high enrichment of Mo in black shale and depletion in red shale, may indicate its accumulation is highly favorable in oxygen deficient environments. Indeed, Mo is reported to be highly correlated with organic matter content (Tribovillard et al, 2004; Wilde et al, 2004). However, the geochemistry behind this observation is not fully

understood. Organic carbon may provide a substrate for Mo scavenging, or, by facilitating sulfate reduction under anoxic condition, Mo may be sequestered by sulfide (Helz et al, 1996; Tribovillard et al, 2004). Nevertheless, the enrichment factor itself cannot identify the phases containing specific trace metals in the Newark Basin Lockatong formation black shale.

As and Mo as Pyrite and Organic Carbon Proxies in Lockatong Formation

Arsenic exposure is one of the major environmental health concerns and the mechanisms of its natural release from the geosphere to the biosphere, is of great interest and importance. Since the mechanism by which arsenic is mobilized from subsurface minerals depends on the solid phases it is associated with, it is essential to determine the arsenic depositional environment in sedimentary rocks.

The abundance of arsenic versus total sulfur in the Lockatong formation black shale was determined. The positive correlation was recognized except for three outliers ($y=35.5x+1.08$, $R^2=0.93$). The three outliers represented two with very high arsenic and low sulfur content and one with high sulfur point and low arsenic concentration. Because of the nearly fixed proportion of total sulfur present as pyrite in black shale, arsenic was also closely correlated with pyritic sulfur ($y=0.0044x+3.43$, $R^2=0.81$) (Fig. 2.7). Arsenic can replace sulfur in iron sulfide to form FeAsS like precipitates (Bostick and Fendorf, 2003). Indeed, high arsenic spots within pyrite mineral in a black shale thick section from the Lockatong formation were observed with wavelength dispersive spectrometry (Serfes,

2005). It was recognized in other studies that pyrite serves as an ultimate source for arsenic in sedimentary shales and its weathering may contribute to the dissolved arsenic in aqueous phases (Ahmed et al., 2004; Lowers et al., 2007; Peters and Burkert, 2008).

Mo is also highly enriched in the Lockatong formation black shale. However, the solid phases containing Mo in black shale may be different from that of arsenic. Mo (normalized by Al) did not strongly track the concentration of pyritic sulfur (R^2=0.29) in the present study. However, the correlation between Mo/Al and the organic carbon in black shale was positive except for two outliers (not shown) (Fig 2.8). These outliers were for samples with two of the highest Mo/Al values corresponding to the two most elevated organic carbon concentrations in the black shale, respectively: 0.017 (Mo/Al ratio) to 0.9% organic carbon and 0.00029 (Mo/Al ratio) to 0.77% of organic carbon. These conditions may indicate the extremely anoxic environments associated with Mo deposition, which was further confirmed by two of the lowest Th/U values 1.1 and 1.3. The positive association between Mo and organic carbon was only found in black shale, not in red shale.

Data from various Mesozoic geological formations showed Mo enrichment was not positively correlated with pyrite abundance but with the amount of sulfur-containing organic matter (Tribovillard et al., 2004). Our study is in agreement with these observations. Mo was also considered to be a useful proxy for original total organic carbon content in the oxygen deficient depositional environment instead of the organic carbon/pyritic sulfur ratios in normal oxic marine shales (Wilde et al., 2004). In modern

euxinic sediments of the Cariaco Basin, a high correlation between total organic carbon (TOC) content and Mo/Al ratio was also observed (Lyons et al., 2003). The close correlation between organic carbon and Mo/Al ratios implies that biological activity may be involved in Mo deposition in black shale. However, the mechanism of Mo sequestered by organic matter is not fully understood. The conservative molybdate (MoO_4^{2-}) begins to convert to the more reactive thiomolybdate (MoS_4^{2-}) through several intermediate products in the presence of H_2S, for example, $MoO_xS_{(4-x)}^{2-}$ (Helz et al, 1996; Erikson and Helz, 2000). The subsequent sequestration of Mo may be involved with sulfur rich organic matter and/or iron rich particles (Helz et al, 1996; Tribovillard et al, 2004). The availability of dissolved sulfide is critical in Mo sequestration; however, the role of organic matter in this process is unclear. Organic matter may simply drive the system to generate hydrogen sulfide, or, in addition to that, also provide a substrate for Mo scavenging (Wilde et al, 2004; Lyons et al., 2003). Iron may play a complimentary role in Mo capture together with organic matter, in which iron sulfides may act as a trap for Mo and form Mo–Fe–S clusters on the iron particle surface. However, in our study, no strong positive relation was recognized between pyritic sulfur and Mo/Al and no correlation was observed between AVS and Mo/Al. This may suggest that Mo was more likely to be fixed with organic matter, but not the pyrite in the Newark Basin Lockatong formation black shale. We are unable to tell how Mo was associated with organic matter at the molecular level and this prevents us from interpreting the mechanism of Mo deposition in the black shale.

Many chemical and biological processes are involved in the accumulation of trace elements in depositional environments. Some of these processes as they may have influenced the accumulation of As and Mo in the Newark Basin are illustrated in Figure 2.10. Interestingly, dissolved sulfide plays a critical role for both depositional processes. In an anoxic lake bottom, sulfate was reduced to sulfide with organic matter as electron donor. Sulfide further reacted with available reactive ferrous iron and generated iron mono-sulfide. Iron mono-sulfide may have been converted to pyrite with continuous supply of hydrogen sulfide. If dissolved arsenic was available, it may have been incorporated into pyrite and form arsenian pyrite. Mo, on the other hand, may have clustered with iron sulfide forming iron-molybdenum-sulfur clusters and deposited . However, in the present study, the correlation between molybdenum and pyritic S as well as AVS in the black shale was not observed, thus, this may not likely be the pathway for Mo deposition in this case. On the other hand, sulfide may react with organic matter and generate sulfurized organic matter. In this case, sufurized organic matter may have complexed with Mo and deposited , a more likely scenario for the Newark Basin .

The release of As and Mo into groundwater from sedimentary rocks

The Passaic formation wells in Newark Basin were analyzed for their aqueous chemical composition and the arsenic concentration was strongly and positively correlated to Mo except for two outliers ($y=0.552x-2.28$, $R^2=0.85$) (Fig. 2.11). Passaic and Lockatong formation shales both belong to the Upper Triassic period with the

Passaic on top of the Lockatong. In contrast to the lithological composition of the Lockatong formation, the Passaic formation is mostly composed of red mudstone, siltstone, sandstone and conglomerate with lesser gray and black shale. A positive correlation between arsenic and molybdenum in Lockatong formation black shale was observed except for three points representing extremely high Mo concentrations (Fig. 2.9). In contrast, red shale has much lower abundance of arsenic and molybdenum compared to black shale and no correlations were found between the two from Lockatong Formation red shale elemental analysis. The dissolved arsenic and molybdenum in red shale groundwater may come from desorption or dissolution of solid phases. However, whether the "ultimate" source of trace elements are from the local red shale or distant black shale cannot be determined provided the datasets in present study and more research needs to be done for the attribution.

2.4 Conclusion

The quantification of sulfur species in black shale can help to determine the abundance of pyrite in sedimentary rocks and together with the analysis of trace metals, the association between important trace elements and the solid phases can then be deduced. The original solid phase hosting of these trace metals may affect their mobilization to the aqueous phase and this may further impact the local environment.

In the present study, we determined that pyrite was a very important component of the total sulfur (more than 50%) in Lockatong formation black shale. The sulfur speciation of black shale indicated a tight correlation between total sulfur and pyritic

sulfur and an inverse relationship between pyritic sulfur and acid volatile sulfur. Inverse relationships between Th/U and pyritic S and positive correlations between Th/U and acid volatile S at different depths in the Lockatong formation indicated that the oxygenation condition was one of the factors controlling the deposition of sulfur species in the sediments. Moreover, trace metal enrichment factors were analyzed and arsenic and molybdenum were two highly enriched elements in the black shale. Further analysis showed that the arsenic content was closely linked to pyrite and molybdenum was associated with organic matter. The As and Mo depositional mechanisms, both of which were mediated by dissolved sulfide, determined their concentrations and host phases in the black shale. The concentration of arsenic was positively correlated to that of molybdenum in a red shale groundwater well in the Newark Basin (Passaic formation) The ultimate source of these trace elements are of great interest and needs to be investigated in future research.

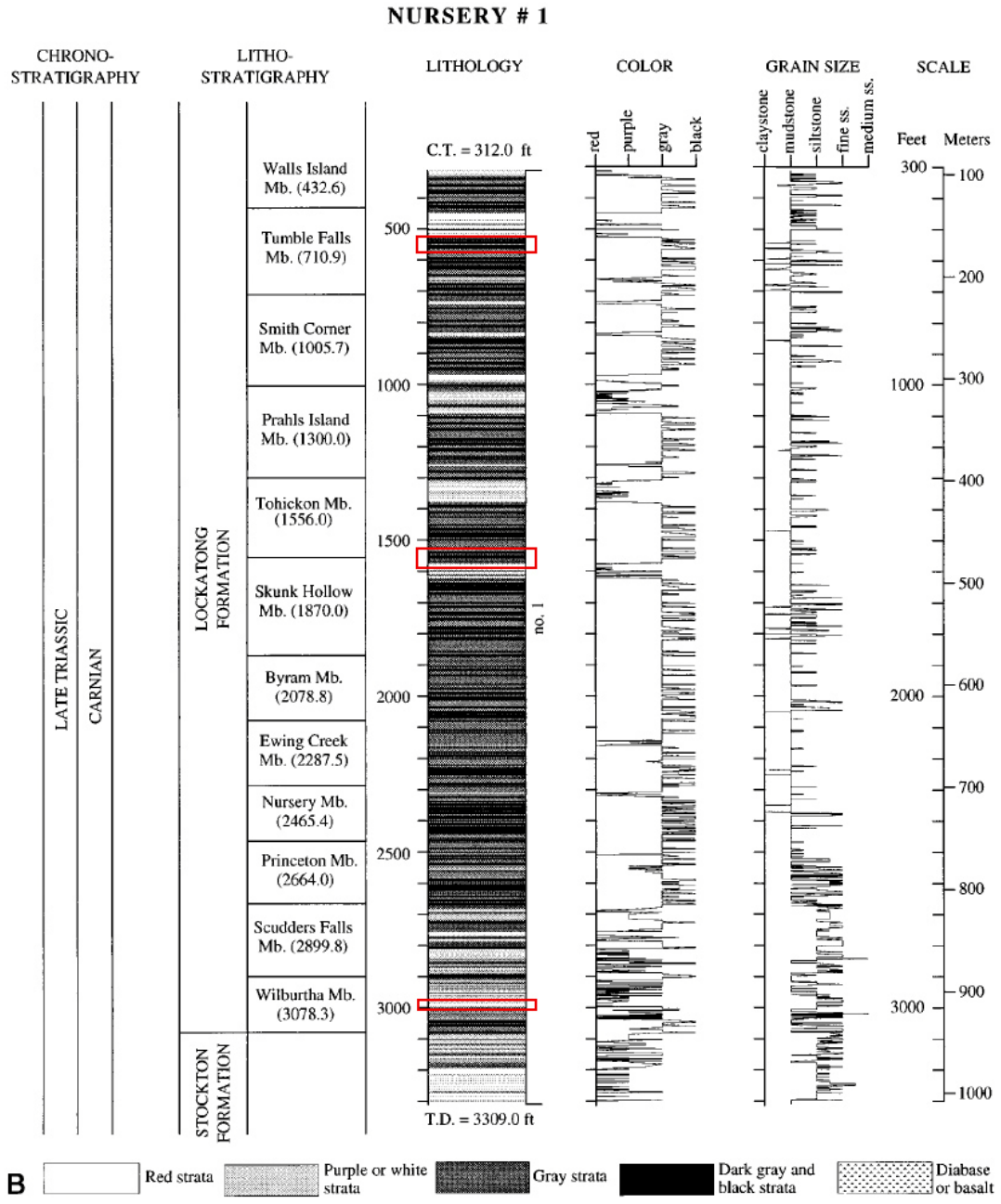

Figure 2.1. Lithology logs from the cores from the Newark Basin Coring Project: the Nursery. Red frames indicated the part of samples were taken and analyzed for abundance of various chemical elements.

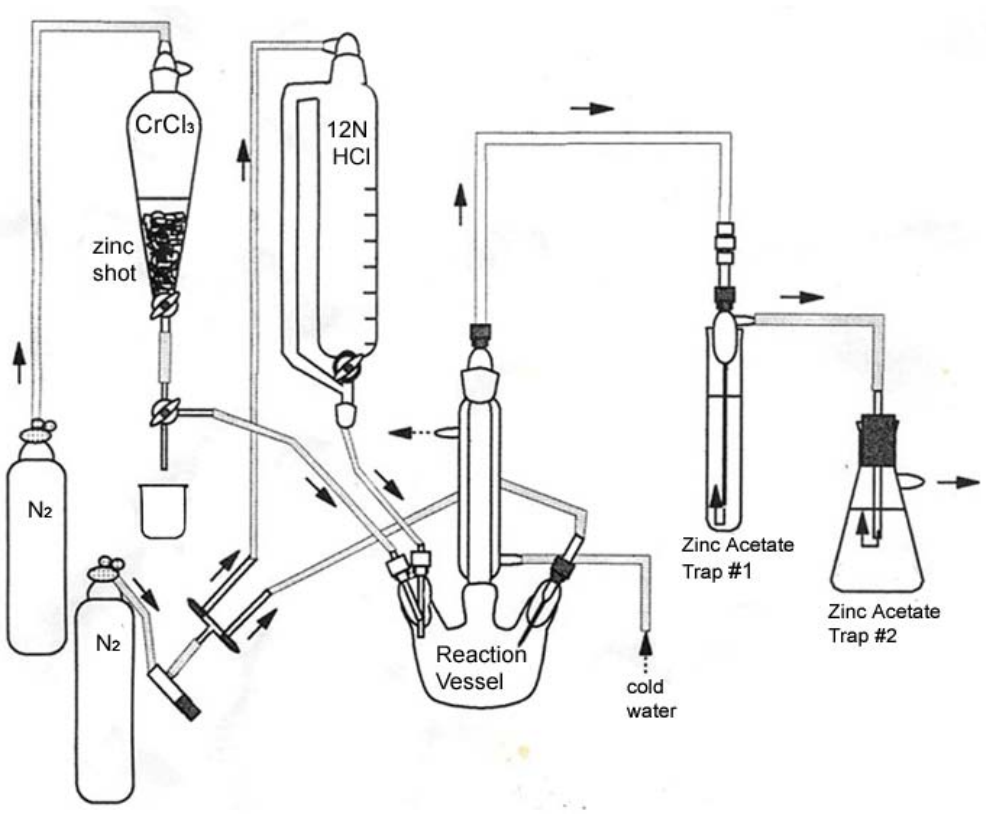

Figure 2.2. The apparatus setting of pyritic sulfur and acid volatile sulfur, after Elswick's lab in University of Cincinnati (Bonilla, 2005)

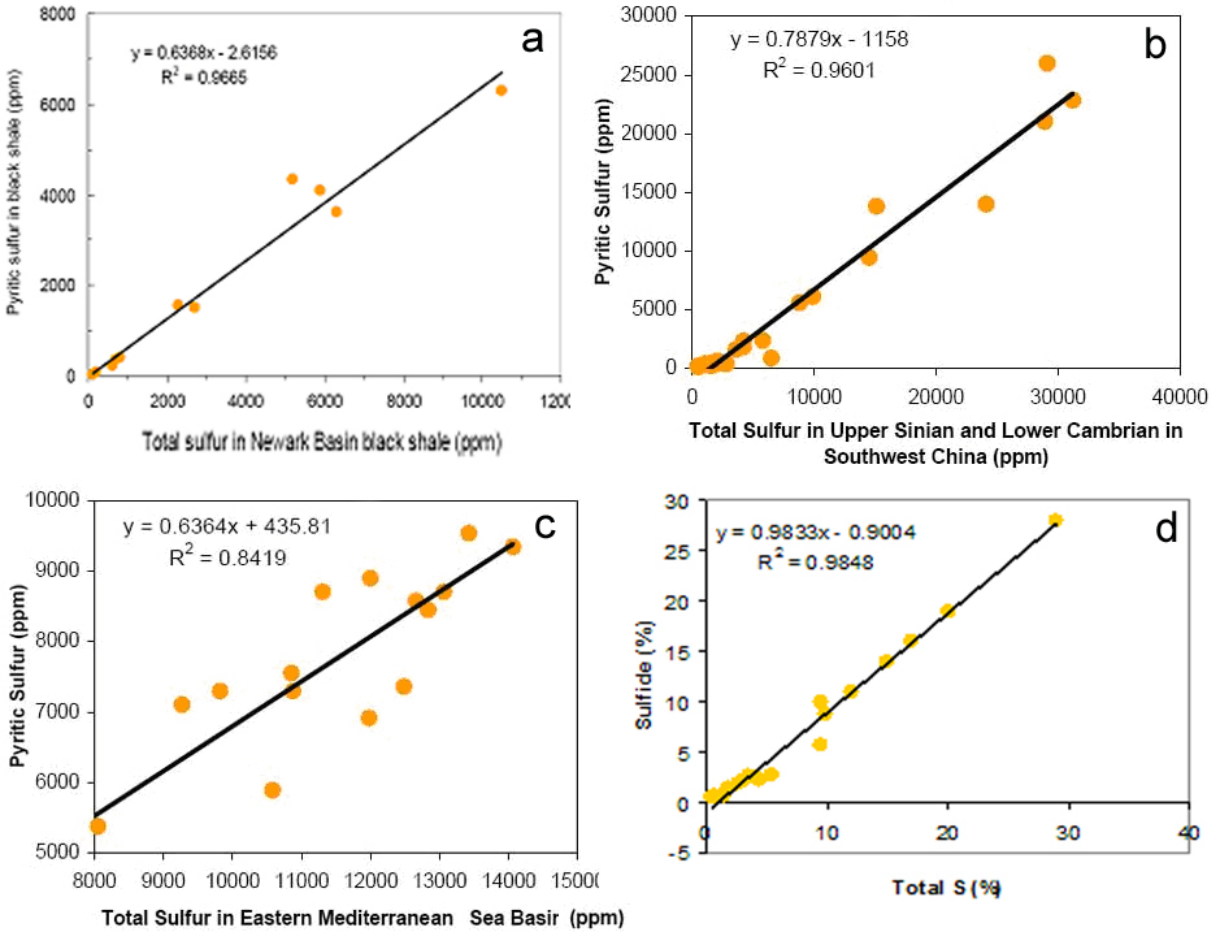

Figure 2.3. Relationship between pyritic sulfur and total sulfur in

a) Late Triassic Newark Basin (Lockatong formation) black shale

b) Pyritic in southwest China sedimentary rock

c) Mediterranean Sea basin

d) New Albany black shale in Kentucky

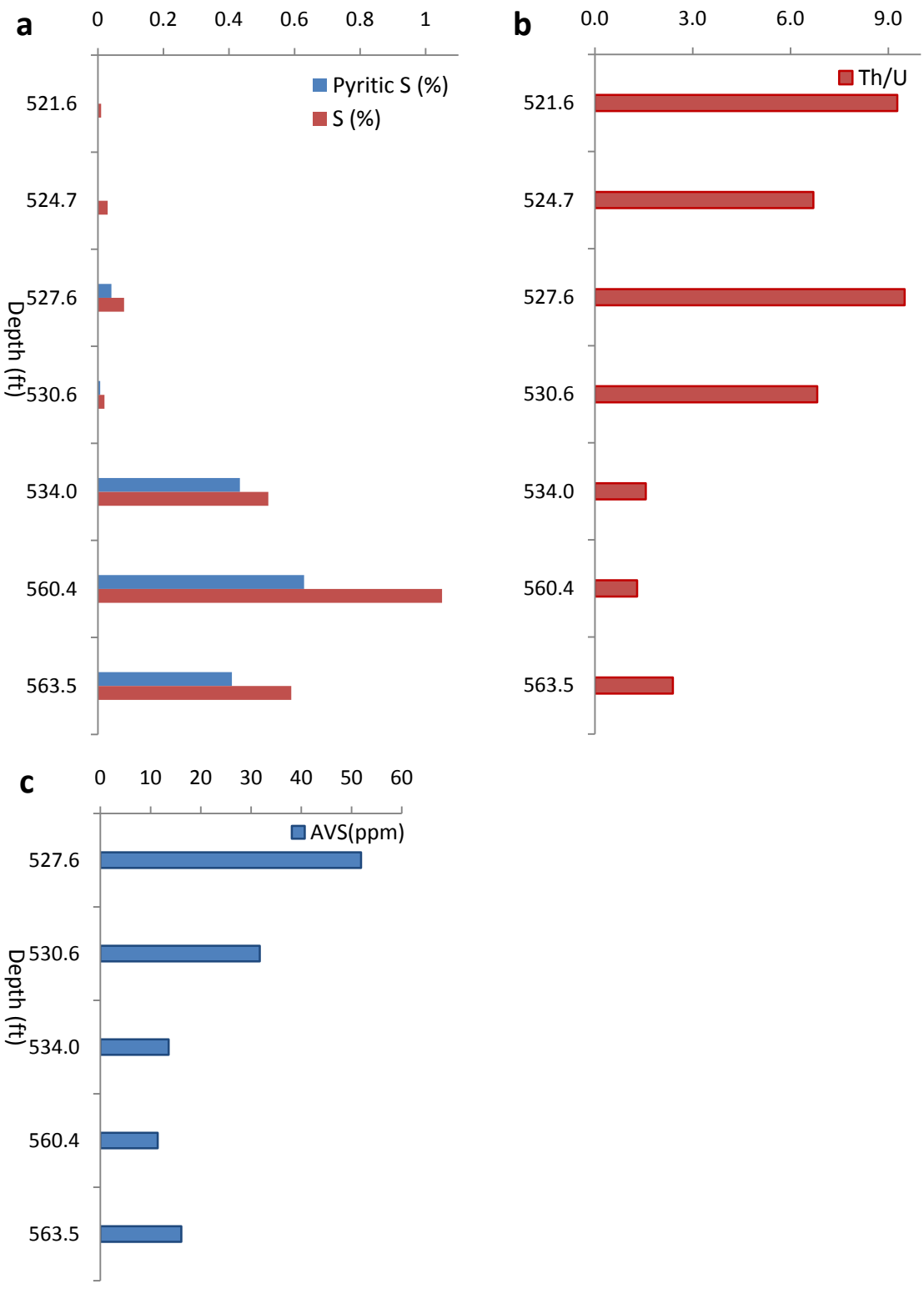
a
0
0.2
0.4
0.6
0.8
1
Pyritic S (%)
S (%)
Depth (ft)
521.6
524.7
527.6
530.6
534.0
560.4
563.5
b
0.0
3.0
6.0
9.0
Th/U
521.6
524.7
527.6
530.6
534.0
560.4
563.5
c
0
10
20
30
40
50
60
AVS(ppm)
Depth (ft)
527.6
530.6
534.0
560.4
563.5

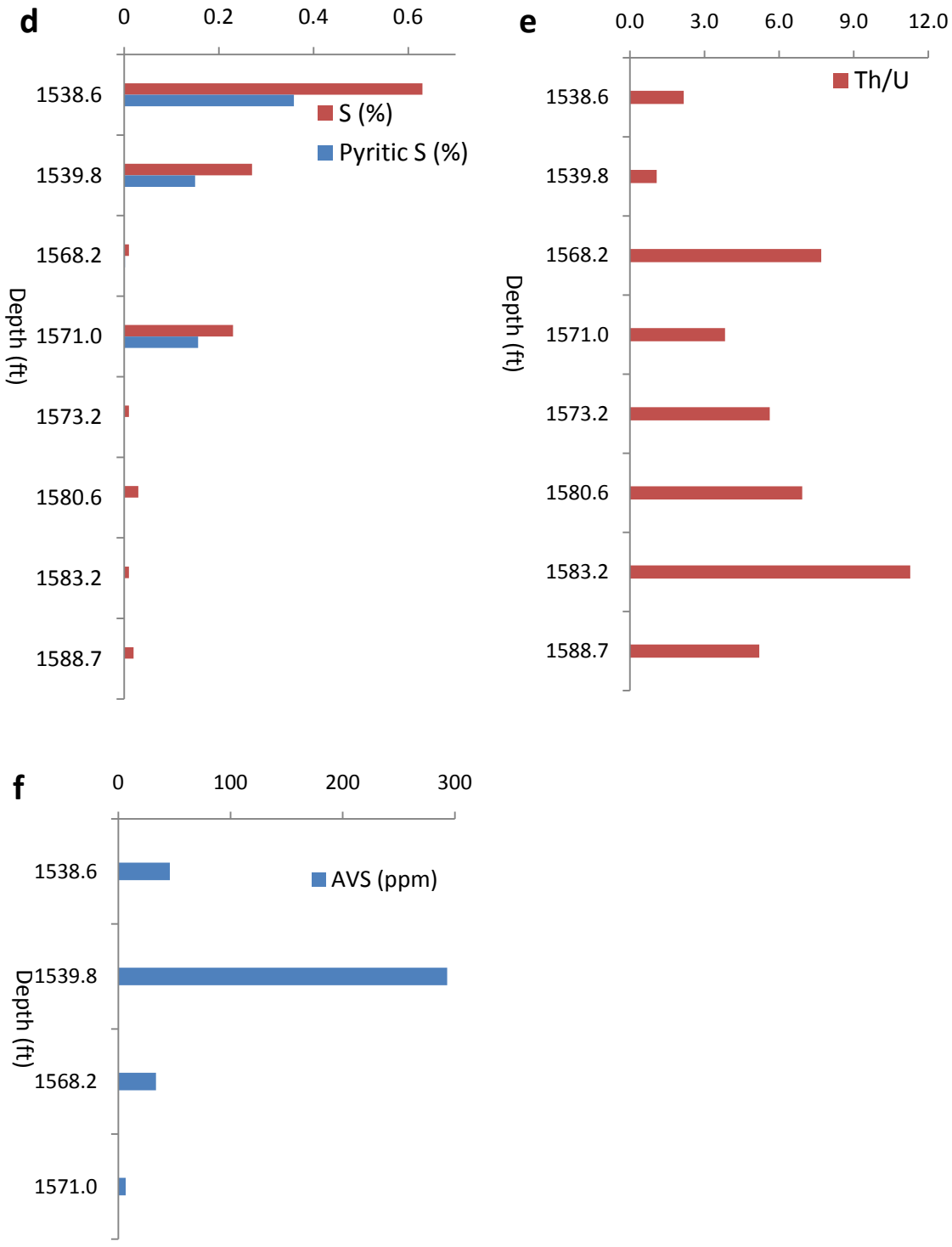

Figure 2.4. The depth profile of pyritic sulfur/total sulfur, AVS and Th/U in Newark Basin Lockatong formation. a) ,b), c) are at depth around 550 ft; d), e), f) are at depth around 1500 ft.

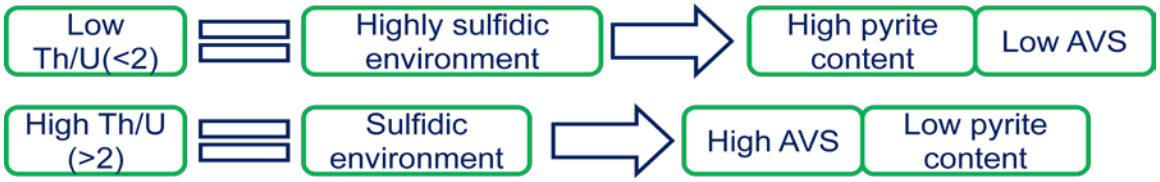

Figure 2.5. The relationship between redox index Th/U and pyrite and AVS amount in shale

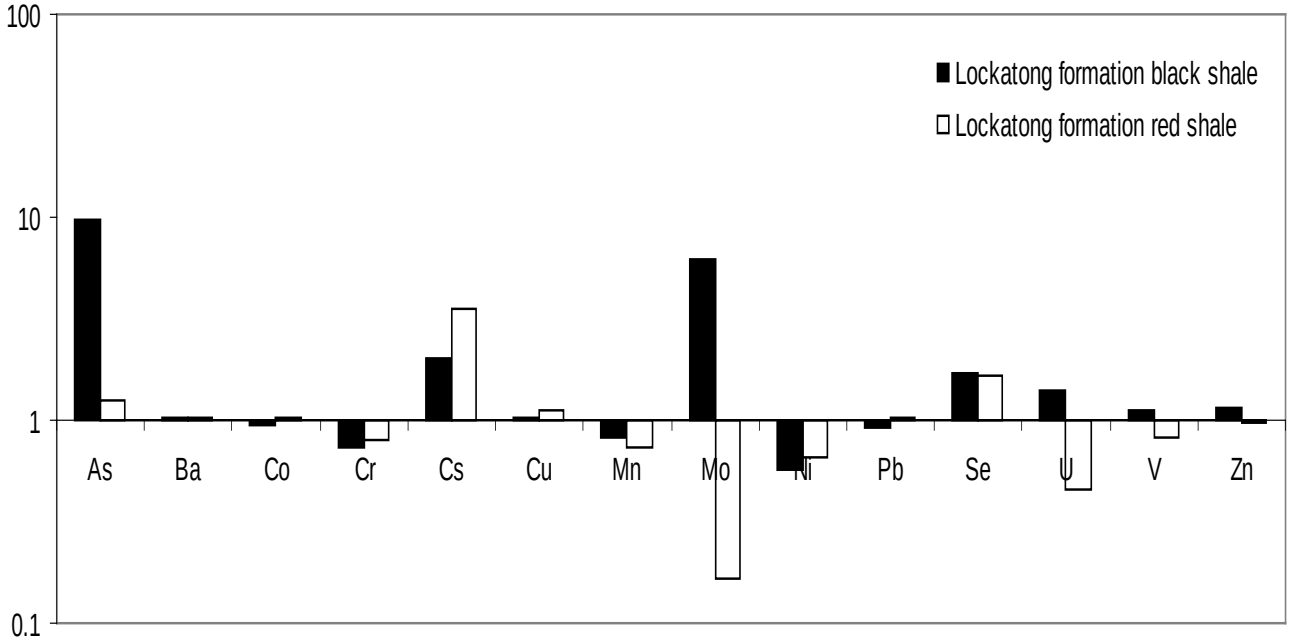

Fig 2.6. Enrichment factors for trace elements in red and black shale of Newark Basin Lockatong formation.

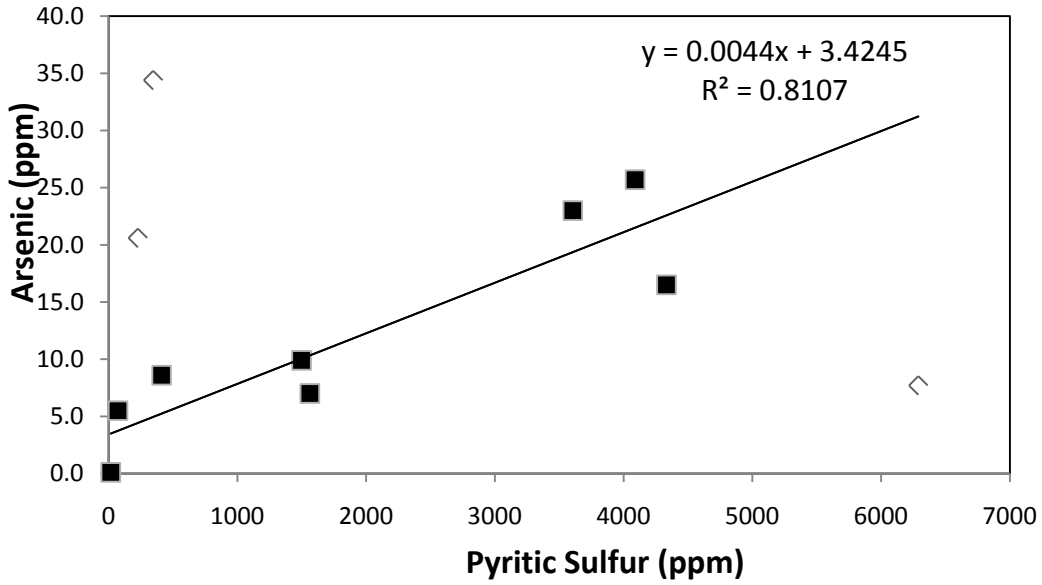

Figure 2.7. Arsenic versus pyritic sulfur in Lockatong formation black shale. Correlation is for all points except three outliers (open symbols).

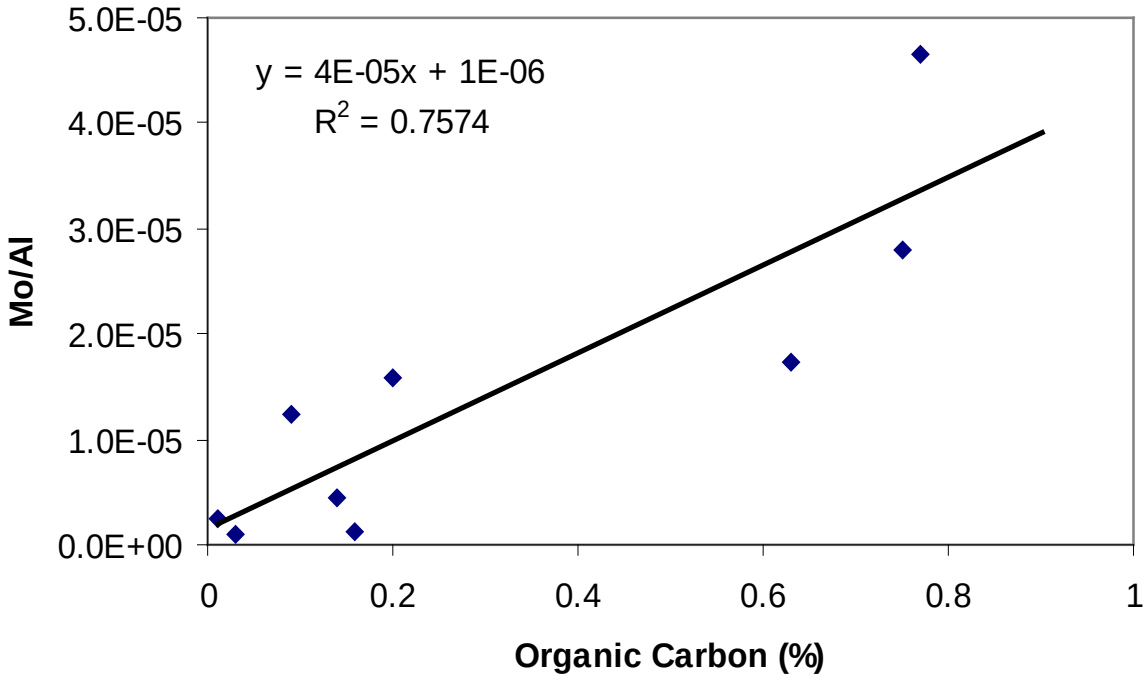

Fig 2.8. Mo normalized by Al versus organic carbon content in Lockatong formation black shale.

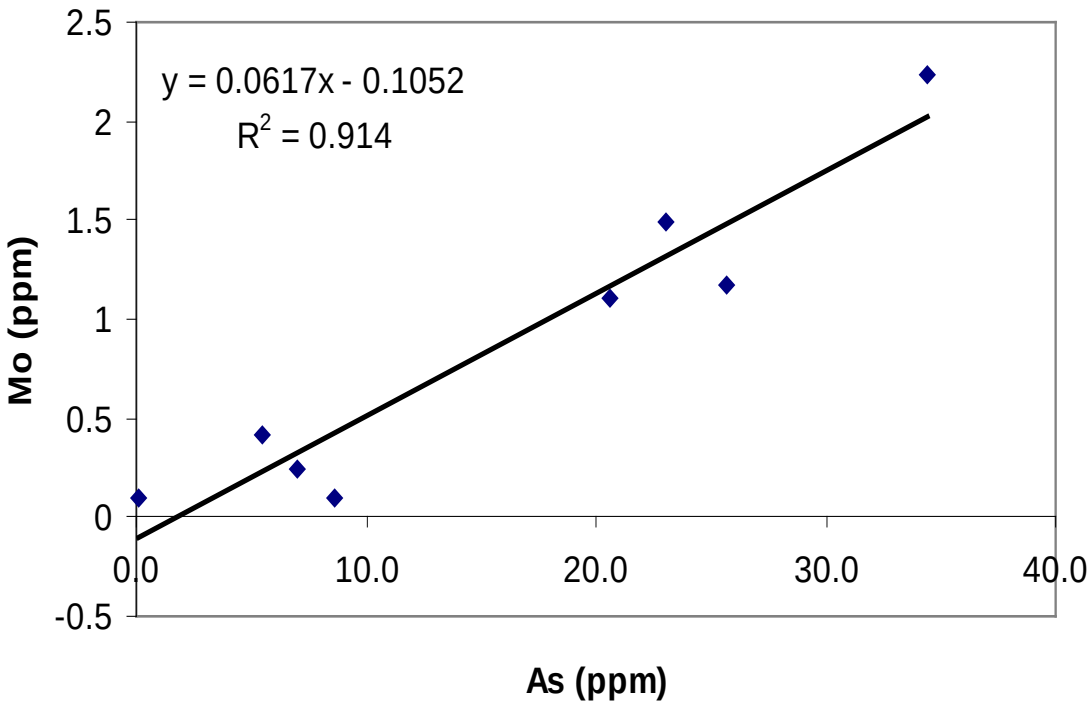

Fig 2.9. As versus Mo concentrations in Lockatong formation black shale.

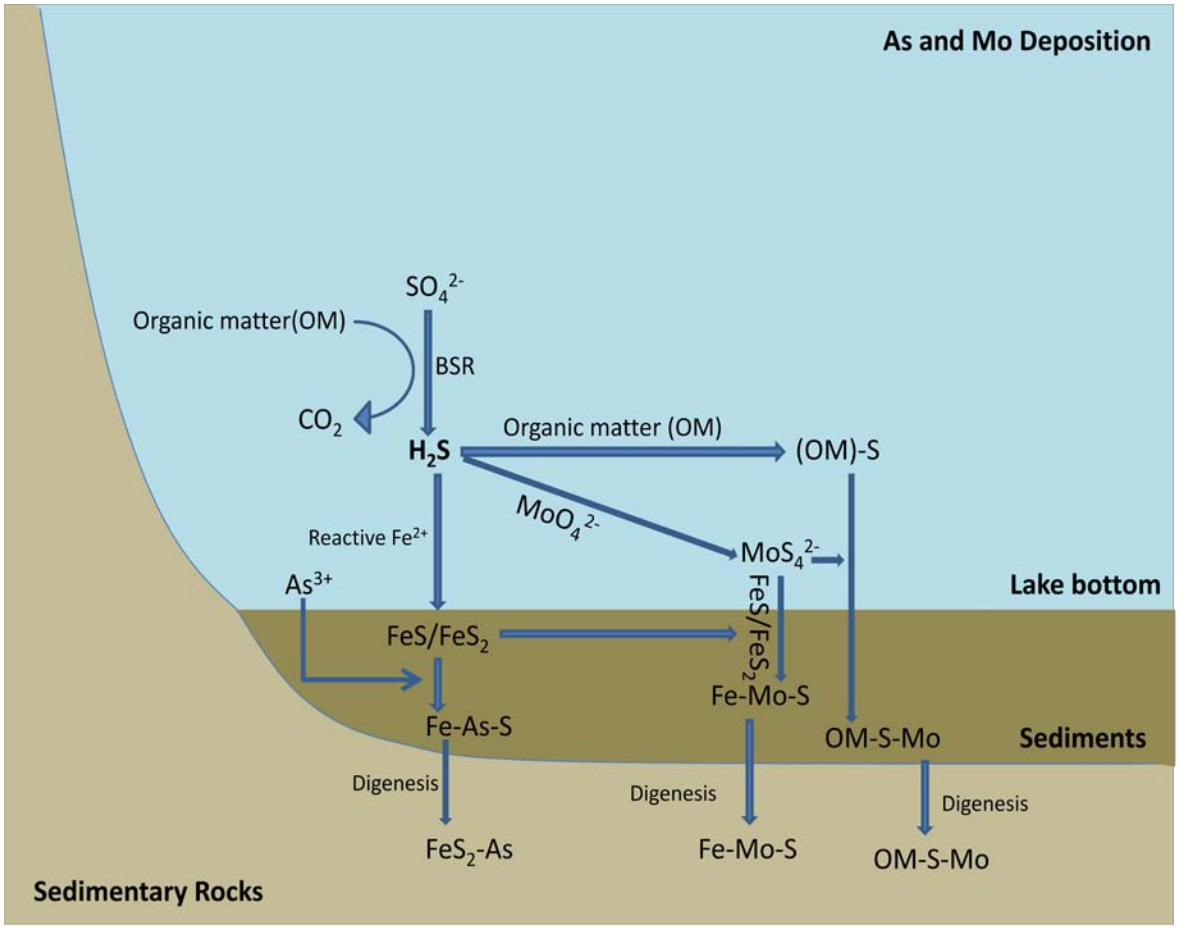

Fig. 2.10. The hypothesized As and Mo depositional mechanisms in the anoxic lake bottom of Newark Basin.

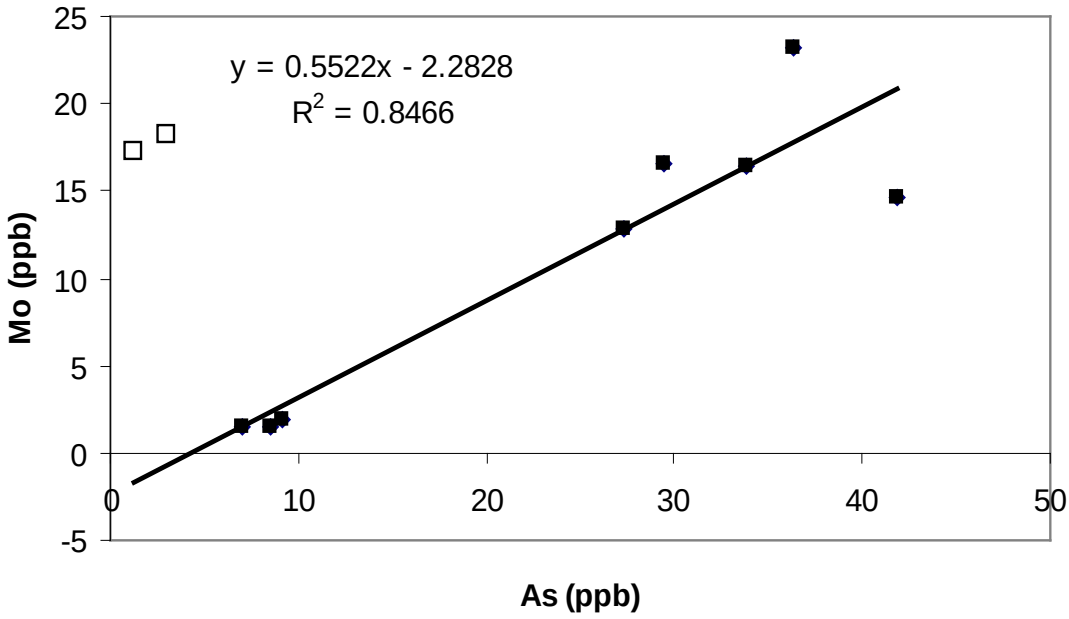

Fig 2.11. Mo versus As in Passaic formation groundwater, data from Serfes PhD dissertation (Serfes, 2005)

References

Ahmed K. M., Bhattacharya P., Hasan M. A., Akhter S. H., Alam S. M. M., Bhuyian M. A. H., Imam M. B., Khan A. A., and Sracek O. (2004) Arsenic enrichment in groundwater of the alluvial aquifers in Bangladesh: an overview. *Applied Geochemistry* **19**(2), 181-200.

Arndt, S., H. J. Brumsack, et al. (2006). Cretaceous black shales as active bioreactors: A biogeochemical model for the deep biosphere encountered during ODP Leg 207 (Demerara Rise). *Geochimica Et Cosmochimica Acta* **70**(2): 408-425.

Bartlett J. K. and Skoog D. A. (1954) Colorimetric Determination of Elemental Sulfur in Hydrocarbons. *Anal. Chem.* **26**(6), 1008-1011.

Benning L. G., Wilkin R. T., and Barnes H. L. (2000) Reaction pathways in the Fe-S system below 100[degree sign]C. *Chemical Geology* **167**(1-2), 25-51.

Berner R. A. (1970) Sedimentary pyrite formation. *Am J Sci* **268**(1), 1-23.

Berner R. A. (1999) Atmospheric oxygen over Phanerozoic time. *Proc Natl Acad Sci U S A.* **96**(20), 10955-10957.

Berner R. A. and Canfield D. E. (1989) A new model for atmospheric oxygen over Phanerozoic time. *Am J Sci* **289**(4), 333-361.

Berner R. A. and Raiswell R. (1984) C/S method for distinguishing freshwater from marine sedimentary rocks. *Geology* **12**(6), 365-368.

Bonilla, A (2005) Geochemistry of Arsenic and Sulfur in Southwest Ohio: Bedrock, Outwash Deposits and Groundwater, University of Cincinnati, Master thesis.

Bostick B. C. and Fendorf S. (2003) Arsenite sorption on troilite (FeS) and pyrite (FeS2). *Geochimica et Cosmochimica Acta* **67**(5), 909-921.

Burton E. D., Bush R. T., and Sullivan L. A. (2006) Fractionation and extractability of sulfur, iron and trace elements in sulfidic sediments. *Chemosphere* **64**(8), 1421-1428.

Canfield D. E., Raiswell R., Westrich J. T., Reaves C. M., and Berner R. A. (1986) The use of chromium reduction in the analysis of reduced inorganic sulfur in sediments and shales. *Chemical Geology* **54**, 149-155.

Canfield D. E., Thamdrup B., and Fleischer S. (1998) Isotope fractionation and sulfur metabolism by pure and enrichment cultures of elemental sulfur-disproportionating bacteria. *Limnology and Oceanography* **43**(2), 253-264.

Cline J. D. (1969) Spectrophotometric Determination of Hydrogen Sulfide in Natural Waters. *Limnology and Oceanography* **14**(3), 454-458.

Crusius J., Calvert S., Pedersen T., and Sage D. (1996) Rhenium and molybdenum enrichments in sediments as indicators of oxic, suboxic and sulfidic conditions of deposition. *Earth and Planetary Science Letters* **145**(1-4), 65-78.

Dean W. E., Gardner J. V., and Piper D. Z. (1997) Inorganic geochemical indicators of glacial-interglacial changes in productivity and anoxia on the California continental margin. *Geochimica et Cosmochimica Acta* **61**(21), 4507-4518.

Donald R. and Southam G. (1999) Low temperature anaerobic bacterial diagenesis of ferrous monosulfide to pyrite. *Geochimica Et Cosmochimica Acta* **63**(13-14), 2019-2023.

Erickson B.E. and Helz G.R. 2000, Molybdenum (VI) Speciation in Sulfidic Waters; Stability and Lability of Thiomolybdates, *Geochimica et Cosmochimica Acta* , **64**, 1149-1158.

Goldhaber M. B. (2003) Sulfur-rich Sediments. In *Treatise on Geochemistry*, Vol. 7 (ed. H. D. Holland and K. K. Turekian), pp. 257-288. Elsevier.

Grosbois C., Schafer J., Bril H., Blanc G., and Bossy A. (2009) Deconvolution of trace element (As, Cr, Mo, Th, U) sources and pathways to surface waters of a gold mining-influenced watershed. *Science of The Total Environment* **407**(6), 2063-2076.

Guo Q., Shields G. A., Liu C., Strauss H., Zhu M., Pi D., Goldberg T., and Yang X. (2007) Trace element chemostratigraphy of two Ediacaran-Cambrian successions in South China: Implications for organosedimentary metal enrichment and silicification in the Early Cambrian. *Palaeogeography, Palaeoclimatology, Palaeoecology* **254**(1-2), 194-216.

Helz, G.R., Miller, C.V., Charnock, J.M., Mosselmans, J.F.W., Parttrick, R.A.D., Garner, C.D. and Vaughan, D.J. 1996. Mechanism of molybdenum removal from the sea and its concentration in black shales: EXAFS evidence. *Geochimica et Cosmochimica Acta*, **60**, 3631-3642.

Henneke E., Luther G. W., De Lange G. J., and Hoefs J. (1997) Sulphur speciation in anoxic hypersaline sediments from the eastern Mediterranean Sea. *Geochimica et Cosmochimica Acta* **61**(2), 307-321.

Holser W. T., Schidlowski M., Mackenzie F. T., and Maynard J. B. (1988) Geochemical cycles of carbon and sulfur. In *Chemical Cycles in the Evolution of the Earth* (ed. C. B. Gregor, R. M. Garrels, F. T. Mackenzie, and J. B. Maynard), pp. 105–173. Wiley.

Huertadiaz M. A. and Morse J. W. (1992) Pyritization of Trace-Metals in Anoxic Marine-Sediments. *Geochimica Et Cosmochimica Acta* **56**(7), 2681-2702.

Hunger S. and Benning L. G. (2007) Greigite: a true intermediate on the polysulfide pathway to pyrite. *Geochem Trans* **8**, 1.

Jones B. and Manning D. A. C. (1994) Comparison of Geochemical Indexes Used for the Interpretation of Palaeoredox Conditions in Ancient Mudstones. *Chemical Geology* **111**(1-4), 111-129.

Lavergren U., Astrom M. E., Bergback B., and Holmstrom H. (2009) Mobility of trace elements in black shale assessed by leaching tests and sequential chemical extraction. *Geochemistry-Exploration Environment Analysis* **9**, 71-79.

Lei, J., R. Li, et al. (2001). "Characteristics of sulfur species and their implications in Lower Cambrian black shales from southern margin of Yangtze Platform." Science in China Series D: Earth Sciences **44**(5): 455-467.

Leventhal J. S. (1995) Carbon-sulfur plots to show diagenetic and epigenetic sulfidation in sediments. *Geochimica et Cosmochimica Acta* **59**(6), 1207-1211.

Lowers H. A., Breit G. N., Foster A. L., Whitney J., Yount J., Uddin M. N., and Muneem A. A. (2007) Arsenic incorporation into authigenic pyrite, Bengal Basin sediment, Bangladesh. *Geochimica et Cosmochimica Acta* **71**(11), 2699-2717.

Lyons T. W., Werne J. P., Hollander D. J., and Murray R. W. (2003) Contrasting sulfur geochemistry and Fe/Al and Mo/Al ratios across the last oxic-to-anoxic transition in the Cariaco Basin, Venezuela. *Chemical Geology* **195**(1-4), 131-157.

McLennan S. M. (2001) Relationships between the trace element composition of sedimentary rocks and upper continental crust. *Geochem. Geophys. Geosyst.* **2**.

Morse J. W. and Cornwell J. C. (1987) Analysis and Distribution of Iron Sulfide Minerals in Recent Anoxic Marine-Sediments. *Marine Chemistry* **22**(1), 55-69.

Morse J. W., Millero F. J., Cornwell J. C., and Rickard D. (1987) The Chemistry of the Hydrogen-Sulfide and Iron Sulfide Systems in Natural-Waters. *Earth-Science Reviews* **24**(1), 1-42.

Morse J. W. (2002) Sedimentary Geochemistry of the Carbonate and Sulphide Systems and their Potential Influence on Toxic Metal Bioavailability In *Chemistry of marine water and sediments* (ed. A. Gianguzza, E. Pelizzetti, and S. Sammartano), pp. 184-185. Springer.

Muller A. (2002) Pyritization of iron and trace metals in anoxic fjord sediments (Nordasvannet fjord, western Norway). *Applied Geochemistry* **17**(7), 923-933.

Ogendi G. M., Hannigan R. E., and Farris J. L. (2007) Toxicity of metal-enriched black shale-draining surface waters to Ceriodaphnia dubia, and Pimephales promelas. *Journal of Agricultural, Food, and Environmental Sciences* **1**(1), 1-15.

Peng B., Piestrzynski A., Pieczonka J., Xiao M., Wang Y. Z., Xie S. R., Tang X. Y., Yu C. X., and Song Z. (2007) Mineralogical and geochemical constraints on environmental impacts from waste rock at Taojiang Mn-ore deposit, central Hunan, China. *Environmental Geology* **52**(7), 1277-1296.

Peng B., Song Z., Tu X., Xiao M., Wu F., and Lv H. (2004) Release of heavy metals during weathering of the Lower Cambrian Black Shales in western Hunan, China. *Environmental Geology* **45**, 1137-1147.

Peters S. C. and Burkert L. (2008) The occurrence and geochemistry of arsenic in groundwaters of the Newark basin of Pennsylvania. *Applied Geochemistry* **23**(1), 85-98.

Petsch S. T. (2003) Ch.11: The Global Oxygen Cycle. In *Treatise on Geochemistry* Vol. 8 (ed. H. D. Holland and K. K. Turekian), pp. 515-556. Elsevier Science.

Popa R. and Kinkle B. K. (2000) Discrimination among iron sulfide species formed in microbial cultures. *Journal of Microbiological Methods* **42**(2), 167-174.

Pratt L. M. and Davis C. L. (1992) Intertwined fates of metals, sulfur and organic carbon in black shales. In *Geochemistry of organic matter in sediments and sedimentary rocks*, Vol. 27 (ed. L. M. Pratt, J. B. Comer, and S. C. Brassell), pp. 1-27.

Raiswell R. and Berner R. A. (1986) Pyrite and organic matter in Phanerozoic normal marine shales. *Geochimica et Cosmochimica Acta* **50**(9), 1967-1976.

Rickard D. and Luther G. W. (1997) Kinetics of pyrite formation by the H2S oxidation of iron(II) monosulfide in aqueous solutions between 25 and 125 degrees C: The mechanism. *Geochimica Et Cosmochimica Acta* **61**(1), 135-147.

Rickard D. and Morse J. W. (2005) Acid volatile sulfide (AVS). *Marine Chemistry* **97**(3-4), 141-197.

Rimmer S. M. (2004) Geochemical paleoredox indicators in Devonian-Mississippian black shales, Central Appalachian Basin (USA). *Chemical Geology* **206**(3-4), 373-391.

Savage, K. S., T. N. Tinglea, et al. (2000). Arsenic speciation in pyrite and secondary weathering phases, Mother Lode Gold District, Tuolumne County,California. *Applied Geochemistry* **15**: 1219-1244.

Scholz F. and Neumann T. (2007) Trace element diagenesis in pyrite-rich sediments of the Achterwasser lagoon, SW Baltic Sea. *Marine Chemistry* **107**(4), 516-532.

Schoonen M. A. A. (2004) Mechanisms of sedimentary pyrite formation. In *Sulfur Biogeochemistry: Past and Present* (ed. J. P. Amend, K. J. Edwards, and T. W. Lyons). Geological Society of America.

Schoonen M. A. A. and Barnes H. L. (1991a) Reactions Forming Pyrite and Marcasite from Solution .1. Nucleation of Fes2 Below 100-Degrees-C. *Geochimica Et Cosmochimica Acta* **55**(6), 1495-1504.

Schoonen M. A. A. and Barnes H. L. (1991b) Reactions Forming Pyrite and Marcasite from Solution .2. Via Fes Precursors Below 100-Degrees-C. *Geochimica Et Cosmochimica Acta* **55**(6), 1505-1514.

Serfes M. E. (2005) Arsenic Occurrence, Sources, Mobilization, Transport and Prediction in the Major Bedrock Aquifers of the Newark Basin, Rutgers University, PhD dissertation.

Taylor S. R. and Mclenna S. M. (1985) *The Continental Crust: Its Composition and Evolution.* Blackwell.

Thornburg, K. and N. Sahai (2004). Arsenic Occurrence, Mobility, and Retardation in Sandstone and Dolomite Formations of the Fox River Valley, Eastern Wisconsin. *Environ. Sci. Technol.* **38**(19): 5087-5094.

Tribovillard N., Riboulleau A., Lyons T., and Baudin F. (2004) Enhanced trapping of molybdenum by sulfurized marine organic matter of marine origin in Mesozoic limestones and shales. *Chemical Geology* **213**(4), 385-401.

Tuttle M. L., Breit G. N., and Goldhaber M. B. (2003) Geochemical Data from New Albany Shale, Kentucky: A Study in Metal Mobility During Weathering of Black Shales. USGS.

Tuttle M. L. W., Breit G. N., and Goldhaber M. B. Weathering of the new albany shale, kentucky: II. redistribution of minor and trace elements. *Applied Geochemistry*. **24** (8), 1549-1564

Wilde P., Lyons T. W., and Quinby-Hunt M. S. (2004) Organic carbon proxies in black shales: molybdenum. *Chemical Geology* **206**(3-4), 167-176.

Wilkin R. T. and Barnes H. L. (1996) Pyrite formation by reactions of iron monosulfides with dissolved inorganic and organic sulfur species. *Geochimica Et Cosmochimica Acta* **60**(21), 4167-4179.

Wu C., Zeng F., Lei J., and Zhao R. (1999) Referential significance of sulfur isotopes and separation of S species in black shales of Southwest China. *Chinese Science Bulletin* **44**(17), 1612-1616.

Yin H. B., Fan C. X., Ding S. M., Zhang L., and Zhong J. C. (2008) Geochemistry of iron, sulfur and related heavy metals in metal-polluted Taihu Lake sediments. *Pedosphere* **18**(5), 564-573.

Zhu W., Young L. Y., Yee N., Serfes M., Rhine E. D., and Reinfelder J. R. (2008) Sulfide-driven arsenic mobilization from arsenopyrite and black shale pyrite. *Geochimica et Cosmochimica Acta* **72**(21), 5243-5250.

CHAPTER 3

SULFIDE-DRIVEN ARSENIC MOBILIZATION FROM ARSENOPYRITE AND BLACK SHALE PYRITE

(Published in GCA, Zhu et al, 2008)

Abstract

We examined the hypothesis that sulfide drives arsenic mobilization from pyritic black shale by a sulfide-arsenide exchange and oxidation reaction in which sulfide replaces arsenic in arsenopyrite forming pyrite, and arsenide (As(-1)) is concurrently oxidized to soluble arsenite (As^{3+}). This hypothesis was tested in a series of sulfide-arsenide exchange experiments with arsenopyrite (FeAsS), homogenized black shale from the Newark Basin (Lockatong formation), and pyrite isolated from Newark Basin black shale incubated under oxic (21% O_2), hypoxic (2% O_2, 98% N_2), and anoxic (5% H_2, 95% N_2) conditions. The oxidation state of arsenic in Newark Basin black shale pyrite was determined using X-ray absorption-near edge structure spectroscopy (XANES). Incubation results show that sulfide (1 mM initial concentration) increases arsenic mobilization to the dissolved phase from all three solids under oxic and hypoxic, but not anoxic conditions. Indeed under oxic and hypoxic conditions, the presence of sulfide resulted in the mobilization in 48 h of 13 to 16 times more arsenic from arsenopyrite and 6 to 11 times more arsenic from isolated black shale pyrite than in sulfide-free controls. XANES results show that arsenic in Newark Basin black shale pyrite has the same oxidation state as that in FeAsS (-1) and thus extend the sulfide-arsenide exchange mechanism of arsenic mobilization to sedimentary rock, black shale

pyrite. Biologically active incubations of whole black shale and its resident microorganisms under sulfate reducing conditions resulted in seven-fold higher mobilization of soluble arsenic than sterile controls. Taken together, our results indicate that sulfide-driven arsenic mobilization would be most important under conditions of redox disequilibrium, such as when sulfate-reducing bacteria release sulfide into oxic groundwater, and that microbial sulfide production is expected to enhance arsenic mobilization in sedimentary rock aquifers with major pyrite-bearing, black shale formations.

3. 1 Introduction

Arsenic has long been recognized as a toxic metalloid (National Research Council: Subcommittee to Update the 1999 Arsenic in Drinking Water Report, 2001). The U.S. EPA lowered the arsenic standard for drinking water to 10 μg L^{-1} in 2001 (EPA, 2001), yet more than ten million people in the U.S. are exposed to potentially harmful levels (>10 μg L^{-1}) of arsenic in their drinking water (Ryker, 2003; Welch et al., 2000).

The release of arsenic into the environment can occur as a result of human activities related to agriculture (Reedy et al., 2007; Signes-Pastor et al., 2007) and mining (Bayard et al., 2006; Carrillo and Drever, 1998; Kwong et al., 2007; Lazareva and Pichler, 2007). However, arsenic is also a component of subsurface rocks in many aquifers and is released through natural weathering processes (Ahmed et al., 2004; Dowling et al., 2002; Lowers et al., 2007; Polizzotto et al., 2005). Natural sources of arsenic include sulfide minerals (e.g. pyrite, troilite, arsenopyrite, realgar, orpiment) and arsenic adsorbed onto mineral oxides (Smedley and Kinniburgh, 2002). Arsenopyrite (FeAsS) and arsenic-rich pyrites ($FeAs_xS_{2x}$) are commonly found in hydrothermal sulfide deposits and diagenetic sediments with high sulfur and organic matter contents such as black shale (Blanchard et al., 2007; Brown et al., 1999; Farquhar et al., 2002; Kober et al., 2005; Lowers et al., 2007; Paikaray et al., 2005; Wilkin, 2001). Under anoxic conditions and with high (mM) concentrations of arsenic, arsenite partitioned onto pyrite appears to form a surface solid phase of arsenopyrite by substitution for sulfur (Bostick and Fendorf, 2003). Therefore, arsenopyrite may provide a model mineral for the study of arsenic mobilization from pyrite.

During pyrite weathering, associated trace metals and metalloids including As, Cd, and Pb are released to the dissolved phase (Bednar et al., 2002) and such trace elements may in fact accelerate pyrite weathering compared to the pure mineral (Lehner and Savage, 2008; Lehner et al., 2007; Savage et al., 2000). The release of arsenic from arsenopyrite and arsenic-rich pyrite has been examined under oxidizing conditions (Craw et al., 2003; Komnitsas et al., 1995; Nesbitt and Muir, 1998; Nesbitt et al., 1995; Yu et al., 2004) and at the extremely low pH of acid mine drainage (Komnitsas et al., 1995; Yu et al., 2004), but not at neutral pH and under hypoxic or redox disequilibrium conditions where sulfide and oxygen or other oxidants may coexist due to biological activity and groundwater flow.

Sulfide is produced by sulfate reducing anaerobes in groundwater only under anoxic conditions where sulfate is present at concentrations high enough to support its use as a terminal electron acceptor (Roesler et al., 2007; Saunders et al., 2005; Singleton, 1993). Under such conditions, dissolved arsenite and arsenate may react with sulfide to form solid phases (Das et al., 1996; O'Day et al., 2004) or aqueous complexes (Stauder et al., 2005). In addition, soluble arsenite may adsorb onto iron sulfide minerals such as troilite and pyrite (Bostick and Fendorf, 2003; Farquhar et al., 2002; Lowers et al., 2007; Wolthers et al., 2005). The interactions between sulfide and solid phase iron arsenides, however, have not been systematically examined.

Arsenic may be mobilized from arsenopyrite by reaction with sulfide in the presence of oxygen (or another oxidant) through sulfide-arsenide exchange:

$$FeAsS + HS^- + H^+ + 5/4O_{2(aq)} + ½H_2O \rightarrow FeS_2 + As(OH)_{3(aq)} \quad (1)$$

This reaction is thermodynamically very favorable ($\Delta G°'_{298}$ = -510 kJ mol^{-1} at pH 8; see Appendix II for species free energies and in situ concentrations) as are other analogous reactions in which Fe(III) serves as the oxidant in the conversion of arsenide to arsenite. Sulfide-arsenide exchange in arsenopyrite is thought to be important in geothermal systems (Ballantyne and Moore, 1988; Heinrich and Eadington, 1986), but has not been examined at ambient groundwater conditions of low temperature and neutral pH. The oxidation of arsenopyrite by oxygen ($FeAsS + 3/4O_{2(aq)} + 3/2H_2O \rightarrow FeS + As(OH)_{3(aq)}$) occurs in the absence of dissolved sulfide, but it is thermodynamically less favorable ($\Delta G°'_{298}$ = -271 kJ mol^{-1}) than sulfide-arsenide exchange, particularly under hypoxic conditions. The mobilization of arsenic and sulfur from arsenopyrite was recently shown to be enhanced by an autotrophic arsenite oxidizing microorganism (Rhine et al., 2008), but whether this mobilization involves direct oxidation of mineral arsenide or results from a shift in the redox poise of dissolved arsenic remains to be determined.

Since arsenic has been shown to substitute for sulfur in pyrite (Savage et al., 2000) and form an arsenopyrite-like solid (Blanchard et al., 2007; Bostick and Fendorf, 2003; Simon et al., 1999), we hypothesized that sulfide may drive the release of arsenic from black shale pyrites. To examine this hypothesis, we measured the sulfide-driven mobilization of arsenic from arsenopyrite, whole black shale, and isolated black shale

pyrite under various redox conditions (hypoxic, oxic, and anoxic) and determined the oxidation state of arsenic in Newark Basin (Lockatong formation) black shale pyrite.

3. 2 Materials and Methods

Materials

Sulfide-arsenide exchange was examined in arsenopyrite, homogenized black shale, and isolated black shale pyrites. Arsenopyrite (FeAsS) was obtained from a commercial supplier and verified as to element content and mineral structure by XRF and X-ray diffraction analyses. Partially weathered black shale (fractured, water-saturated) was collected from an outcrop of the Newark Basin's Lockatong formation near Trenton, New Jersey (As concentration = 6 to 26 mg kg^{-1}). Black shale pyrites (1 to 5 mm prior to pulverization, As concentration = 0.2 to 0.6% by micro-XRF) were chiseled from Newark Basin (Lockatong formation) rock cores. All reagents were analytical grade and solutions were prepared with ultrapure water.

Abiotic arsenic mobilization experiments

Arsenic mobilization from arsenopyrite, homogenized black shale, and isolated black shale pyrites was examined in batch incubation experiments conducted in the presence or absence of sulfide, under oxic, hypoxic, or anoxic (arsenopyrite and homogenized black shale only) conditions. Rock samples were pulverized to a fine powder, over 95 percent of which passed through an 80-mesh screen. Visual inspection indicated that clay material accounted for less than 10% of the pulverized black shale

pyrite samples. A constant mass of each material (arsenopyrite 0.02 g, black shale 0.2 g, pyrite 0.09 g) was added to 40 ml of 10 mM HEPES-KOH (pH 8) buffer solutions in 50 ml polypropylene tubes and incubated in duplicate. A solution of sodium bisulfide (NaHS, Aldrich) was prepared in deoxygenated (N_2 purged) ultrapure water and added to an initial concentration of 1 mM. Sulfide-free control experiments were also performed for each material. Solids were sterilized by autoclaving at 121 ℃ for 25 minutes or immersion in ethanol overnight. The HEPES buffer was sterilized by autoclaving. After sterilization, solids were rinsed with sterile buffer solution three times in order to remove loosely bound arsenic including iron arsenate or iron arsenite surface coatings on arsenopyrite or pyrite (Nesbitt et al., 1995). Oxic experiments were performed using air-equilibrated buffer. Hypoxic conditions were established in a glove bag flushed with high purity N_2 for 10 minutes For hypoxic and anoxic experiments, buffer solutions were purged with high purity N_2 for at least 30 minutes During hypoxic incubations, oxygen concentrations increased from 30 μM to 70 μM over three days. Anoxic conditions were established in an anaerobic chamber (N_2:H_2=95:5) where oxygen is strictly excluded. Subsamples were removed from anoxic incubation tube within the chamber to avoid oxygen exposure. All batch experiments were conducted at room temperature (20 ℃).

Batch reactors were sampled for soluble arsenic at 0.5 h after initiation and once or twice a day up to 4 days thereafter. Prior to sampling, tubes were centrifuged at 3200 rpm for 5 minutes and one to ten ml of particle-free supernatant was taken and preserved with EDTA (final concentrations of 1.25 mM for arsenopyrite samples, 0.125 mM for black shale and pyrite samples) in 15 ml polypropylene tubes. Samples were stored in

the dark at 4 ℃ until analysis. The addition of EDTA was necessary to preserve arsenic oxidation states (Bednar et al., 2002). Arsenic concentrations and speciation were determined within 48 hours of collection.

Biological arsenic mobilization from black shale under sulfate reducing conditions

Biological mobilization of arsenic from homogenized black shale under sulfate reducing conditions was examined in 84 day batch incubation experiments. Slurries of unsterilized, pulverized Newark Basin black shale (10% w/v) were prepared in triplicate in acid-washed, 160 ml serum bottles with sterilized, deoxygenated (N_2 purged) BT culture media (41 mM phosphate, pH 7) containing 0.4 mM sulfate and 10 mM acetate. For biologically active treatments, unsterilized black shale was used as the microbiological inocculum. For abiotic controls, dry pulverized shale was autoclaved under argon gas for 30 minutes, three times over three days prior to preparation of slurries. Biologically active and sterile slurries were incubated at 30 ℃ in the dark and thoroughly mixed each day. Samples for arsenic analysis were collected periodically from the overlying water of settled slurries (prior to mixing).

Analytical techniques

Soluble arsenic in the abiotic mobilization experiments was measured by anodic stripping voltammetry (ASV) using a gold-plated, nano-array carbon electrode (TraceDetect Nano-Band^{TM}) with a platinum wire auxiliary electrode and a Ag/AgCl/KCl reference electrode (Huang and Dasgupta, 1999). Reagent grade concentrated hydrochloric acid and nitric acid were used to acidify samples to pH less than 2 before

analysis. Arsenite was reductively plated as elemental arsenic on the electrode at a potential of -400 mV for 20 to 60 s. Arsenic was stripped from the electrode by anodic scanning from -400 mV to +800 mV with a step voltage of 17 mV and a frequency of 1250 s^{-1}. Since ASV only detects As(III), total dissolved As was detected after reduction of As(V) to As(III) with sodium thiosulfate (0.5 N) for at least four minutes (Anezaki et al., 1999). Sodium arsenite ($NaAsO_2$) was dissolved in 1% (v/v) HCl to make a 1000 ppm As(III) stock solution. Working solutions of As(III) were prepared daily from the stock solution. Calibration was performed before each group of analyses. The detection limit of As(III) analysis by ASV was 4 nM based on three times the standard deviation of the blank. The pH in each solution was measured using an Accumet Basic (Fisher scientific) pH electrode and dissolved oxygen was measured using a DO electrode (model 850, Thermo Orion). Total soluble arsenic in the biological mobilization experiment was measured by ICP-MS at Rutgers Environmental and Occupational Health Sciences Institute (Xie et al., 2006).

The oxidation state of arsenic in Newark Basin pyrite was determined by X-ray absorption-near edge structure (XANES) spectroscopy. Arsenic K-edge absorption spectra were collected at the National Synchrotron Light Source at Brookhaven National Laboratory on beamline X-11A. Experiments were conducted using isolated black shale pyrites (As concentration = 0.2 to 0.6%) chiseled from Newark Basin (Lockatong formation) rock cores and pulverized to a fine powder. K-edge data were calibrated by defining the inflection point of the gold L_3-edge. The energy value assigned to the Au L_3-edge was 11.919 keV. Gold foil spectra were also measured between sample runs.

XANES measurements were collected from 11.800 to 12.200 keV in fluorescence mode. For data analysis, the background was subtracted and the jump height was normalized to unity using the software WinXAS (Ressler, 1997). Experimental spectra of the pulverized black shale pyrite were compared to powder arsenic reference standards including the As(III) oxide, sodium arsenite ($NaAsO_2$), the As(II) sulfide, realgar (AsS), and the As(-I) iron sulfide, arsenopyrite (FeAsS).

3.3 Results

Sulfide-driven arsenic mobilization from arsenopyrite

Arsenic mobilization from arsenopyrite was enhanced by sulfide under oxic and hypoxic, but not anoxic conditions. In the absence of sulfide, 2 to 5 μM of soluble arsenic was released from arsenopyrite in 24 h under all redox conditions (Fig 3.1). The release of soluble arsenic from arsenopyrite (as well as from whole black shale and black shale pyrite, see below) in the absence of sulfide was likely due to the dissolution of small amounts of arsenate or arsenite solids left on the mineral surfaces after rinsing with buffer. With the addition of 1 mM sulfide, however, more than 20 μM of soluble arsenic was released from arsenopyrite in 24 h under oxic and hypoxic conditions (Fig 3.1). In addition, the release of soluble arsenic from arsenopyrite continued in the oxic and hypoxic incubations for up to 72 h in the sulfide treatments, but ceased after 24 h in those without sulfide (Fig 3.1). Sulfide did not enhance arsenic mobilization from arsenopyrite in the anoxic treatment. Among all incubations, the highest total soluble arsenic concentrations after 72 h were found in the hypoxic-sulfide treatment, followed by the

oxic-sulfide treatment (Fig 3.1). Note that only 20-25% of the initial added sulfide was consumed by reaction with oxygen in oxic and hypoxic treatments without minerals or shale over 72 hours.

Both arsenite and arsenate were generated by decomposition of arsenic mobilized from arsenopyrite in oxic and hypoxic incubations (Fig 3.2). The temporal patterns of total arsenic mobilization from arsenopyrite was similar to that of arsenite indicating that arsenate (difference between total arsenic and arsenite) was produced from the oxidation of mobilized arsenite.

Sulfide-driven arsenic mobilization from homogenized black shale and isolated black shale pyrite

The general patterns of arsenic mobilization from homogenized whole black shale and isolated black shale pyrite were similar to those observed with arsenopyrite; arsenic mobilization was higher in the presence than absence of sulfide and the rates and extents of arsenic mobilization were higher under hypoxic than oxic conditions (Figs 3.3 and 3. 4). In contrast to the arsenopyrite experiments, however, soluble arsenic concentrations declined after 50 h in oxic and hypoxic incubations of whole black shale and black shale pyrite in the presence of sulfide (Fig 3.3) and all arsenic mobilized from whole black shale and black shale pyrite was present as arsenate. Soluble arsenic was below detection (4 nM) in anoxic incubations of whole black shale in both sulfide and sulfide-free treatments.

XANES spectroscopy of arsenic in black shale pyrite

The energy positions of the XANES edge for arsenic in sodium arsenite, realgar, and arsenopyrite were 11.870, 11.868, and 11.867 keV, respectively (Fig 3.5). The XANES data indicate that the position of the As K-edge shifts to lower energies with decreasing oxidation states. The peak position of the edge measured for arsenic in black shale pyrite was 11.867 keV. A comparison of inflection points of the XANES spectra indicates that the arsenic hosted in the Newark Basin black shale pyrite has the same oxidation state (-1) as arsenic in the arsenopyrite standard.

Biological arsenic mobilization from homogenized black shale under sulfate reducing conditions

Immediately following the addition of unsterilized and autoclaved black shale to deoxygenated culture media (within 10 minutes), 1.0 μM and 1.5 μM, respectively, of soluble arsenic was released (0 d in Fig 3.6). These initial concentrations of soluble arsenic were likely due to the desorption of loosely bound arsenate or arsenite associated with the unrinsed black shale. (Note that the concentration of shale was 20 times higher in these mobilization experiments than in the sulfide-arsenide exchange experiments with homogenized black shale and isolated black shale). After the initial release of adsorbed arsenic, little or no arsenic was mobilized from the black shale during the first 14 d of the incubations under biologically active or sterile conditions (Fig 3.6). However, from 14 to 42 d, more than 2 μM arsenic was mobilized from the black shale in the biologically active treatment, while only 0.3 μM arsenic was mobilized in the sterile control (Fig 3.6). The time lag of arsenic mobilization in the biologically active treatment during the first

14 d may reflect the acclimation of the microbial community to the experimental media. After 42 d, the concentration of soluble arsenic remained constant in the biologically active treatment, but decreased in the sterile control.

3.4 Discussion

Sulfide-driven arsenic mobilization from arsenopyrite and pyritic black shale

The results presented here show that sulfide increases the mobilization of arsenic from arsenopyrite, whole black shale, and isolated black shale pyrite under hypoxic and oxic conditions compared with sulfide-free controls. We propose that this mobilization occurs via sulfide-arsenide exchange as in reaction 1. Other processes that could have driven arsenic release in our experiments include the oxidation of arsenopyrite or arsenian pyrite and sulfide complexation of dissolved arsenic. Sulfide-free controls showed little arsenic mobilization (Figs 3.1-4) confirming that purely oxidative arsenic mobilization did not occur to a major extent. Sulfide complexation of dissolved arsenic (i.e. formation of thioarsenites or thioarsenates) should have driven arsenic mobilization under anoxic as well as oxic and hypoxic conditions, but arsenic mobilization was lowest in the anoxic treatments.

For arsenopyrite, sulfide-arsenide exchange is thought to be important in low pH, geothermal systems (Ballantyne and Moore, 1988; Heinrich and Eadington, 1986), but our results demonstrate its potential importance in low temperature circumneutral pH settings as well. We can extend this mechanism to black shale arsenian pyrite using

arsenopyrite as a model mineral for sulfide-driven arsenic mobilization and by comparing the chemical forms of arsenic in black shale pyrites and arsenopyrite. It was previously shown by X-ray photoelectron spectroscopy that 85% of the arsenic in arsenopyrite is present as arsenide (-1 oxidation state) with the remaining 15% present as elemental arsenic (Nesbitt et al., 1995). Furthermore, previous XANES measurements have shown that arsenic is present as As(-1) in arsenian pyrite (Savage et al., 2000; Simon et al., 1999). Our XANES results (Fig 3.5) are consistent with these studies and show that arsenic in Newark Basin black shale pyrite is most likely present as arsenide (-1 oxidation state). Black shale arsenian pyrite may therefore be susceptible to the same sulfide-driven arsenic mobilization process as occurs in arsenopyrite.

The lack of an effect of sulfide on arsenic mobilization from arsenopyrite and whole black shale under anoxic conditions indicates that sulfide-driven arsenic mobilization from both materials requires an oxidant as in reaction 1.

All three materials released more arsenic under hypoxic (30 to 70 μM O_2) than oxic conditions. This may have resulted from the formation of iron oxide crusts on pyrite surfaces in the oxic treatments that slowed or prevented reactions of solid phase arsenic with sulfide (Komnitsas et al., 1995; Nesbitt et al., 1995; Schaufuss et al., 2000; Walker et al., 2006; Yu et al., 2004). In addition, the oxidation of sulfide was more rapid under oxic than hypoxic conditions decreasing sulfide's reactive lifetime.

In the proposed sulfide-arsenide exchange reaction, arsenic is mobilized as arsenite, but soluble arsenate represented 30% to 70% of dissolved arsenic in the oxic and hypoxic incubations of arsenopyrite and was the only soluble form of arsenic detected in the whole black shale and black shale pyrite experiments. Soluble arsenate in these experiments was likely produced by the oxidation of mobilized arsenite in solution. Since the concentrations of dissolved arsenic were 100 times lower in the black shale and black shale pyrite incubations than in the arsenopyrite incubations, only partial oxidation of mobilized arsenite occurred with arsenopyrite, while with the black shale and black shale pyrite, arsenite oxidation was nearly complete. Desorption of arsenate from arsenopyrite and pyrtite surfaces can occur (Yu et al., 2004), but much if not all adsorbed arsenate should have been removed by rinsing with incubation buffer prior to the start of these experiments (Nesbitt et al., 1995). Another possible source of arsenate is the production of thioarsenate ($H_2AsO_3S^-$) by the reaction of arsenite and sulfide or elemental sulfur (Stauder et al., 2005), however, this would only be possible in the sulfide treatments.

The precipitation of orpiment could not have removed soluble arsenite in the whole black shale and black shale pyrite experiments since it was undersaturated in these incubations. However, arsenite could have been selectively removed from solution by adsorption since at pH 8, arsenite shows greater adsorption on iron sulfide minerals than arsenate (Bostick and Fendorf, 2003).

Although the mechanistic details of sulfide-arsenide exchange will require further study, it is likely that this reaction proceeds by the initial binding of sulfide to iron on arsenopyrite or arsenian pyrite surfaces destabilizing solid phase arsenide. Destabilized arsenide on the surface of these minerals would be susceptible to oxidation by aqueous or solid phase oxidants. The oxidation and subsequent hydrolysis of arsenic would lead to the release of soluble arsenite and allow bound sulfide to form pyrite.

Implications for the environment

Groundwater arsenic concentrations in sedimentary rock aquifers often exceed the U.S. Maximum Contaminant Level of 10 $\mu g\ L^{-1}$ (0.13 μM) (Ryker, 2003; Welch et al., 2000). Although the weathering of pyritic black shale appears to be the ultimate source of arsenic to groundwater in sedimentary rock aquifers (Peters and Burkert, 2008), the mechanism of arsenic mobilization is unclear. Our results indicate that a sulfide-arsenide exchange and oxidation reaction may drive arsenic mobilization from sedimentary rock pyrites. This mechanism will be most important at the boundary of oxidizing and reducing environments that support sulfate reducing bacteria. Such conditions of redox disequilibrium occur in confined aquifers where oxygenation rates are slow and hypoxic and anoxic groundwaters mix (Massmann et al., 2003; Yamanaka et al., 2007).

The redox stoichiometry of sulfide-arsenide exchange indicates that if sulfide is present, arsenic may be mobilized from arsenopyrite and arsenic-rich pyrite only when an oxidant is available. In natural groundwater, Fe(III), Mn(IV), or nitrate could serve as oxidants in sulfide-driven arsenic mobilization in the absence of oxygen. Indeed the

energetics of sulfide-driven arsenic mobilization from arsenopyrite (at pH 8) are favorable for reactions with $Fe(OH)_3$ ($\Delta G°'_{298}$ = -143 kJ mol^{-1}), MnO_2 ($\Delta G°_{298}$ = -405 kJ mol^{-1}), or nitrate ($\Delta G°_{298}$ = -360 kJ mol^{-1}). Analogous thermodynamic calculations are not possible for arsenian pyrite which is a heterogeneous solid of variable composition. However, we can predict that arsenic-enriched pyrite surfaces of arsenian pyrite are less stable than pure arsenopyrite. In this case, sulfide-arsenide exchange with arsenian pyrite will be even more favorable than that for arsenopyrite. Arsenic mobility in fractured rock aquifers containing pyritic black shale will therefore be determined in part by the concentrations of sulfide and available oxidant. Sulfide-driven arsenic mobilization reactions will proceed until the surfaces of the exposed arsenopyrite or arsenian pyrite are depleted of arsenic and enriched in pure pyrite. Once new arsenic-rich surfaces become exposed through the oxidation of surface pyrite and/or the formation of new fractures in the shale, the process will begin again.

The mobilization of arsenic in biologically active incubations under sulfate reducing conditions (N_2 atmosphere, sulfate, organic carbon) was seven times higher than in sterile controls (Fig 3.6). One explanation for this result is that sulfide generated by sulfate reducing bacteria in the biologically active incubations drove arsenic mobilization from the solid phase as in our abiotic experiments, although other direct or indirect, microbially-catalyzed processes resulting in the dissolution of the solid phase are also possible. The continuous mobilization of arsenic over a period of four weeks in the biologically active treatments (Fig 3.6), compared with a time scale of arsenic release of only two days in the abiotic sulfide exchange experiments (Fig 3.3), reflects the

continuous production of sulfide by sulfate reducing bacteria during their growth and provides a more realistic model of how this process may occur in an aquifer. Sulfate reduction has been shown to lower dissolved arsenic levels in unconsolidated glacial aquifers, presumably through the precipitation of arsenic sulfides and/or iron sulfides (Kirk et al., 2004). In sedimentary rock aquifers with major formations of pyritic black shale, however, our results suggest that microbial sulfide production will enhance arsenic mobilization to groundwater.

The importance of sulfide-arsenide exchange to arsenic mobilization in a given black shale aquifer will depend on the relative rates of this and competing processes. Our results show that the abiotic mobilization of arsenic from arsenopyrite and black shale arsenian pyrite by reaction with oxygen is much slower than that of sulfide-arsenide exchange (Figs 3.1-4). Moreover, the maximum specific rate of arsenic mobilization from arsenopyrite by sulfide exchange observed here (5.4×10^{-3} d^{-1}) is comparable to that for biological mobilization of arsenic from arsenopyrite catalyzed by a dense, lab-grown culture of an arsenic oxidizing aerobe (9.3×10^{-3} d^{-1}) (Rhine et al., 2008). This indicates that, if conditions are favorable (sulfide and an oxidant are present), sulfide-arsenide exchange has the potential to compete with biologically-driven mobilization of arsenic from arsenian pyrite.

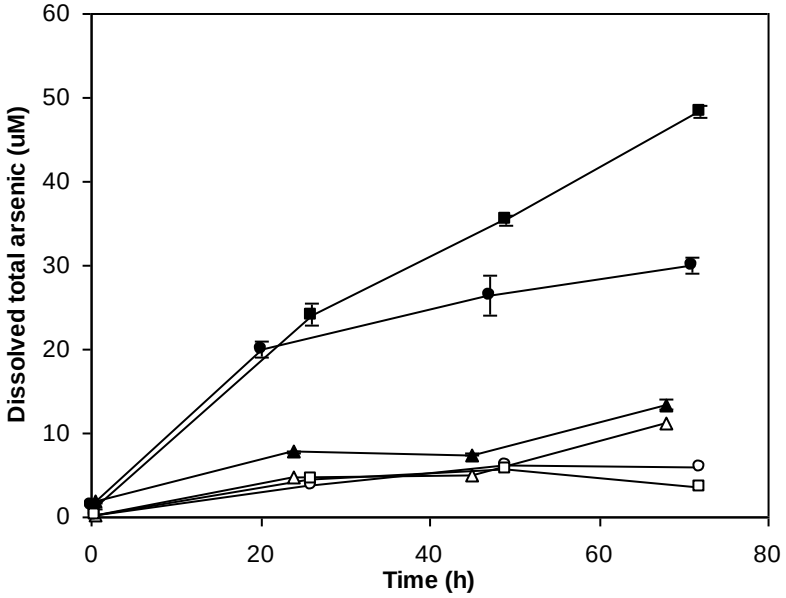

Figure 3.1. Mobilization kinetics of total arsenic from arsenopyrite incubated at pH 8 under oxic (20% O_2; circles), hypoxic (≈2% O_2; squares), and anoxic (5% H_2, 95% N_2; triangles) conditions with (filled) or without (open) 1 mM sulfide. Means of duplicate incubations are plotted; error bars show upper and lower values.

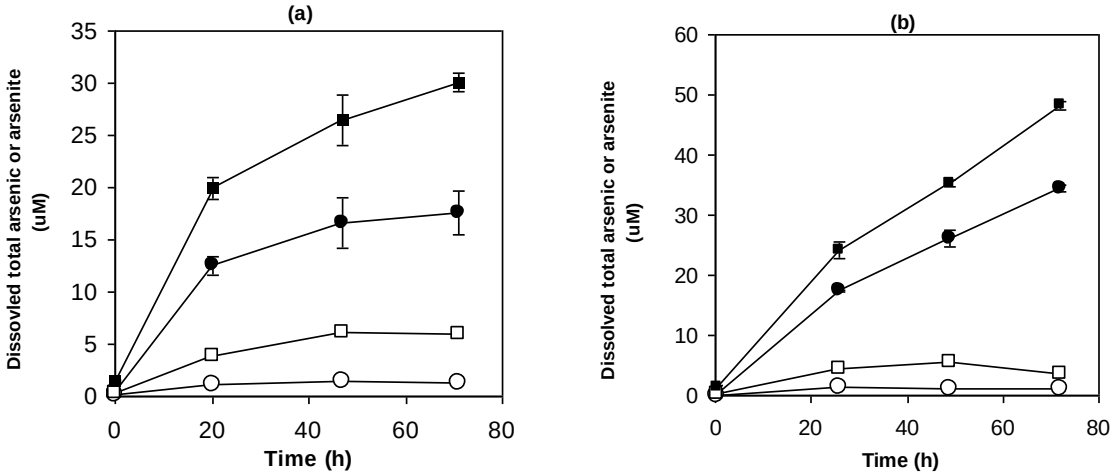

Figure 3.2. Mobilization kinetics of total arsenic (squares) and arsenite (circles) from arsenopyrite under oxic (a), and hypoxic (b) conditions with (filled) or without (open) 1 mM sulfide. Arsenite was measured by ASV in acidified samples and total arsenic was measured after reduction with thiosulfate. Means of duplicate incubations are plotted; error bars show upper and lower values.

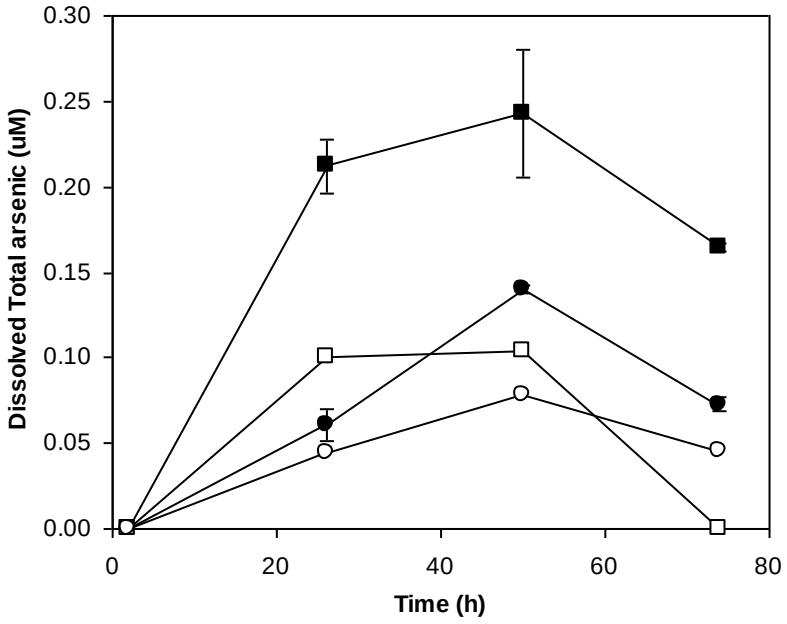

Figure 3.3. Mobilization kinetics of total arsenic from homogenized Newark Basin black shale under oxic (circles) and hypoxic (squares) conditions with (filled) or without (open) 1 mM sulfide. Means of duplicate incubations are plotted; error bars show upper and lower values.

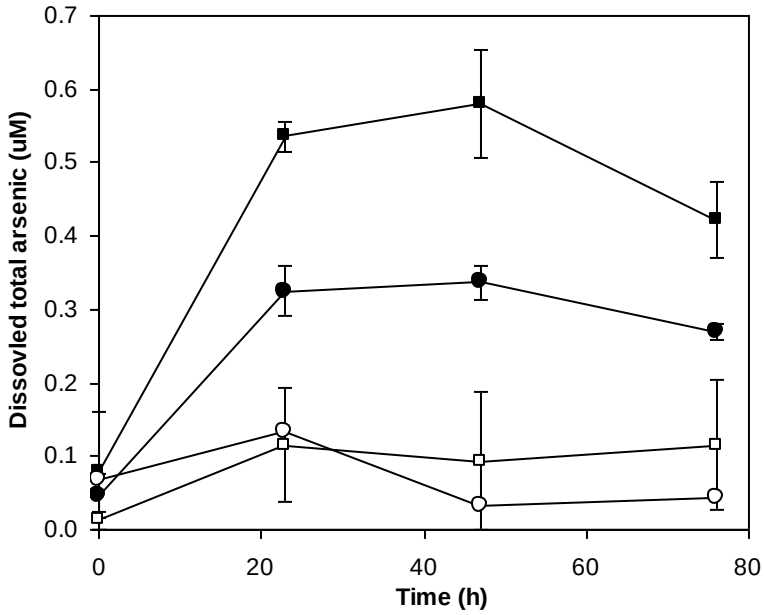

Figure 3.4. Mobilization kinetics of total arsenic from isolated Newark Basin black shale pyrite under oxic (circles) and hypoxic (squares) conditions with (filled) or without (open) 1 mM sulfide. Means of duplicate incubations are plotted; error bars show upper and lower values.

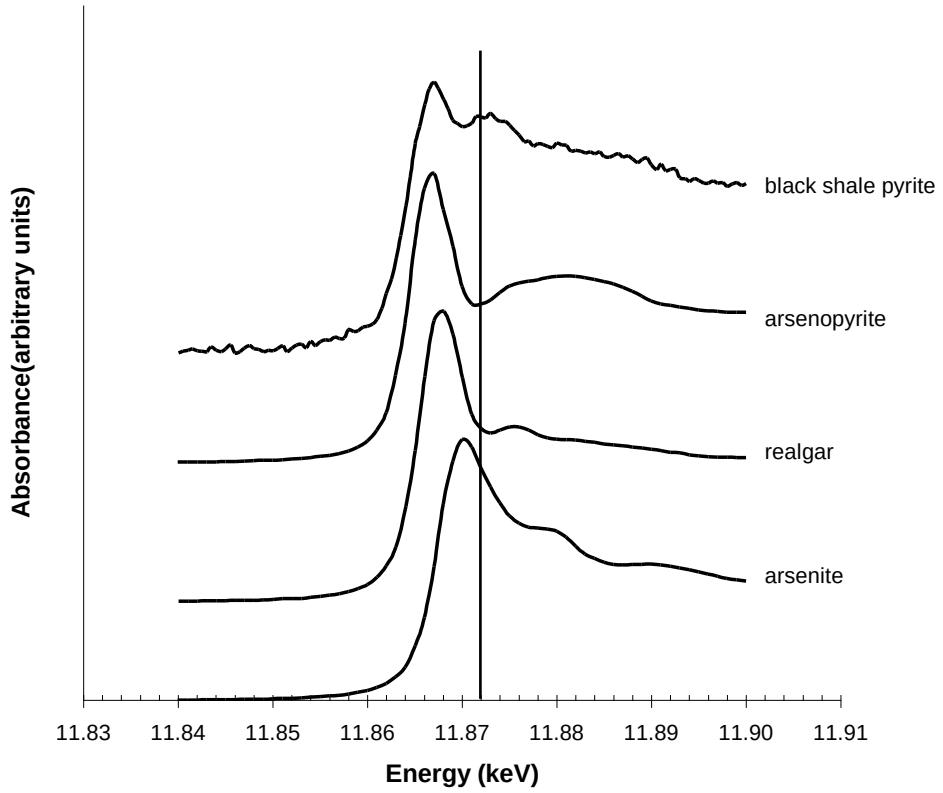

Figure 3.5. Arsenic K-edge x-ray absorption-near edge structure (XANES) for the As(III) oxide, sodium arsenite ($NaAsO_2$), the As(II) sulfide, realgar (AsS), the As(-I) iron sulfide, arsenopyrite (FeAsS), and arsenian pyrite isolated from Newark Basin (Lockatong formation) black shale. Vertical line shows peak arsenic absorbances for arsenopyrite and Newark Basin arsenian pyrite (11.867 keV).

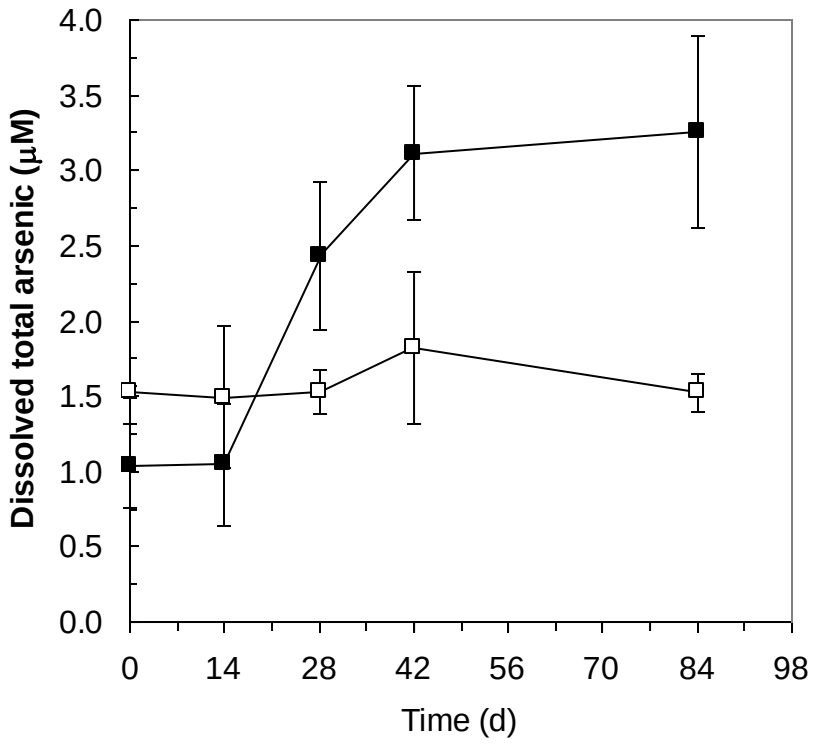

Figure 3.6. Arsenic mobilization from homogenized Newark Basin black shale incubated under biologically active, sulfate reducing (filled squares) and sterile (open squares) conditions. Values are means of triplicate incubations ± 1 standard deviation.

References

Ahmed K. M., Bhattacharya P., Hasan M. A., Akhter S. H., Alam S. M. M., Bhuyian M. A. H., Imam M. B., Khan A. A. and Sracek O. (2004) Arsenic enrichment in groundwater of the alluvial aquifers in Bangladesh: an overview. *Appl. Geochem.* **19**, 181-200.

Anezaki K., Nukatsuka I. and Ohzeki K. (1999) Determination of arsenic(III) and total arsenic(III,V) in water samples by resin suspension graphite furnace atomic absorption spectrometry. *Anal. Sci.* **15**, 829.

Ballantyne J. M. and Moore J. N. (1988) Arsenic geochemistry in geothermal systems. *Geochim. Cosmochim. Acta* **52**, 475-483.

Bayard R., Chatain V., Gachet C., Troadec A. and Gourdon R. (2006) Mobilisation of arsenic from a mining soil in batch slurry experiments under bio-oxidative conditions. *Water Res.* **40**, 1240-1248.

Bednar A. J., Garbarino J. R., Ranville J. F. and Wildeman T. R. (2002) Preserving the distribution of inorganic arsenic species in groundwater and acid mine drainage samples. *Environ. Sci. Technol.* **36**, 2213-2218.

Blanchard M., Alfredsson M., Brodholt J., Wright K. and Catlow C. R. A. (2007) Arsenic incorporation into FeS_2 pyrite and its influence on dissolution: A DFT study. *Geochim. Cosmochim. Acta* **71**, 624-630.

Bostick B. C. and Fendorf S. (2003) Arsenite sorption on troilite (FeS) and pyrite (FeS_2). *Geochim. Cosmochim. Acta* **67**, 909-921.

Brown G. E. J., Foster A. L. and Ostergren J. D. (1999) Mineral surfaces and bioavailability of heavy metals: A molecular-scale perspective *Proc. Natl. Acad. Sci. U. S. A.* **96**, 3388-3395.

Carrillo A. and Drever J. I. (1998) Adsorption of arsenic by natural aquifer material in the San Antonio-El Triunfo mining area, Baja California, Mexico. *Environmental Geology* **35**, 251-257.

Craw D., Falconer D. and Youngson J. H. (2003) Environmental arsenopyrite stability and dissolution: theory, experiment, and field observations. *Chem. Geol.* **199**, 71-82.

Das D., Samanta G., Mandal B. K., Chowdhury T. R., Chowdhury P. P., Basu G. K., Chanda C. R. and Chakraborti D. (1996) Arsenic in groundwater in six districts of West Bengal, India. *Environmental Geochemistry and Health* **18**, 5-15.

Dowling C. B., Poreda R. J., Basu A. R. and Peters S. L. (2002) Geochemical study of arsenic release mechanisms in the Bengal Basin groundwater. *Water Resour. Res.* **38**, 1173.

Farquhar M. L., Charnock J. M., Livens F. R. and Vaughan D. J. (2002) Mechanisms of arsenic uptake from aqueous solution by interaction with goethite, lepidocrocite, mackinawite, and pyrite: An X-ray absorption spectroscopy study. *Environ. Sci. Technol.* **36**, 1757-1762.

Heinrich C. A. and Eadington P. J. (1986) Thermodynamic predictions of the hydrothermal chemistry of arsenic, and their significance for the paragenetic sequence of some cassiterite-arsenopyrite-base metal sulfide deposits. *Econ. Geol.* **81**, 511-529.

Huang H. and Dasgupta P. K. (1999) A field-deployable instrument for the measurement and speciation of arsenic in potable water. *Anal. Chim. Acta* **380**, 27-37.

Kirk M. F., Holm T. R., Park J., Jin Q., Sanford R. A., Fouke B. W. and Bethke C. M. (2004) Bacterial sulfate reduction limits natural arsenic contamination in groundwater. *Geol.* **32**, 953-956.

Kober R., Welter E., Ebert M. and Dahmke A. (2005) Removal of arsenic from groundwater by zerovalent iron and the role of sulfide. *Environ. Sci. Technol.* **39**, 8038-8044.

Komnitsas K., Xenidis A. and Adam K. (1995) Oxidation of pyrite and arsenopyrite in sulphidic spoils in lavrion. *Miner. Eng.* **8**, 1443-1454.

Kwong Y. T. J., Beauchemin S., Hossain M. F. and Gould W. D. (2007) Transformation and mobilization of arsenic in the historic Cobalt mining camp, Ontario, Canada. *J. Geochem. Explor.* **92**, 133-150.

Lazareva O. and Pichler T. (2007) Naturally occurring arsenic in the Miocene Hawthorn Group, southwestern Florida: Potential implication for phosphate mining. *Appl. Geochem.* **22**, 953-973.

Lehner S. and Savage K. (2008) The effect of As, Co, and Ni impurities on pyrite oxidation kinetics: Batch and flow-through reactor experiments with synthetic pyrite. *Geochim. Cosmochim. Acta* **72**, 1788-1800.

Lehner S., Savage K., Ciobanu M. and Cliffel D. E. (2007) The effect of As, Co, and Ni impurities on pyrite oxidation kinetics: An electrochemical study of synthetic pyrite. *Geochim. Cosmochim. Acta* **71**, 2491-2509.

Lowers H. A., Breit G. N., Foster A. L., Whitney J., Yount J., Uddin M. N. and Muneem A. A. (2007) Arsenic incorporation into authigenic pyrite, Bengal Basin sediment, Bangladesh. *Geochim. Cosmochim. Acta* **71**, 2699-2717.

Massmann G., Tichomirowa M., Merz C. and Pekdeger A. (2003) Sulfide oxidation and sulfate reduction in a shallow groundwater system (Oderbruch Aquifer, Germany). *J. Hydrol.* **278**, 231-243.

Nesbitt H. W. and Muir I. J. (1998) Oxidation states and speciation of secondary products on pyrite and arsenopyrite reacted with mine waste waters and air. *Mineralogy and Petrology* **62**, 123-144.

Nesbitt H. W., Muir J. and Praw A. R. (1995) Oxidation of arsenopyrite by air and air-saturated, distilled water, and implications for mechanism of oxidation. *Geochim. Cosmochim. Acta* **59**, 1773-1786.

O'Day P. A., Vlassopoulos D., Root R. and Rivera N. (2004) The influence of sulfur and iron on dissolved arsenic concentrations in the shallow subsurface under changing redox conditions. *Proc. Natl. Acad. Sci. U. S. A.* **101**, 13703-13708.

Paikaray S., Banerjee S. and Mukherji S. (2005) Sorption of arsenic onto Vindhyan shales: Role of pyrite and organic carbon. *Curr. Sci.* **88**, 1580-1585.

Peters S. C. and Burkert L. (2008) The occurrence and geochemistry of arsenic in groundwaters of the Newark basin of Pennsylvania. *Appl. Geochem.* **23**, 85-98.

Polizzotto M. L., Harvey C. F., Sutton S. R. and Fendorf S. (2005) Processes conducive to the release and transport of arsenic into aquifers of Bangladesh. *Proc. Natl. Acad. Sci. U. S. A.* **102**, 18819-18823.

Reedy R. C., Scanlon B. R., Nicot J. P. and Tachovsky J. A. (2007) Unsaturated zone arsenic distribution and implications for groundwater contamination. *Environ. Sci. Technol.* **41**, 6914-6919.

Ressler T. (1997) WinXAS: A new software package not only for the analysis of energy dispersive XAS data. *J. Phys. IV* **7**, 269-270.

Rhine E. D., Onesios K. M., Serfes M. E., Reinfelder J. R. and Young L. Y. (2008) Arsenic transformation and mobilization from minerals by the arsenite oxidizing strain WAO. *Environ. Sci. Technol.* **42**, 1423–1429.

Roesler A. J., Gammons C. H., Druschel G. K., Oduro H. and Poulson S. R. (2007) Geochemistry of flooded underground mine workings influenced by bacterial sulfate reduction. *Aquat. Geochem.* **13**, 211-235.

Ryker S. J. (2003) Arsenic in ground water used for drinking water in the United States. In: Welch, A. H. and Stollenwerk, K. G. Eds.), *Arsenic in Ground Water: Geochemistry and Occurrence*. Kluwer Academic Publishers, Norwell, Massachusetts.

Saunders J. A., Mohammad S., Korte N. E., Lee M. K., Fayek M., Castle D. and Barnett M. O. (2005) Groundwater geochemistry, microbiology, and mineralogy in two arsenic-bearing Holocene alluvial aquifers from the United States, *Advances in Arsenic Research*.

Savage K. S., Tinglea T. N., O'Day P. A., Waychunas G. A. and Bird D. K. (2000) Arsenic speciation in pyrite and secondary weathering phases, Mother Lode Gold District, Tuolumne County,California. *Appl. Geochem.* **15**, 1219-1244.

Schaufuss A. G., Nesbitt H. W., Scaini M. J., Hoechst H., Bancroft M. G. and Szargan R. (2000) Reactivity of surface sites on fractured arsenopyrite (FeAsS) toward oxygen. *Am. Mineral.* **85**, 1754-1766.

Signes-Pastor A., F. Burló K. M. and Carbonell-Barrachina A. A. (2007) Arsenic biogeochemistry as affected by phosphorus fertilizer addition, redox potential and pH in a west Bengal (India) soil. *Geoderma* **137**, 504-510.

Simon G., Huang H., Penner-Hahn J. E., Kesler S. E. and Kao L.-S. (1999) Oxidation state of gold and arsenic in gold-bearing arsenian pyrite. *Am. Mineral.* **84**, 1071-1079.

Singleton R., Jr (1993) *The sulfate-reducing bacteria: an overview.* Springer Verlag, Inc., New York, N.Y.

Smedley P. L. and Kinniburgh D. G. (2002) A review of the source, behaviour and distribution of arsenic in natural waters. *Appl. Geochem.* **17**, 517-568.

Stauder S., Raue B. and Sacher F. (2005) Thioarsenates in sulfidic waters. *Environ. Sci. Technol.* **39**, 5933-5939.

Walker F. P., Schreiber M. E. and Rimstidt J. D. (2006) Kinetics of arsenopyrite oxidative dissolution by oxygen. *Geochim. Cosmochim. Acta* **70**, 1668-1676.

Welch A. H., Westjohn D. B., Helsel D. R. and Wanty R. B. (2000) Arsenic in ground water of the United States—Occurrence and geochemistry. *Ground Water* **38**, 589-604.

Wilkin R. T. (2001) Iron sulfide-arsenite interactions: Adsorption behavior onto iron monosulfides and controls on arsenic accumulation in pyrite. *USGS Workshop on Arsenic in the Environment*, Denver. (abstr.).

Wolthers M., Charlet L., van Der Weijden C. H., van der Linde P. R. and Rickard D. (2005) Arsenic mobility in the ambient sulfidic environment: Sorption of arsenic(V) and arsenic(III) onto disordered mackinawite. *Geochim. Cosmochim. Acta* **69**, 3483-3492.

Xie R. M., Johnson W., Spayd S., Hall G. S. and Buckley B. (2006) Arsenic speciation analysis of human urine using ion exchange chromatography coupled to inductively coupled plasma mass spectrometry. *Anal. Chim. Acta* **578**, 186-194.

Yamanaka M., Nakano T. and Tase N. (2007) Sulfate reduction and sulfide oxidation in anoxic confined aquifers in the northeastern Osaka Basin, Japan. *J. Hydrol.* **335**, 55-67.

Yu Y., Zhu Y., Williams-Jonesb A. E., Gao Z. and Li D. (2004) A kinetic study of the oxidation of arsenopyrite in acidic solutions: implications for the environment. *Appl. Geochem.* **19**, 435-444.

Zhu W., Young L. Y., Yee N., Serfes M., Rhine E. D., and Reinfelder J. R. (2008) Sulfide-driven arsenic mobilization from arsenopyrite and black shale pyrite. *Geochimica et Cosmochimica Acta* **72**(21), 5243-5250.

CHAPTER 4

MICROBIAL COLONIZATION OF IRON SULFIDE SUBSTRATE IN SUBSURFACE ENVIRONMENT

Abstract

Thick biofilms were observed on the surfaces of pyrite bearing black shale sections during their in situ incubation in groundwater for 1 month. The microbial colonization pattern on the black shale sections observed under epi-fluorescence microscope indicated preferential microbial attachment to pyrite rather than the shale matrix. Scanning electron microscopy (SEM) further confirmed the colonization preference and revealed the co-occurrence of secondary iron minerals and bacterial shaped pits on pyrite which indicates biological involvement in the formation of these secondary solid phases. Molecular characterization of attached bacterial communities on pyrite, arsenopyrite and quartz sand minerals incubated in the groundwater was achieved by isolating bacterial DNA and performing polymerase chain reaction-denaturing gradient gel electrophoresis (PCR-DGGE). The 16S rDNA sequences obtained from all three materials suggested that majorities of the attached bacteria belong to phylum proteobacteria, and most of them are members of Fe (III)-reducing Geobacteraceae in the δ-proteobacteria. Other groups such as β and ε-proteobacteria whose members are able to oxidize iron or sulfur were also identified in the biofilm that attached to arsenopyrite. For pyrite, attached microbes were recognized as members from β and δ-proteobacteria. δ - proteobacteria and one Gram Positive *Clostridium* species were also detected in the biofilm on quartz sand. This study

indicated that microbes may play an essential role in the transformation of iron sulfides and their secondary minerals such as iron hydroxide in the pyrite bearing substrata in contact with slightly acidic groundwater.

4.1 Introduction

The subsurface environment on Earth can be viewed as an electron reservoir and reduced iron sulfur minerals such as pyrite in the underlying substrata play a major role as electron source for biological activities. Weathering of pyrite has profound impact on the iron and sulfur redox cycles in the environment. Pyrite oxidation can be achieved via either biotic or abiotic pathways and microbially catalyzed pyrite oxidation is faster than chemical reaction. The Fe (II) in pyrite can function as electron donor for iron oxidizing microorganisms under oxic or anoxic conditions. Sulfur oxidizing microorganisms can also obtain energy by oxidizing the reduced sulfur in pyrite. From a thermodynamically point of view, much more energy can be harnessed from the oxidation of reduced sulfur compounds than the ferrous iron (Hazeu et al., 1986; Malki et al., 2006). The energy harvested via iron sulfides oxidation can facilitate the growth of chemolithotrophic microorganisms that mediate the process (Edwards, 2004; McCollom, 2000).

In natural environment, pyrite weathering is indisputably involved with or even controlled by biological activities. The mechanism of microbially involved pyrite oxidation is controversial. Two basic mechanisms were proposed, the “direct” (attach to mineral surface and dissolve sulfides without a soluble electron shuttle) or the “indirect” (not attach to mineral surface and oxidize the metal sulfide via Fe(II)/Fe(III) shuttle) pathways (Rodriguez et al., 2003a; Rodriguez et al., 2003b; Schippers and Sand, 1999). The direct attack was initiated by cells attaching to the exposed sulfide surfaces. Dissolution of the mineral was achieved by transferring electrons from the mineral substrate to an appropriate electron acceptor. On the other hand, the indirect attack was achieved by microorganisms

accelerate the regeneration of ferric iron in the solution and this soluble ferric iron further oxidizes the reduced iron sulfide minerals (Harneit et al., 2006; Konhauser, 2006; Malki et al., 2006; Sand et al., 1995).

Diverse microorganisms within domains of Achaea and Bactria are involved in the pyrite weathering process. There has been abundant research concerning the biological control of the pyrite oxidation at low pH, for example, in the bioleaching industry or acid mine drainage environment (Bond and Banfield, 2001; Edwards et al., 2000; Edwards et al., 1999; Meyer et al., 1999). Acidophilic bacteria such as members from genera *Thiobacillus* and *Leptospirillum* and achaea microbe *Ferroplasma acidarmanus* are usually identified in the acid mine drainage process (Baker and Banfield, 2003; Edwards et al., 2000). However, at neutral or slightly acidic pH, pyrite weathering had been discounted despite its importance in local iron and sulfur geochemistry. Neutrophillic iron oxidizers such as aerobic *Gallionella ferruginea* and anaerobic and nitrate-dependent *Thiobacillus denitrificans* can facilitate the solid iron oxidizing process (Ehrlich, 2002; Weber et al., 2006).

The bio-oxidation products of pyrite were characterized as biogenic Fe(III) oxides, including 2-line ferrihydrite, goethite, hematite and mixed phase Fe(II)-Fe(III) minerals, Fe-complex ligands and etc (Chaudhuri et al., 2001; Lack et al., 2002; Toner et al., 2009; Weber et al., 2006). The generated iron(III) may serve as electron acceptors under anoxic condition and the reduction processes are also considered to be biologically mediated in nature, coupled with the oxidation of organic matter, hydrogen or S(0) (Chapelle and

Lovley, 1992; Lovley, 1995; Lovley, 1997). Phylogenetically diversed iron reducers throughout the Archaea and Bacteria have been identified for using Fe (III) as electron acceptors. Pure cultures of Fe (III) reducing extremophiles such as thermophilic and hyperthermophilic microorganisms have been obtained from extreme environments (Lovley et al., 2004). At circumneutral pH, family Geobacteraceae from ε-proteobacteria, *Shewanella putrefaciens* from γ-proteobacteria together with other ferric iron respirers have been well characterized in terrestrial and subsurface environment (Ehrlich, 2002; Lovley, 2001). Besides, some microbes that belong to β-proterobacteria and *Geothrix fermentans* from Acidobacteria might also be responsible for iron reduction in sediments and aquifers (Coates et al., 1999; Cummings et al., 1999; Karrie A. Weber, 2006). Moreover, fermentative microorganisms may also contribute to the Fe (III) reduction process, yet, it was considered as a minor role in iron geochemical cycling compare to the respiratory iron reduction (Weber et al., 2006).

In summary, the transformations among different oxidation states of sulfur and iron in the subsurface environment are tightly intertwined with microbiological activities. The pre-incubation of black shale thick sections in a Lockatong formation sedimentary rock aquifer in West Trenton, New Jersey showed abundant biomass colonized on the surface of pyrite mineral. The hypothesis of our research was that autotrophic microorganisms might be identified from the biomass since they are able to utilize the iron sulfide mineral as electron sources. However, the possible existence of heterotrophs cannot be excluded. The dissolution of the minerals by chemoautotrophic microorganisms may provide electron acceptors such as ferric iron and/or sulfate to heterotrophs and with the availability of

organic matter, heterotrophic microorganisms may present and play an important role in the subsurface iron or sulfur transformation processes. A study on the composition of the microbial community that colonizes on iron sulfide minerals was thus conducted for a detailed understanding of the local sulfur and iron biogeochemical processes.

4.2 Methodology

Site description

The colonization experiment was conducted in a well in the Naval Air Warfare Center (NAWC) in West Trenton, New Jersey. The NAWC lies within the Newark Basin and is characterized by Triassic-age clastic sedimentary rocks, predominately mudstone in the Lockatong Formation, and sandstone in the Stockton Formation (Fig 4.1). The well used in this investigation is in the Lockatong formation and has a total depth of 45 ft with a depth to water of 19.46 ft (Fig 4.2).

The chemical composition of the groundwater in 33BR well where we deployed our samples is presented in table 1. These parameters were measured after pumping out 3 well volumes and therefore are believed to represent aquifer water. The well water was slightly acidic with pH around 4.8, which may be attributed to the weathering of pyrite bearing rocks. The NAWC is a polluted site with soil and groundwater by TCE and other contaminants, however, the well used in this study is located outside of the plume.

Sample deployment

Polished black shale thick sections (2.7 cm X 4.6 cm X 1 mm thick) of the Lockatong Formation used for the colonization experiments were cut from sections of core from the Newark Basin coring project. They were sterilized by ethanol immersion overnight and buffed with fine sandpaper to remove surface oxides or biofilms. Mineral pyrite, arsenopyrite and quartz sand (as control) were crushed into grains between 350 to 1000 μm and packed in 350 μm nylon pouches. The individual pouches were repeatedly sterilized with ethanol immersion overnight and air dried over 3 consecutive days. Thick sections and pouches were deployed into the well depth around 5 ft to the bottom in the Naval Air Testing site in West Trenton for incubations of 4 to 5 weeks during July-September 2007 and 2008 (The apparatus for deployment were illustrated in figure 4.3). Upon retrieval, each thick section was kept moist in polypropylene tubes and pouches were left in deployment cups and placed on ice during transportation. Thick sections for SEM study were fixed immediately upon return to the laboratory (within 1-2 hours) and pouches were stored at –80 ℃ until further use.

Experimental design of microbial community investigation was briefly illustrated in figure 4.4, black shale thick sections were undergone DAPI staining, SEM study as well as the attempt of biofilm enrichment; packed mineral grains were under gone DNA extraction and further molecular biological study.

DAPI staining

Thick sections were transferred to 1 μg/mL DAPI and incubated at room temperature for 30 minutes. Following staining, sections were rinsed in DI water for less than 1 minute to remove unbound DAPI prior to examination. A Zeiss Axioskop epi-fluorescence microscope and Nikon 9900 camera were used for viewing thick sections of black shale and capturing pictures.

Scanning electron microscopy (SEM) and Energy Dispersive Spectrometry (EDS)

Thick sections were fixed immediately after retrieval from the well. Primary fixation was accomplished by immersing thick sections in 2% phosphate buffered formaldehyde (pH 7.3) for 2 hours. Following fixation, thick sections were rinsed twice by immersion in 0.05 M phosphate buffer (pH 7.3) for 15 minutes each time. Thick sections were then dehydrated by immersion in increasing concentrations of ethanol as shown below.

Ethanol Concentration	Time
50% ethanol	15 min
70% ethanol	15 min
80% ethanol	15 min
95% ethanol	15 min
100% ethanol	15 min
100% ethanol	15 min

Dehydrated slides were kept in 100% ethanol until critical point drying. Preserved thick sections were critical point dried (Balzers Union, CPD 020) and sputter coated with gold (Balzers SCD 004) prior to observation using an Amray 1830I scanning electron

microscope at the Rutgers University Division of Life Sciences Electron Imaging Facility. The element composition of a subset of thick sections was examined by energy dispersive spectroscopy (EDS) using a JEOL JXA 8200 electron microprobe in the department of Earth and Planetary Sciences at Rutgers University. The relative atomic abundances of Fe, S, and O were detected based on their Kα electron energies after ZAF matrix correction.

Enrichment of the Biofilm Microorganisms

Biofilm on the black shale thick sections were scraped by sharp blades and transferred into a liquid culture medium containing 10 mL of BT medium (see Appendix III for medium composition) and 10 mM $NaHCO_3$with a mixture of pulverized grains including 40 mg pyrite and 10 mg arsenopyrite. A control tube with same medium composition while absent of any biomass from thick sections was also prepared. Both tubes were kept at room temperature.

Sulfide and arsenite agar plates were made with the BT medium plus 10 mM $NaHCO_3$ and 1.8 g/L agar, with addition of either 5 mM sulfide (NaHS) or 5 mM of arsenite ($NaAsO_2$). After 7 days of incubation, cells were looped from the liquid culture medium and streaked on the plates. Then the plates were stored in the dark at room temperature. After 1 week, small white colonies with similar shape and size were observed on the plates. The colonies on the plates were randomly picked and inoculated into liquid BT medium plus bicarbonate with 5 mM either sulfide or arsenite.

DNA extraction and PCR

Minerals and sand were emptied from nylon pouches and subjected to DNA extraction using PowerSoil DNA isolation kit (MoBio Laboratories, Inc. Carlsbad, CA) according to manufacturer's protocol.

A portion of the extracted DNA was then used to amplify a segment of the bacterial 16*S* rDNA gene by PCR using the USB Taq PCR Kit (USB Corporation, Ohio). Each PCR mixture contained 0.2 μM of each universal bacterial primer (338f and 519r) (1 uL for each), 5 unit/μL Taq DNA polymerase (0.25 uL) and 10X PCR buffer (5 uL), 0.2 mM dNTP-Mix (1 uL) and 2.5 mM $MgCl_2$ (2 uL). DNA template and DI water brought the PCR mixture to a final volume of 50 μL. The PCR protocol included an initial 5 min denaturation at 94 ℃, followed by 30 or 40 thermal cycles of 30s at 94 ℃, 30s at 55 ℃ and 30s at 72 ℃. Amplification was completed with a final extension step at 72 ℃ for 7 min.

Denaturing Gradient Gel Electrophoresis (DGGE) and DNA sequencing

DGGE was carried out in a DCode system manufactured by Bio-Rad laboratories Inc., CA with 30% to 80% of acrylamide gel at 55V for 16 hours. The DGGE profiles were viewed and further examined under UV light. Targeted bands were excised from gel under UV light and placed in 20 uL of sterilized DI water overnight at 4 ℃. PCR was then performed with the eluted DNA template in water and further purified with UltraClean PCR Clean-up kit (Mobio, CA) according to manufacturer's instruction. Cleaned gene segments were sent for sequencing to Genewiz Lab, Inc (NJ).

DNA sequencing results analysis

Sequencing results of the 16*S* rDNA gene segments were analyzed and compared to the sequences in GenBank database by BlastN (National Center for Biotechnology Information database) (http://www.ncbi.nlm.nih.gov). Species that indicated highest similarities to the sample 16s rDNA gene segments were selected as the most relevant.

4.3 Results

DAPI staining

Before incubation, some of the black shale thick sections were DAPI stained and observed under epi-fluorescence microscope as for comparison with the later colonization patterns on the mineral surface. Pyrite grains on the black shale were shown as red squares with the epi-fluorescent light and were free of microorganisms (Fig 4.5). After incubating the black shale thick sections in subsurface well water, thick sections were retrieved, DAPI stained and observed. Favorable colonization of microorganisms on pyrite mineral was detected. Contrast of microbial colonization patterns between pyrite mineral and black shale matrix indicated that microorganisms preferred to attach on the pyrite mineral surface (Fig 4.6). Microorganisms almost covered the pyrite mineral grains except for several streaks on the surface caused by handling. Figure 4.6 (a) indicated small pyrite grains attract microbial colonization relative to shale matrix with pyrite in red and the shale matrix in dark. Below left (Fig. 4.6 (b)), pyrite mineral surface was shown with red autofluorescence. Below right (Fig 4.6 (c)), pyrite mineral surface was with red fluorescence filtered out.

Scanning Electron Microscopy (SEM)

The black shale thick sections were gold plated and observed under scanning electron microscopy (SEM). Several different morphologies of microbes, including rod, oval and stalk shaped cells were detected on sections and most of them were found embedded within extracellular polymeric substances (EPS) (Fig 4.7 (a)). Microbial colonization showed similar preference for pyrite substrate rather than shale matrix, which was in agreement with our DAPI staining observation. Moreover, bacteria shaped pits were observed on the surface of black shale thick sections (4.7 (c)) and the co-occurrence of cells and pits may provide some evidence of biological involvement in the pit formation.

Energy Dispersive Spectroscopy

The elemental composition of the secondary formations on the surface of the pyrite was identified by energy dispersive spectroscopy (EDS). The chemical composition of pyrite on the same surface was also checked as control. Fe, S and other elements such as O, Mg and Ca were identified from the secondary formations while only Fe and S were recognized for the pure pyrite mineral. Higher Fe/S ratio was recognized in the secondary formations when compared to the control pure pyrite (data not shown).

Molecular study of attached microbes

No growth was observed from the liquid culture medium of either sulfide or arsenite utilizing bacteria in a month. Thus, the attempt of culturing the microbes from the biofilm that attached to the black shale thick section surfaces was unsuccessful. However,

the incubation of mineral grains in nylon packs in the well groundwater and extraction of the bacterial 16*S* rDNA from the mineral biofilms successfully provided us with the information on the microbial genotypes that attached to the mineral.

DGGE

Similar profiles were observed from the biofilms that were extracted from quartz sand, pyrite and arsenopyrite. Yet, some bands were recognized only within profiles of arsenopyrite or pyrite. Forty-five Bands in total were excised from DGGE gel and all were amplified by PCR with primer 338f. Among them, 33 of the bands were recognized with positive DNA results confirmed by agarose gel check and 12 of them did not successfully get amplified. Bands that successfully amplified were purified and then sent for sequencing. 24 of them were returned with useable sequences that were with at least 100 distinguishable base pairs (Fig 4.9).

16S rDNA sequencing results

The sequences of gene segments obtained from the biofilms were compared with other sequences deposited in GenBank database by BlastN. It is notable that the biofilm bacteria were mostly comprised by members of the Proteobacteria phylum, including those in β-, δ- and ε-proteobacteria families. Microbes from the pyrite biofilm appeared to be closely related to the β- and δ-proteobacteria and microbes from the arsenopyrite biofilm were associated with β-, ε-and δ-proteobacteria (Table 4.2). Quartz sand was colonized by members from δ-proteobacteria and Gram positive bacteria (Table 4.2).

All three biofilms were detected microorganisms that closely related to *Geobacter sp*. from δ-proteobacteria. Some of the sequences from arsenopyrite biofilm were recognized belong to β- and ε-proteobacteria, such as sequences that share high similarities to *Decholoromonas*, *Ferribacterium*, *Thiobacillus* in β-proteobacteria and *Sulfurricurvum kujiense* in ε-proteobacteria (Table 4.3). Some of the species from *Decholoromonas* and *Thiobacillus* genera were iron oxidizing autotrophs. *Sulfurricurvum kujiense*, which was found 100% identical with the sequence from arsenopyrite biofilm, is a sulfide oxidizing autotroph. On the biofilm of pyrite, similar sequences were found from β-proteobacteria. Yet, no ε-proteobacteria was identified.

4.4 Discussion

Microbial activities play a significant role in the transformations of iron and sulfur among their different oxidation states in nature. Abundant research has examined pyrite oxidation at extremely low pH and various kinds of acidophilic bacteria have been recognized in the process. However, much less attention has been given to the biological iron sulfide transformation at circumneutral or slightly acidic environment. Indeed, the pH for most subsurface environments such as groundwater or aquifer sediments usually ranges from slightly acidic to slightly alkaline, depending on local geochemical controls. At different pH conditions, one would expect major microorganisms and pathways for pyrite oxidation and subsequent transformations may not be the same as in acid mine drainage.

On the contrary of abundant research regarding microbial colonization on pyrite in acid mine drainage, the colonization of microbes on sulfide minerals at slightly acidic to

neutral pH has not been widely documented. In the most thorough study of this phenomenon, pyrite and other sulfide minerals were deployed to the seafloor for two months and all exposed mineral surfaces were observed to be covered by biofilms with various degrees of thickness upon retrieval (Edwards et al., 2003a). Neutrophilic iron oxidizing bacteria were enriched and isolated from the incubated minerals indicating biological involvement in iron sulfide weathering in the marine environment (Edwards et al., 2003b). However, in the terrestrial environment, such research has not been done yet.

The preferred colonization of microbes on the pyrite mineral rather than on the shale matrix was shown by both DAPI and SEM results (Fig 4.6 and 4.7). This indicated the close association between the microorganisms and iron sulfide minerals. A monolayer biofilm may be developed by the initial attachment of cells on the mineral surface; an extracellular polymeric substances (EPS) layer may be formed (Schippers et al, 1999). EPS plays an important role in the direct contact of bacteria with minerals and promotes the dissolution of metal sulfides through the complexation of Fe (III) ions that attack the mineral surfaces (Sand and Gehrke, 2006). As a result, the bacteria shaped pits on the black shale thick sections may be generated by the embedment of cells in the EPS.

The clustered secondary formations adjacent to pits or cells have a consistent morphological appearance with previously observed iron oxides generated by Fe- oxidizing bacteria (Malik et al., 2001; Mikkelsen et al., 2007). Indeed, the exoploymers of *Gallionella ferruginea,* an iron oxidizing, chemolithotrophic bacteria that lived in low-oxygen conditions was observed in the form of twisted Fe oxides stalk on the surface (Fig.

4.8). Microbes were usually encrusted with bacteriogenic iron oxide precipitate (Ehrlich, 2002). Observations of co-occurrence of cells and secondary formations may suggest the iron sulfide mineral utilization by microorganisms. One possibility is that the autotrophic microbes might produce these secondary formations by using iron sulfide as energy substrates.

Indeed, autotrophic microorganisms were detected within the biofilm of the arsenopyrite and pyrite minerals. Some of the sequences revealed high similarities to the sulfur and iron oxidizing microorganism species that belonged to Proteobacteria phylum. For example, ε-proteobacteria had been identified from the recovered 16*S* rDNA sequences from arsenopyrite biofilm. It is one of the dominant bacterial groups from some subaqueous sulfidic microbial mat communities (Engel et al., 2004). The most closely related species to our ε-proteobacteria that found in the arsenopyrite biofilm was *Sulfuricurvum kujiense*. This chemolithoautotrophic sulfur-oxidizing strain is able to use elemental sulfur, sulfide and thiosulfate as energy sources (Kodama and Watanabe, 2003).

Beta-proteobacteria is one of the major bacterial groups detected in acid mine drainage environment. The recovered 16*S* rDNA sequences that identified as β-proteobacteria were also detected in biofilms of both arsenopyrite and pyrite, including *Thiobacillus*, *Dechloromonas* and *Ferribacterium*. One of the closely related isolates of these sequences was within the genus of *Thiobacillus*. Most *Thiobacillus* species are thermophilic and acidophilic with several exceptions which only grow at neutral pH, and they are able to oxidize iron and inorganic sulfur compounds. Some other sequences were

found sharing high similarities to *Dechloromonas sp. HZ*, a chemoautotrophic facultative anaerobe (Zhang et al., 2002). Moreover, species in *Dechloromonas* genus have been observed with the ability of metabolizing Fe (II) coupled with perchlorate/chlorate (Weber et al., 2006). Sequence that closely related to *Ferribacterium* was also recognized in the iron sulfide mineral biofilm. One of the heterotrophic species in *Ferribacterium* was a dissimilatory Fe (III) reducing bacteria that capable of coupling the oxidation of acetate and other organic acids to the reduction of ferric iron (Cummings et al, 1999). However, although we observed the stalk structures on the surface of black shale that highly resembled to *Gallionella,* we did not find sequences that belong to this genus. The recognition of these microbes further supports the hypothesis that microbial activities were involved with iron and sulfur oxidation on the mineral surface.

Besides autotrophic bacteria, heterotrophs like iron reducers such as the *Ferribacterium*, were also recognized from the biofilm. Biogenic iron oxyhydroxide can be reduced by iron reducers when coupled with organic matter or other electron donors. δ-proteobacteria probably composed a predominant population (more than half of the analyzed sequences) in all three biofilms from pyrite, arsenopyrite and quartz sand. Some of the δ- proteobacteria were most closely related to *Geobacter* species in the *Geobacteraceae* family, which is one of the most predominant Fe (III) reducers in a variety of subsurface environments (Holmes et al., 2002). Generally speaking, δ-proteobacteria family could represent anaerobic iron reducing heterotrophs (Devereux et al., 1989; Lovley, 1997). It should be pointed out that in the well, iron reducing species like *Geobacter* and *Ferribacterium* may be supported by Fe oxides from the well casing, but the mineral

incubations were protected from falling debris by their plastic cups.

With EDS, it was observed that the secondary formations occurred on the surface of pyrite mineral on black shale thick sections were composed by Fe, S and O as well as other metals such as Ca and Mg. With a higher ratio of Fe/S compared to pure pyrite, these secondary formations on the surface of pyrite mineral were likely to be amorphous iron oxyhydroxide that transformed from pyrite. Given that the black shale thick sections were polished before deploying to the groundwater, they must have been formed during the incubation. From a biological view, the iron in the secondary formations may serve as the electron acceptors for heterotrophic microbial respiration. The energy source for these heterotrophs could come from the organic matter that were trapped by the biofilm on the iron sulfide mineral surface or from the groundwater. High dissolved iron concentration (825 μg/L) was detected in the studied groundwater well and aqueous Fe^{2+} should compose most of the dissolved iron with pH at around 4.8 and Eh at around -88 mV (Table 4.1). The occurrence of abundant ferrous iron in the Lockatong formation groundwater could be due to the reduction of solid secondary iron (III) minerals on black shale surfaces by *Geobacter* species over thousands of years.

Besides the Proteobacteria phylum, other bacteria were also recognized in the biofilm. For example, a sequence that was very closely related to Gram positive bacteria *Clostridium* was detected in quartz sand. Some strains such as *Clostridium butyricum* and *Clostridium beijerinckii* can respire Fe (III) heterotrophically and the latter preferably reduces amorphous Fe (O)OH to the crystalline forms (Dobbin et al., 1999; Munch and

Ottow, 1980).

Compared to the proteobacteria microorganisms identified at low pH acid mine conditions, of which most belong to the β and γ subdivisions (Bond et al., 2000; Hallberg et al., 2006; Yang et al., 2008), δ-proteobacteria was not often reported in acid mine drainage locations (Bond et al., 2000; Bruneel et al., 2006; Hao et al., 2007). Yet in our study, *Geobacter* was one of the dominant bacterial groups. This may be attributed to the presence of Fe (III), primarily as solid secondary minerals on black shale surfaces.

Moreover, if compared to the microbial community composition in the black shale at other locations, such as the New Albany shale in Clay City, Kentucky, USA, *Dechloromonas* in the β-proteobacteria family was also identified as well as the Gram+ eubacteria, *Clostridium* from the black shale, which was in agreement with our study. However, γ-proteobacteria were also recognized, similar to the acid mine drainage microbial community, probably due to the high weathering rates of the pyrite in local black shale as very acidic water was identified from the weathering profile. Similar to most of the acid mine studies, no δ-proteobacteria was detected (Pestch et al, 2005).

4.5 Conclusion and implications

Iron is the fourth most abundant elements in earth's crust, the redox reaction of iron is critical to support some of the microbial activities in soil, sediments and aqueous environments. Ferrous iron can be used as electron donor or source of energy under oxic or

anoxic conditions and ferric iron can function as an electron acceptor in anaerobic respiration. The oxidation and reduction of iron are important components of iron cycling in the biosphere which controls the mobilization of iron and accumulation of iron as secondary formations. It is now accepted that microbial metabolism primarily controls iron redox chemistry in most environments (Weber et al., 2006).

Autotrophs such as sulfur and iron oxidizing microorganisms were hypothesized to exist in the biofilm of iron sulfide minerals because of the low organic carbon concentration in groundwater. Indeed, 16*S* rDNA from sulfide mineral biofilms had sequences that sharing high similarities to autotrophic bacteria such as *Sulfuricurvum kujiense*, *Dechloromonas sp. HZ* and *Thiobacillus*. Metal sulfide oxidation is the main energy-delivering process for these autotrophic microorganisms (Kock and Schippers, 2008). Yet, with the formation of the biofilm and extracellular polymeric substances, organic matter may be trapped within the biofilm. Upon the secondary formation of iron (oxy) hydroxide by the autotrophs, it is likely that heterotrophic microorganisms may use the trapped organic matter as electron donors in dissimilatory Fe (III) reduction. Iron reducing microorganisms with sequences of 99% to 100% similarities to *Geobacter sp*. were detected in the biofilms of all three solids and their existence may be explained by this process. However, one thing to notice is that the iron casing of the well may be rusted over time and contribute to the existence of iron hydroxide in the well.

The identification of diverse groups of bacteria from pyrite, arsenopyrite and quartz sand biofilms may well exemplify the structure of microbial communities that inhabit

subsurface environments containing iron sulfide minerals at slightly acidic pH. Several redox processes including iron sulfide oxidation, Fe (III) reduction may occur within various microenvironments or during different time periods given the appropriate environmental conditions such as pH and oxygenation. The influence of microbiological activities on iron and sulfur geochemistry has long been recognized for its importance at the very low pH environment. This study indicates that microbes may also play an essential role in the transformation of iron sulfides and their secondary formations in the underlying substrata at slightly acidic pH condition. Moreover, the microbial activities may also raise environmental concerns, for example, the iron reducers may help arsenic releasing from arsenic absorbing or bearing solid phases such as iron oxides to groundwater (Kelly et al., 2005). Further investigation of the ecology and biochemistry of microbial transformation of iron minerals under such conditions might help us to better understand the natural factors controlling this process.

Table 4.1. Groundwater chemistry of NAWC well 33BR

Parameter	Value
pH	4.6~4.8
DO	2.5~2.7 mg/L
Eh	-88~-83 mV
Ca	56 mg/L
Mg	21 mg/L
Na	22 mg/L
K	2.5 mg/L
Fe	0.825 mg/L
Mn	0.555 mg/L
Ba	0.2 mg/L
SO_4^{2-}	26 mg/L
NO_3^-	0.2 mg/L
Cl^-	53 mg/L
$S2^-$	0.035 mg/L
As (total)	2 µg/L

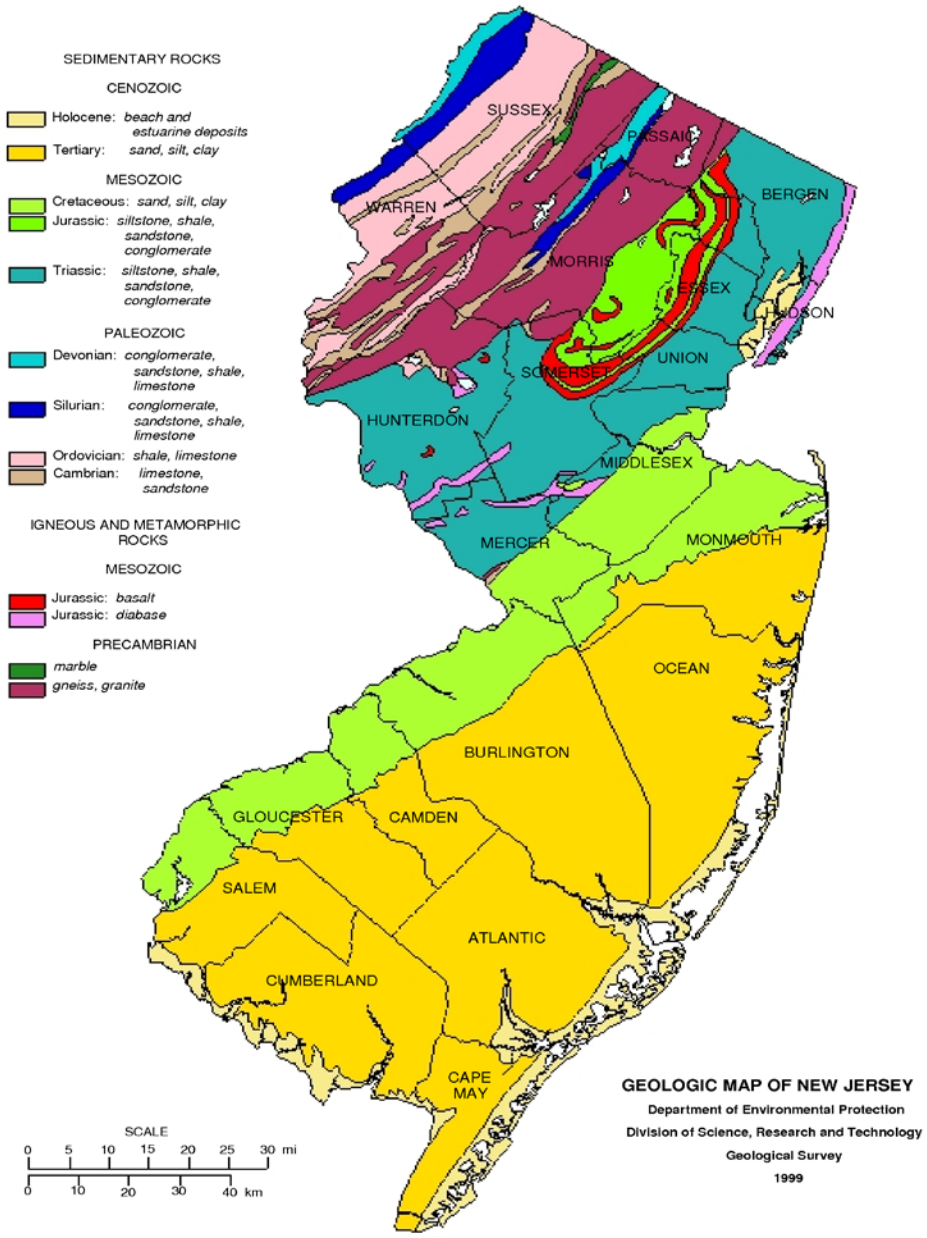

Figure 4.1. Geological map of New Jersey http://www.state.nj.us/dep/njgs/

Figure 4.2. Air view of the Naval air warfare center. Red circle indicated the sampling and deploy well.

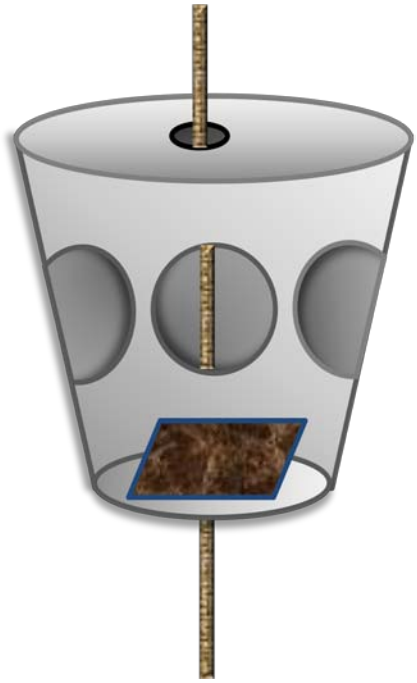

Figure 4.3. Apparatus of sample deployment to the Naval air warfare center well.

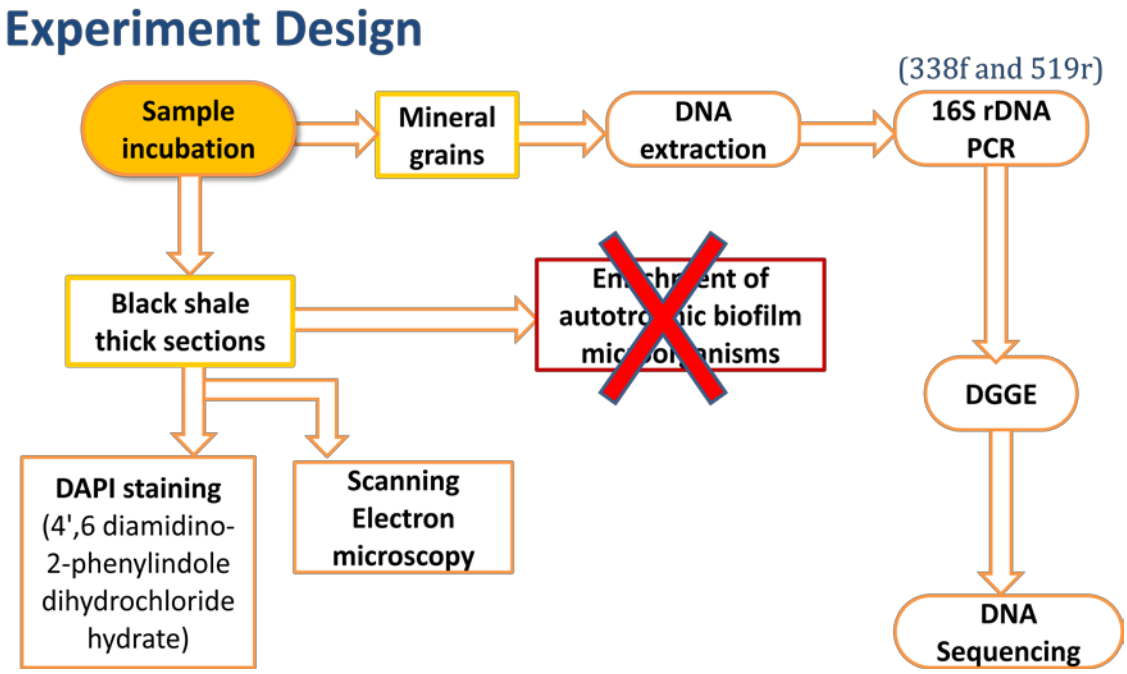

Figure 4.4. Experimental design of the investigation regarding microbial colonization on the pyritic black shale

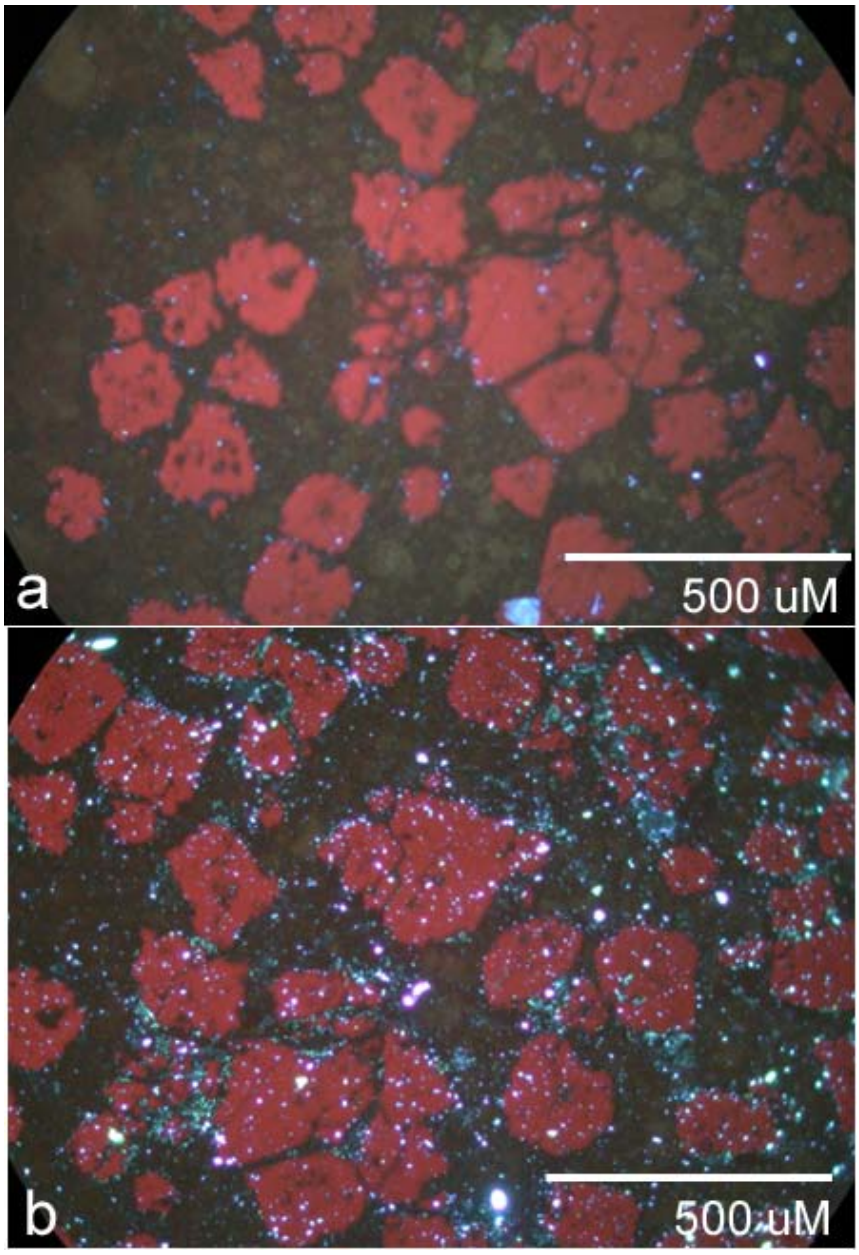

Figure 4.5. Comparison among DAPI Staining of black shale thick sections with square pyrite grains shown with red fluorescence.

a) Sterilized black shale thick section without DAPI staining

b) Sterilized black shale thick section with DAPI staining

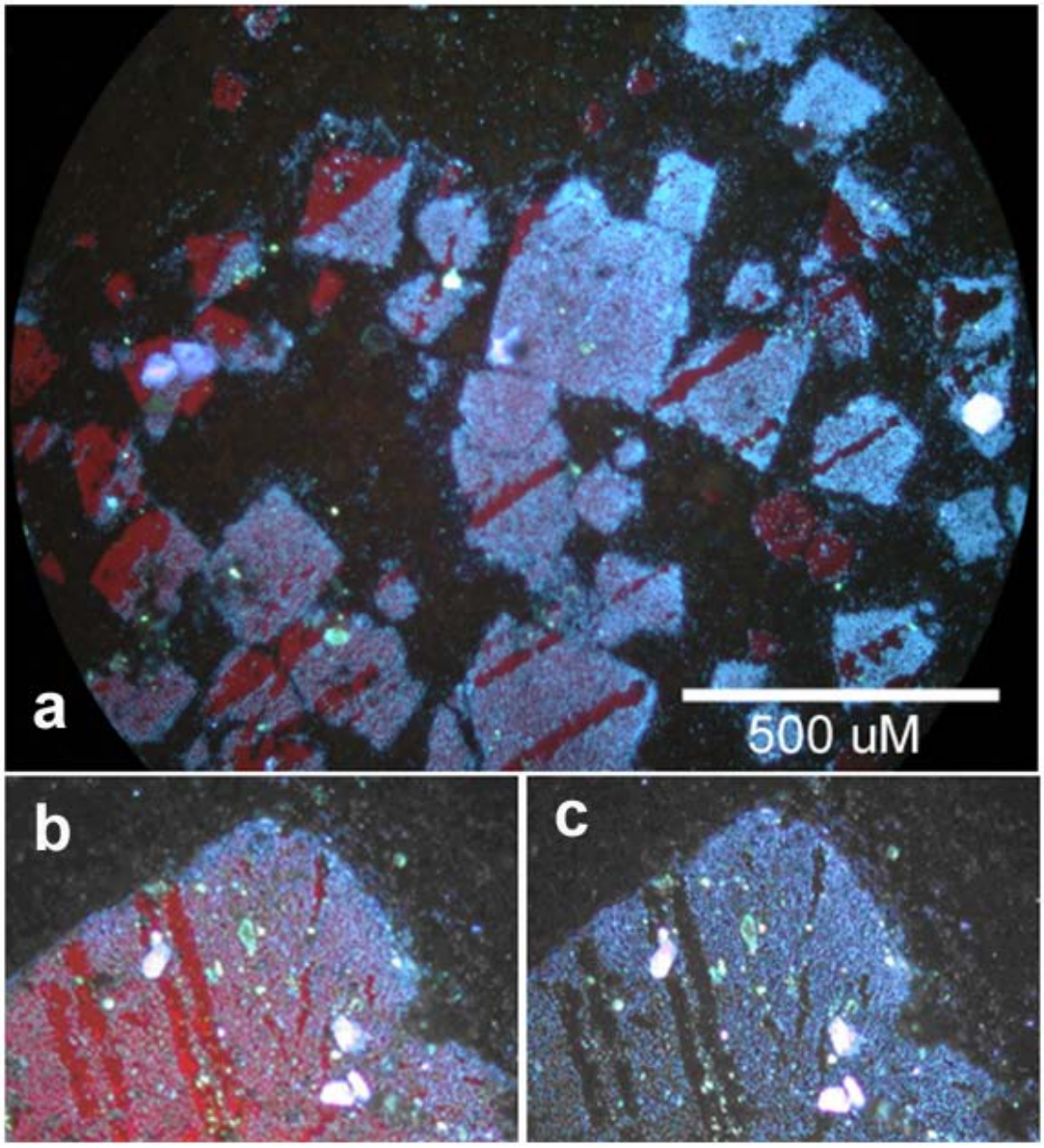

Figure 4.6. DAPI staining of microorganisms colonized on black shale thick sections. Red areas are the pyrite and the shale matrix is dark.

Above, small pyrite grains attract microbial colonization relative to shale matrix. Below left, pyrite mineral surface shown with red autofluorescence.Below right, pyrite mineral surface with red fluorescence filtered out.

Figure 4.7. Scanning electron microscopy observation of biofilm–cells were embedded within EPS and more associated with pyrite than shale matrix.

a) Preference of microbes colonized on pyrite mineral to shale matrix

b) Cells embedded with EPS, as indicated by red circle

c) Bacteria shaped pit

d) Embedded cells and adjacent secondary mineral cluster

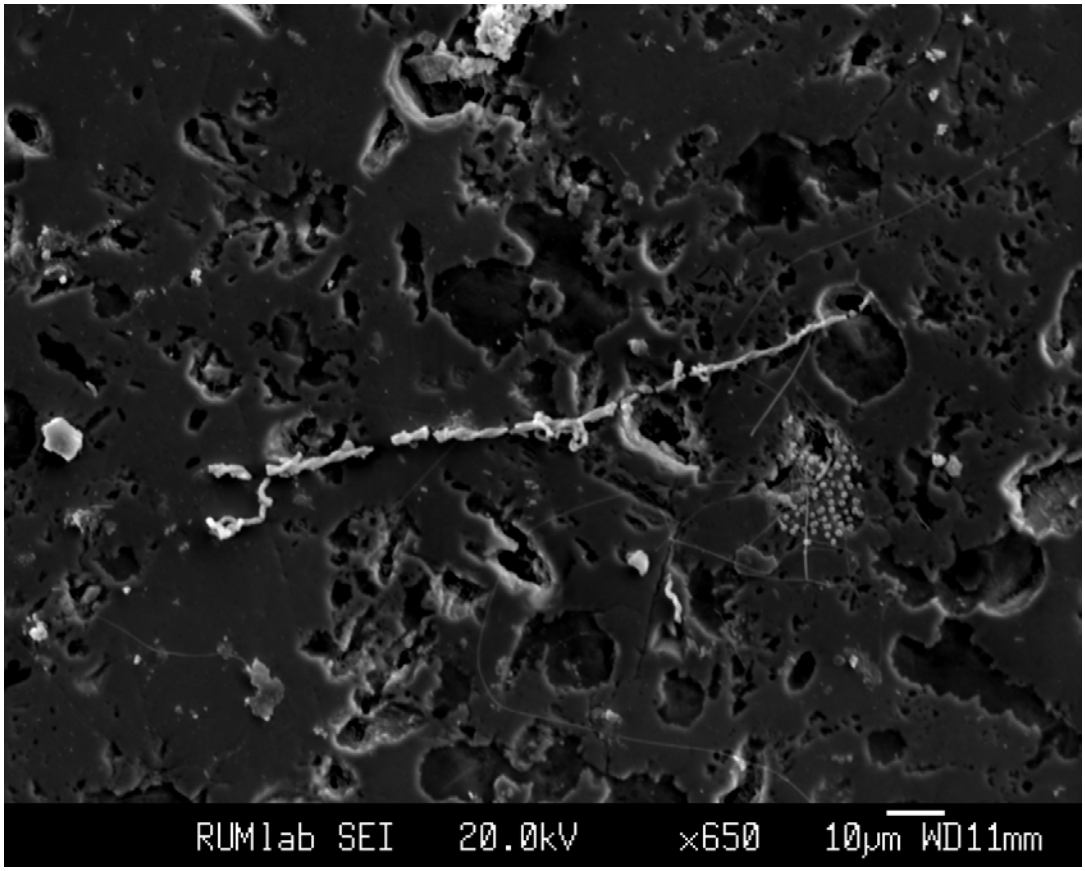

Figure 4. 8. SEM image of the exopolymers from *G. ferruginea* on the black shale thick section incubated in groundwater

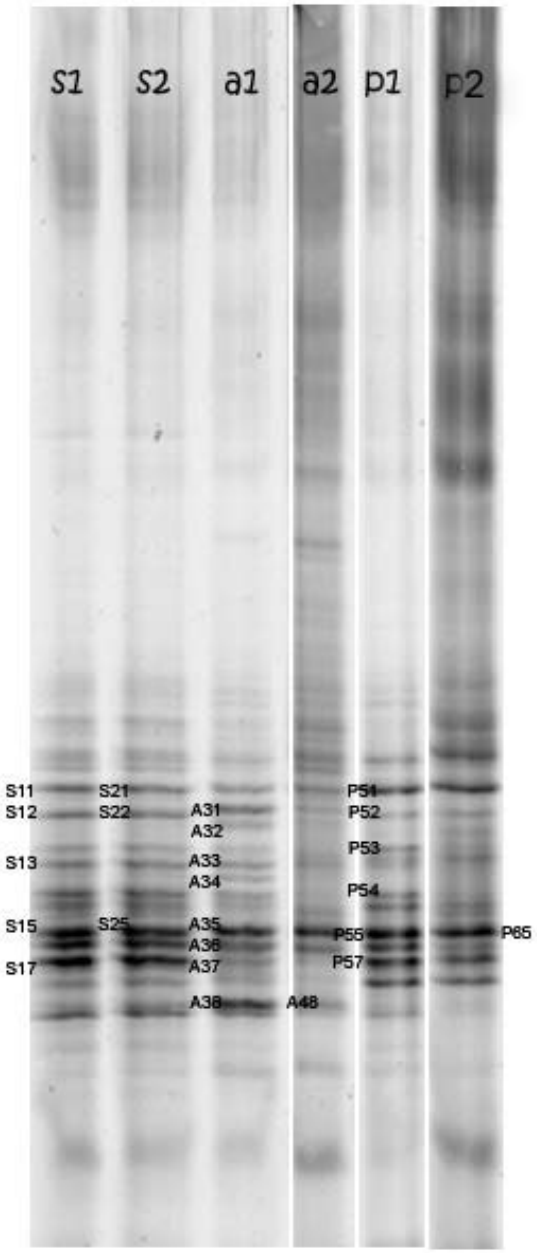

Figure 4.9. DGGE (30% to 80%, 55V, 16h) profile of PCR amplified 16*S* rDNA gene products. The letters represented different bands showed in the figure.

Table 4.3 The phylogenetic position of each band excised from DGGE

	Bands	Phylogenetic position
Arsenopyrite	A34	ε-proteobacteria
	A31, A48	β-proteobacteria
	A33, A35, A38	δ-proteobacteria
Pyrite	P54	β-proteobacteria
	P51,P52,P53,P55,P57,P65	δ-proteobacteria
Quartz sand	S11,S21,S13,S15,S17,S25	δ-proteobacteria
	S12,S22	Gram + eubacteria

Table 4.2. Bacteria detected from biofilms attached to pyrite, arsenopyrite minerals and quartz sand in the subsurface well.

Mineral	Similarity (%)	Nearest Relative (a)	Phylogenetic position	Physiology of Nearest Relative
Arsenopyrite	100%	*Sulfuricurvum kujiense* (b)	Epsilon proteobacteria	Sulfide oxidizing, Autotroph
	93%	*Dechloromonas sp. HZ*	Beta proteobacteria	Hydrogen oxidizing Chemolithoautrophic
	97%	*Thiobacillus*	Beta proteobacteria	Sulfur, iron oxidizing Autotroph
	96%	Uncultured *Ferribacterium sp.*	Beta proteobacteria	Fe(III) reduction Heterotroph
	100%	*Geobacter sp.*	Delta proteobacteria	NO_3^-, Mn(IV), Fe(III) reduction Heterotroph
Pyrite	93%	*Dechloromonas sp. HZ* (c)	Beta proteobacteria	Hydrogen oxidizing Chemolithoautroph
	97%	*Thiobacillus*	Beta proteobacteria	Sulfur, iron oxidizing Autotroph
	100%	*Geobacter sp.*	Delta proteobacteria	NO_3^-, Mn(IV), Fe(III) reduction Heterotroph
Sand	92%	*Clostridium*	Gram+ Eubacteria	Anaerobic, Fermentative
	99%	*Geobacter sp.*	Delta proteobacteria	NO_3^-, Mn(IV), Fe(III) reduction Heterotroph

(a) Based on phylogenetic relationship shown in Fig 4.9 and on BlastN analyzed using GenBank database

(b) From (Kodama and Watanabe, 2003)

(c) From (Zhang et al., 2002)

References

Baker B. J. and Banfield J. F. (2003) Microbial communities in acid mine drainage. *Fems Microbiology Ecology* 44(2), 139-152.

Bond P. L. and Banfield J. F. (2001) Design and performance of rRNA targeted oligonucleotide probes for in situ detection and phylogenetic identification of microorganisms inhabiting acid mine drainage environments. *Microbial Ecology* 41(2), 149-161.

Bond P. L., Smriga S. P., and Banfield J. F. (2000) Phylogeny of Microorganisms Populating a Thick, Subaerial, Predominantly Lithotrophic Biofilm at an Extreme Acid Mine Drainage Site. *Appl. Environ. Microbiol.* 66(9), 3842-3849.

Bruneel O., Duran R., Casiot C., Elbaz-Poulichet F., and Personne J. C. (2006) Diversity of Microorganisms in Fe-As-Rich Acid Mine Drainage Waters of Carnoules, France. *Appl. Environ. Microbiol.* 72(1), 551-556.

Chapelle F. H. and Lovley D. R. (1992) Microbial Fe(III) Reduction Coupled to Organic Material Oxidation - a Mechanism for the Development of High Iron Concentrations in Ground-Water. *Abstracts of Papers of the American Chemical Society* 203, 148-GEOC.

Chaudhuri S. K., Lack J. G., and Coates J. D. (2001) Biogenic Magnetite Formation through Anaerobic Biooxidation of Fe(II). *Appl. Environ. Microbiol.* 67(6), 2844-2848.

Coates J., Ellis D., Gaw C., and Lovley D. (1999) Geothrix fermentans gen. nov., sp. nov., a novel Fe(III)-reducing bacterium from a hydrocarbon-contaminated aquifer. *International journal of systematic bacteriology.* 49(4), 1615-22.

Cummings D. E., Caccavo Jr F., Spring S., and Rosenzweig R. F. (1999) Ferribacterium limneticum, gen. nov., sp. nov., an Fe(III)-reducing microorganism isolated from mining-impacted freshwater lake sediments. *Archives of Microbiology* 171(3), 183-188.

Devereux R., Delaney M., Widdel F., and Stahl D. A. (1989) Natural relationships among sulfate-reducing eubacteria. *J. Bacteriol.* 171(12), 6689-6695.

Dobbin P. S., Carter J. P., Garc-Salamanca San Juan C., von Hobe M., Powell A. K., and Richardson D. J. (1999) Dissimilatory Fe(III) reduction by Clostridium beijerinckii isolated from freshwater sediment using Fe(III) maltol enrichment. *FEMS Microbiology Letters* 176(1), 131-138.

Edwards K. J. (2004) Formation and degradation of seafloor hydrothermal sulfide deposits. *Sulfur Biogeochemistry: Past and Present* 379(0), 83-96.

Edwards K. J., Bond P. L., and Banfield J. F. (2000) Characteristics of attachment and growth of *Thiobacillus caldus* on sulphide minerals: a chemotactic response to sulphur minerals? *Environmental Microbiology* 2(3), 324-332.

Edwards K. J., Goebel B. M., and Rodgers T. M., et al. (1999) Geomicrobiology of Pyrite (FeS2) Dissolution: Case Study at Iron Mountain, California. *Geomicrobiology Journal* 16, 155-179.

Edwards K. J., McCollom T. M., Konishi H., and Buseck P. R. (2003a) Seafloor bioalteration of sulfide minerals: results from in situ incubation studies. *Geochimica et Cosmochimica Acta* 67(15), 2843-2856.

Edwards K. J., Rogers D. R., Wirsen C. O., and McCollom T. M. (2003b) Isolation and characterization of novel psychrophilic, neutrophilic, Fe-oxidizing, chemolithoautotrophic alpha- and, gamma-Proteobacteria from the deep sea. *Applied and Environmental Microbiology* 69(5), 2906-2913.

Ehrlich H. L. (2002) 15. Geomicrobiology of Iron. In *Geomicrobiology*. Marcel Dekker, Inc.

Engel A. S., Porter M. L., Stern L. A., Quinlan S., and Bennett P. C. (2004) Bacterial diversity and ecosystem function of filamentous microbial mats from aphotic (cave) sulfidic springs dominated by chemolithoautotrophic "Epsilonproteobacteria". *FEMS Microbiology Ecology* 51(1), 31-53.

Flynn T.M., Sanford R.A., and Bethke C.M.(2008) Attached and suspended microbial communities in a pristine confined aquifer. *Water Resour. Res.* 44.

Hallberg K. B., Coupland K., Kimura S., and Johnson D. B. (2006) Macroscopic Streamer Growths in Acidic, Metal-Rich Mine Waters in North Wales Consist of Novel and Remarkably Simple Bacterial Communities. *Appl. Environ. Microbiol.* 72(3), 2022-2030.

Hao C., Zhang H., Haas R., Bai Z., and Zhang B. (2007) A Novel Community of Acidophiles in an Acid Mine Drainage Sediment. *World Journal of Microbiology and Biotechnology* 23, 15-21.

Harneit K., Goksel A., Kock D., Klock J. H., Gehrke T., and Sand W. (2006) Adhesion to metal sulfide surfaces by cells of *Acidithiobacillus ferrooxidans, Acidithiobacillus thiooxidans* and *Leptospirillum ferrooxidans*. *Hydrometallurgy* 83(1-4), 245-254.

Hazeu W., Bijleveld W., Grotenhuis J. T. C., Kakes E., and Kuenen J. G. (1986) Kinetics and energetics of reduced sulfur oxidation by chemostat cultures of *Thiobacillus ferrooxidans*. *Antonie van Leeuwenhoek* 52(6), 507-518.

Holmes D. E., Finneran K. T., O'Neil R. A., and Lovley D. R. (2002) Enrichment of members of the family Geobacteraceae associated with stimulation of dissimilatory metal reduction in uranium-contaminated aquifer sediments. *Applied and Environmental Microbiology* 68(5), 2300-2306.

Weber K.A., Urrutia M.M., Churchill P.F., Kukkadapu R. K., Roden E. E., (2006) Anaerobic redox cycling of iron by freshwater sediment microorganisms. *Environmental Microbiology* 8(1), 100-113.

Kelly W. R., Holm T. R., Wilson S. D., and Roadcap G. S. (2005) Arsenic in Glacial Aquifers: Sources and Geochemical Controls. *Ground Water* 43(4), 500-510.

Kock D. and Schippers A. (2008) Quantitative Microbial Community Analysis of Three Different Sulfidic Mine Tailing Dumps Generating Acid Mine Drainage. *Appl. Environ. Microbiol.* 74(16), 5211-5219.

Kodama Y. and Watanabe K. (2003) Isolation and Characterization of a Sulfur-Oxidizing Chemolithotroph Growing on Crude Oil under Anaerobic Conditions. *Appl. Environ. Microbiol.* 69(1), 107-112.

Konhauser K. (2006) Microbial Weathering. In *Introduction to Geomicrobiology*, pp. 192-234. Blackwell Publishing.

Lack J. G., Chaudhuri S. K., Chakraborty R., Achenbach L. A., and Coates J. D. (2002) Anaerobic Biooxidation of Fe(II) by Dechlorosoma suillum. *Microbial Ecology* 43(4), 424-431.

Lovley D. R. (1995) Microbial Reduction of Iron, Manganese, and Other Metals. *Advances in Agronomy, Vol 54* 54, 175-231.

Lovley D. R. (1997) Microbial Fe(III) reduction in subsurface environments. *Fems Microbiology Reviews* 20(3-4), 305-313.

Lovley D. R. (2001) Reduction of iron and humics in subsurface environments. In *Subsurface Microbiology and Biogeochemistry* (ed. J. K. Fredrickson and M. Fletcher), pp. 193-217. Wiley-Liss, Inc.

Lovley D. R., Holmes D. E., Nevin K. P., and Poole. (2004) Dissimilatory Fe(III) and Mn(IV) Reduction. In *Advances in Microbial Physiology*, Vol. Volume 49, pp. 219-286. Academic Press.

Maidak B. L., Cole J. R., Parker C. T., Jr., Garrity G. M., Larsen N., Li B., Lilburn T. G., McCaughey M. J., Olsen G. J., Overbeek R., Pramanik S., Schmidt T. M., Tiedje J. M., and Woese C. R. (1999) A new version of the RDP (Ribosomal Database Project). *Nucl. Acids Res.* 27(1), 171-173.

Malik A., Dastidar M. G., and Roychoudhury P. K. (2001) Biodesulphurization of coal: Mechanism and rate limiting factors. *Journal of Environmental Science and Health Part a-Toxic/Hazardous Substances & Environmental Engineering* 36(6), 1113-1128.

Malki M., Gonzez-Toril E., Sanz J. L., Gez F., Rodruez N., and Amils R. (2006) Importance of the iron cycle in biohydrometallurgy. *Hydrometallurgy* 83(1-4), 223-228.

McCollom T. M. (2000) Geochemical constraints on primary productivity in submarine hydrothermal vent plumes. *Deep Sea Research Part I: Oceanographic Research Papers* 47(1), 85-101.

Meyer G., Waschkies C., and Huttl R. F. (1999) Investigations on pyrite oxidation in mine spoils of the Lusatian lignite mining district. *Plant and Soil* 213(1-2), 137-147.

Mikkelsen D., Kappler U., Webb R. I., Rasch R., McEwan A. G., and Sly L. I. (2007) Visualisation of pyrite leaching by selected thermophilic archaea: Nature of microorganism-ore interactions during bioleaching. *Hydrometallurgy* 88(1-4), 143-153.

Munch J. and Ottow J. (1980) Preferential reduction of amorphous to crystalline iron oxides by bacteria activity. *Soil Science* 129(1), 15-21.

Petsch S.T., Edwards K. J., and Eglinton T.I. (2005) Microbial transformation of organic matter in black shales and implications for global biogeochemical cycles. *Palaeogeography, Palaeoclimatology, Palaeoecology* 219(1-2), 157-170

Rodriguez Y., Ballester A., Blazquez M. L., Gonzalez F., and Munoz J. A. (2003a) New information on the pyrite bioleaching mechanism at low and high temperature. *Hydrometallurgy* 71(1-2), 37-46.

Rodriguez Y., Ballester A., Blizquez M. L., Gonzilez F., and Muioz J. A. (2003b) Study of Bacterial Attachment During the Bioleaching of Pyrite, Chalcopyrite, and Sphalerite. *Geomicrobiology Journal* 20(2), 131.

Sand W. and Gehrke T. (2006) Extracellular polymeric substances mediate bioleaching/biocorrosion via interfacial processes involving iron(III) ions and acidophilic bacteria. *Research in Microbiology* 157(1), 49-56.

Sand W., Gerke T., Hallmann R., and Schippers A. (1995) Sulfur Chemistry, Biofilm, and the (in)Direct Attack Mechanism - a Critical-Evaluation of Bacterial Leaching. *Applied Microbiology and Biotechnology* 43(6), 961-966.

Schippers A., Rohwerder T., and Sand W. (1999) Intermediary sulfur compounds in pyrite oxidation: implications for bioleaching and biodepyritization of coal. *Applied Microbiology and Biotechnology* 52(1), 104-110.

Schippers A. and Sand W. (1999) Bacterial Leaching of Metal Sulfides Proceeds by Two Indirect Mechanisms via Thiosulfate or via Polysulfides and Sulfur. *Appl. Environ. Microbiol.* 65(1), 319-321.

Tamura K, Dudley J, Nei M & Kumar S (2007) MEGA4: Molecular Evolutionary Genetics Analysis (MEGA) software version 4.0. Molecular Biology and Evolution 24: 1596-1599.

Toner B. M., Santelli C. M., Marcus M. A., Wirth R., Chan C. S., McCollom T., Bach W., and Edwards K. J. (2009) Biogenic iron oxyhydroxide formation at mid-ocean ridge hydrothermal vents: Juan de Fuca Ridge. *Geochimica et Cosmochimica Acta* 73(2), 388-403.

Weber K. A., Achenbach L. A., and Coates J. D. (2006) Microorganisms pumping iron: anaerobic microbial iron oxidation and reduction. *Nat Rev Micro* 4(10), 752-764.

Yang Y., Shi W., Wan M. Z., Y.; , Zou L., Huang J., Qiu G., and Liu X. (2008) Diversity of bacterial communities in acid mine drainage from the Shen-bu copper mine, Gansu province, China. *Electronic Journal of Biotechnology [online]*. 11(1).

Zhang H., Bruns M. A., and Logan B. E. (2002) Perchlorate reduction by a novel chemolithoautotrophic, hydrogen-oxidizing bacterium. *Environmental Microbiology* 4(10), 570-576.

CHAPTER 5

SUMMARY AND CONCLUSIONS

5.1 Summary

The investigation of pyrite depositional environment in the Newark Basin Lockatong formation began with the quantification of reduced inorganic sulfur species in the black shale. Both pyrite and acid volatile sulfur were quantified and pyrite was determined to be the most abundant species in total sulfur (more than 50%). A strong positive correlation was observed between total sulfur and pyritic sulfur while an inverse relationship was identified between pyritic sulfur and acid volatile sulfur at different depths. Inverse relationships were revealed between Th/U, which was proportional to redox potential, and pyritic S and positive correlations were found between Th/U and acid volatile S from their depth profiles. These results show that the oxygenation condition was one of the controlling factors for the deposition of different sulfur species in the Newark Basin sedimentary environments.

The trace metal enrichment factors were analyzed and arsenic and molybdenum were two highly enriched elements observed in the black shale. Further analysis showed that the arsenic content was closely linked to pyrite and molybdenum was associated with organic matter. This observation shed light on the original residences of these trace metals and in turn may help to evaluate their mobilization patterns to the aqueous phase. It was observed that the abundance of arsenic was positively correlated to molybdenum in the Lockatong formation black shale. Positive correlation between the two was also

showed in the groundwater of a Passaic formation well, which composed mostly by red shale that has much lower abundance of arsenic and molybdenum compare to black shale. However, no correlations were found between the two trace elements from our red shale elemental analysis. Combine this with the previous observation, it implicates that the black shale may be the ultimate source of arsenic and molybdenum and the weathering of black shale may lead to their mobilization from solid phases.

Although the pyritic black shale appears to be the ultimate source of arsenic to the groundwater in sedimentary rock aquifers, the mechanism of arsenic mobilization is unclear. Arsenic mobilization from solid phases could occur via abiotic and/or biotic pathways. In chapter 3, our results indicated that a sulfide-arsenide exchange and oxidation reaction may drive arsenic mobilization from sedimentary rock pyrites. The redox stoichiometry of sulfide-arsenide exchange indicates that if sulfide is present, arsenic may be mobilized from arsenopyrite and arsenic-rich pyrite only when an oxidant is available. In natural groundwater, Fe (III), Mn (IV) or nitrate could serve as oxidants in sulfide-driven arsenic mobilization in the absence of oxygen. Arsenic mobility in fractured rock aquifers containing pyritic black shale will therefore be determined in part by the concentrations of sulfide and available oxidant. Such conditions of redox disequilibrium occur in confined aquifers where oxygenation rates are slow and hypoxic and anoxic groundwaters mix.

The sulfide in groundwater that may mobilize arsenic from pyritic black shale may be of biological origin. Sulfide can be generated at the boundary of oxidizing and

reducing environments that support sulfate reducing bacteria (SRB). Therefore, the arsenic-sulfide exchange mechanism is likely an indirect biological pathway. Yet, direct biological pathways of weathering pyrite and releasing the incorporated arsenic may also be one of the important mechanisms for arsenic mobilization.

It is now accepted that microbial metabolism primarily controls iron redox chemistry in most environments (Weber et al., 2006). Microbial activities can catalyze iron sulfide mineral oxidation and the redox reactions of iron and sulfur are in turn critical to the growth and metabolism of many autotrophic and heterotrophic microbes. We examined the biofilm that formed on pyrite containing black shale thick sections hincubated in subsurface groundwater in the Newark Basin. Close association between microorganisms and the pyrite mineral was observed by DAPI staining and SEM. Further, the biofilm formed on the pyrite and arsenopyrite minerals were extracted and the 16*S* rDNA of the microbial consortia were obtained and sequenced. High similarities of some of the sequences to the autotrophic bacteria in the proteobacteria phylum such as *Sulfuricurvum kujiense*, *Dechloromonas sp. HZ* and *Thiobacillus* were observed. Moreover, iron reducers with sequences of 99% to 100% similarities to *Geobacter sp*. were detected in the biofilm on the iron sulfide minerals. They may utilize the trapped organic matter as electron donors in dissimilatory Fe (III) reduction, where the Fe (III) may be generated from iron sulfide oxidation. The identification of diverse groups of bacteria from the iron sulfide mineral biofilms may well exemplify the structure of microbial communities that inhabit subsurface environments with slightly aciditic pH where such microbes may be important drivers of iron and sulfur cycling.

Fig 5.1 illustrates the important subsurface redox reactions described in chapter 3 H(the sulfide-arsenide exchange reaction) and chapter 4 (microbial catalyzed iron redox processes). Given the appropriate environmental conditions such as pH and oxygenation, these redox reactions may take place within various microenvironments or during different time periods and become very important components in the local geochemistry of iron, sulfur or trace elements such as arsenic.

5.2 Conclusions

Several conclusions can be drawn from this study. In the first research chapter, we observed that the oxygenation condition is one of the controlling factors for different sulfur species deposition in the sedimentary environment and also identified the residences for enriched arsenic and molybdenum in the black shale (pyrite and organic matter, respectively). These results suggest that As and Mo may be useful proxies for pyritic S and organic carbon deposition. In the second research chapter, arsenic was found to be mobilized by the presence of dissolved sulfide and low levels of oxygen from arsenic containing solid phases such as arsenopyrite and arsenian pyrite. This process will be most important in the anoxic-oxic groundwater interface and the release of arsenic may be of local environmental concern. The third research chapter investigated the microbial consortia colonized on the surface of pyritic minerals. Both autotrophic and heterotrophic bacteria were identified from the biofilm and they may play an important role in the iron and sulfur cycles in the subsurface aqueous and solid phases.

5.3 Suggested future researches

Natural environments are highly variable and the control of the biogeochemistry of Fe, S and trace elements may occur via many different means. More research is needed of subsurface water and rock interactions as well as the impact of microbial activities on the subsurface environment. The following questions/issues should be addressed in future research:

1. Studies of the weathering of black shale with oxidants as to leach arsenic and molybdenum from the solid which may help to answer the question of whether the oxidation of pyrite and organic carbon take place simultaneously or in a certain sequence. It may further confirm or dispute if black shale is the source for arsenic and molybdenum recognized in the Newark Basin wells.

2. The spacial distribution and quantification of trace elements on the pyritic black shale thick sections may be further investigated and mapped. High resolution instruments can be applied for this application (WDS- wavelength dispersive spectroscopy). This may provide us with the information of specific trace elemental residences in the black shale.

3. The weathering of pyrite is of particular interest for its global importance. The consumption of oxygen by pyrite weathering may compete with organic matter in sedimentary shales upon exposure to the atmosphere (Petsch, 2003). The effort of quantifying pyrite weathering globally is important to our understanding of the global oxygen budget.

4. Investigation of the physiological and ecological role of each species of microorganism that colonize black shale pyrite and form the resulting biofilm to determine their own functionalities in iron and sulfur geochemistry of the subsurface environment.

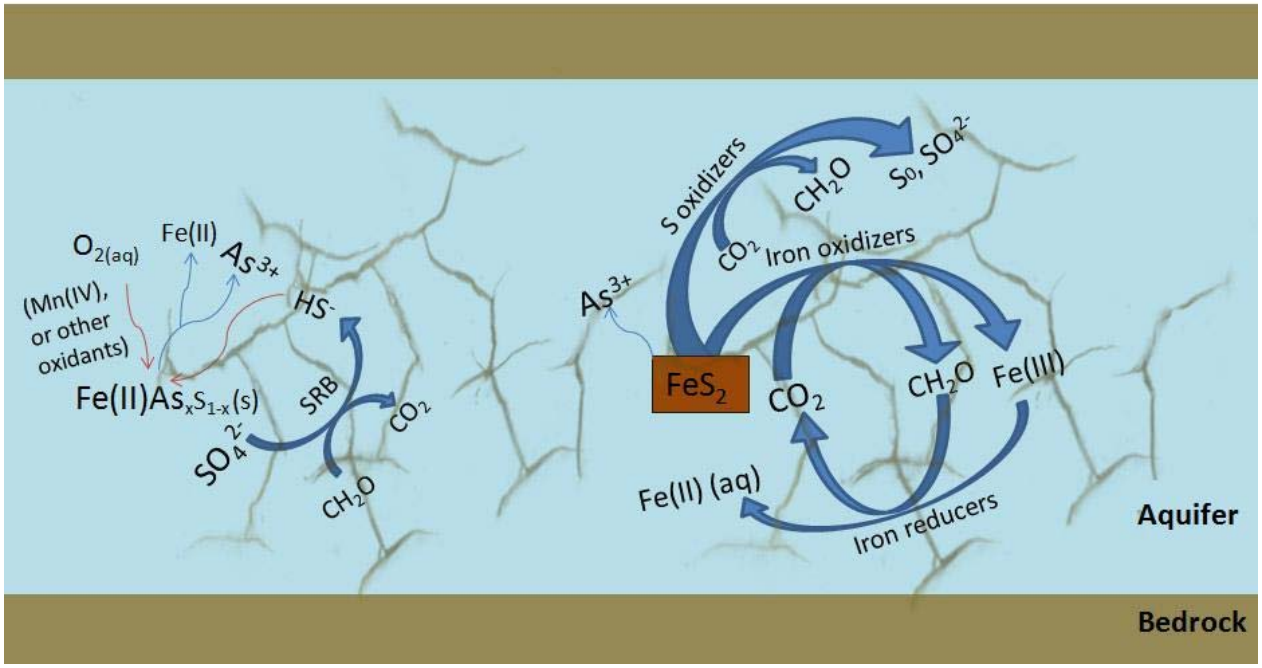

Figure 5.1. The subsurface iron and arsenic geochemistry, illustrated for the redox reactions described in this dissertation.

References

Kelly W. R., Holm T. R., Wilson S. D., and Roadcap G. S. (2005) Arsenic in Glacial Aquifers: Sources and Geochemical Controls. *Ground Water* 43(4), 500-510.

Kock D. and Schippers A. (2008) Quantitative Microbial Community Analysis of Three Different Sulfidic Mine Tailing Dumps Generating Acid Mine Drainage. *Appl. Environ. Microbiol.* 74(16), 5211-5219

Serfes M.E. (2005) Arsenic Occurrence, Sources, Mobilization, Transport and Prediction in the Major Bedrock Aquifers of the Newark Basin, Rutgers University (PhD dissertation)

Tuttle M. L. W., Breit G. N., and Goldhaber M. B. Weathering of the New Albany Shale, Kentucky: II. Redistribution of minor and trace elements. *Applied Geochemistry* In Press, Corrected Proof.

Weber K.A., Achenbach L.A., and Coates J.D. (2006) Microorganisms pumping iron: anaerobic microbial iron oxidation and reduction. *Nat Rev Micro* 4(10), 752-764

APPENDIX I

SAMPLE ID	Core Box	Shallow Depth (ft)	Deeper Depth (ft)	Color	Ag ppm	Al %	As ppm	Ba ppm	Be ppm	Bi ppm	Ca %	Cd ppm
NBL1	299	2999.4	2999.8	Black	0.11	7.04	20.6	390	1.82	0.46	4.97	0.16
NBL2	299	2994.0	2994.4	red	0.02	9.82	4.5	400	3.82	0.6	0.5	0.02
NBL3	299	3001.7	3002.1	Black	0.11	7.94	34.4	320	2.34	0.47	4.28	0.07
NBL4	298	2993.7	2994.0	red	0.04	10.05	5.9	450	4.38	0.97	0.22	<0.02
NBL5	298	2985.0	2985.5	red	0.02	7.73	2.4	310	2.46	0.44	2.27	0.05
NBL6	137	1538.6	1539.0	Black	0.05	8.54	23.0	400	2.46	0.26	3.51	0.09
NBL7	137	1539.8	1540.2	Black	0.04	8.46	9.9	320	2.81	0.42	3.8	<0.02
NBL8	141	1573.2	1573.6	red	<0.01	9.2	0.7	610	2.74	0.55	1.98	0.03
NBL9	142	1588.7	1589.0	red	<0.01	8.97	0.6	480	3.91	0.29	0.94	0.02
NBL10	140	1568.2	1568.7	grey-black	0.04	8.22	**0.1**	620	2.38	0.27	6.38	0.02
NBL11	140	1571.0	1571.4	grey-black	0.03	10.15	7.0	560	4.24	0.65	1.06	<0.02
NBL12	142	1583.2	1583.5	red	0.02	9.04	**0.1**	540	3.36	0.47	1.41	<0.02
NBL13	141	1580.6	1581.0	red	0.03	9.86	1.2	590	3.62	0.66	1.12	<0.02
NBL14	24	527.6	528.0	grey	<0.01	9.21	8.6	410	3.44	0.26	1.36	0.04
NBL15	24	521.6	522.0	red	<0.01	8.9	0.6	550	2.93	0.34	1.98	<0.02
NBL16	28	560.5	560.9	grey-black	0.04	8.37	7.7	310	2.59	0.39	3.17	<0.02
NBL17	25	530.6	531.0	grey-black	0.06	9.09	5.5	460	2.97	0.16	1.56	0.03
NBL18	24	524.6	525.0	red	<0.01	9.35	0.9	530	3.64	0.33	1.4	0.02
NBL19	28	563.5	564.0	grey	<0.01	9.4	25.7	980	1.58	0.36	1.12	0.06
NBL20	25	534.0	534.4	Black	0.05	8.34	16.5	480	1.19	0.4	5.14	0.02

SAMPLE ID	Core Box	Ce ppm	Co ppm	Cr ppm	Cs ppm	Cu ppm	Fe %	Ga ppm	Ge ppm	Hf ppm	Hg ppm	In ppm
NBL1	299	121.5	11.6	47	2.16	6	3.29	19.1	0.21	2.7	0.01	0.08
NBL2	299	77.2	17.2	68	6.41	28.6	5.46	26.8	0.2	3	0.01	0.102
NBL3	299	65.3	17.9	63	4.87	51.2	4.91	22.9	0.17	2.2	<0.01	0.081
NBL4	298	76.9	25.4	69	7.42	69.6	5.39	25.5	0.18	2.9	<0.01	0.101
NBL5	298	97.1	10.5	53	3.34	61.5	4.04	20.7	0.19	2.8	<0.01	0.124
NBL6	137	59.5	18.6	62	5.53	41.6	4.79	22.5	0.13	2.4	0.01	0.084
NBL7	137	61.5	16.8	63	6.15	44	4.74	22.1	0.12	2.6	<0.01	0.073
NBL8	141	58.6	18.2	69	12.45	12.4	5.78	26.7	0.15	2	<0.01	0.083
NBL9	142	48.4	24.2	82	12.85	20.3	5.79	30.7	0.12	2.5	<0.01	0.104
NBL10	140	77.3	15.4	55	4.8	45.8	4.28	20.5	0.14	2.3	<0.01	0.06
NBL11	140	41.9	26.6	81	13.65	93.6	6.54	27.5	0.12	2.4	0.01	0.104
NBL12	142	48.6	18.8	71	11.55	16.9	5.53	27.1	0.13	1.9	0.01	0.115
NBL13	141	45.6	19.8	79	13.95	183	5.95	30.1	0.12	2.5	0.01	0.085
NBL14	24	50.6	20.9	63	16.75	41.1	5.31	25.4	0.11	2.6	<0.01	0.089
NBL15	24	43.2	19.6	71	24.9	31.8	5.65	26	0.13	2.2	<0.01	0.083
NBL16	28	61.6	17.6	62	9.01	44.6	5	23.1	0.11	2.6	<0.01	0.073
NBL17	25	74.5	17	101	9.28	56.8	5.19	27.6	0.13	2.2	0.01	0.096
NBL18	24	46.8	20.5	80	26.6	33.2	5.58	27.1	0.11	2.3	<0.01	0.082
NBL19	28	91.7	21.6	66	3.08	45.7	4.07	30.3	0.12	3.7	<0.01	0.095
NBL20	25	71.3	15	60	5.91	45.8	4.41	20.4	0.11	2.1	<0.01	0.075

SAMPLE ID	Core Box	K %	La ppm	Li ppm	Mg %	Mn ppm	Mo ppm	Na %	Nb ppm	Ni ppm	P ppm	Pb ppm	Rb ppm
NBL1	299	1.96	49.7	20.3	1.75	947	1.11	3.72	14.3	21	1290	17	77.5
NBL2	299	4.07	39.3	82.7	0.66	231	0.19	4.02	17.2	40.5	340	22.9	199.5
NBL3	299	3.88	33.8	75.4	2.51	782	2.23	3	14.9	36	370	16.6	165.5
NBL4	298	5.16	38.7	119.5	0.63	115	0.2	3.36	17.4	50.9	330	28	251
NBL5	298	2.26	47.2	28.7	1.19	1220	0.15	4.13	15.4	31.7	350	22.3	97.8
NBL6	137	4.66	30.1	69.7	3.01	786	1.49	2.74	13.3	41.7	500	17.2	163
NBL7	137	4.42	29.4	99.6	3.49	850	145	3.1	13.6	37.2	490	19.5	163.5
NBL8	141	3.02	30.1	79.7	1.95	980	1.31	4.54	18.8	39.8	610	24.7	125
NBL9	142	3.02	15.4	192.5	1.87	300	1.02	4.25	17.4	57.1	1070	12.9	148.5
NBL10	140	2.01	35.8	34.3	3.12	1110	0.1	4.35	13.3	28.4	560	15.8	89.7
NBL11	140	2.93	22.5	91.1	1.67	406	0.25	4.57	18.8	50.1	580	22.1	166.5
NBL12	142	2.86	28.5	156	1.86	754	0.24	4.34	15.8	42.9	590	22.6	147
NBL13	141	3.03	26.2	123.5	1.69	699	0.2	4.88	18.2	46.6	670	24	166.5
NBL14	24	2.5	27	65.7	2.01	795	0.1	4.51	15.6	51.3	510	14.6	173
NBL15	24	3.05	22.7	144	2.18	1035	0.18	4.14	14.8	42.3	490	14.9	166.5
NBL16	28	3.96	29.9	81.1	3.12	743	22.4	3.05	13.1	39.9	360	21.1	185
NBL17	25	3.32	27.4	93.9	2.17	612	0.41	4	13.5	46.7	480	20.6	168.5
NBL18	24	3.05	21.2	139	2.07	816	0.44	4.43	16.7	48	420	14.9	163.5
NBL19	28	1.71	43.1	45.8	1.34	390	1.17	5.18	17	41.6	880	17.6	60
NBL20	25	3.16	33.7	45.5	3.06	1040	3.89	3.38	12.1	33.4	450	20.8	79.9

SAMPLE ID	Core Box	Re ppm	S %	Sb ppm	Se ppm	Sn ppm	Sr ppm	Ta ppm	Te ppm	Th ppm	Ti %	Tl ppm	U ppm
NBL1	299	<0.002	0.06	0.34	2	2.9	321	1.03	<0.05	33.8	0.352	0.35	7
NBL2	299	<0.002	0.06	1.44	1	4.3	86.5	1.32	0.05	10.7	0.453	0.79	1.9
NBL3	299	0.005	0.07	0.55	1	3.2	353	1.05	<0.05	10.7	0.363	0.71	7.6
NBL4	298	<0.002	0.13	1.77	1	4.4	71.2	1.34	0.08	10.6	0.484	0.99	1.8
NBL5	298	<0.002	0.02	1.17	1	3.5	195.5	1.09	<0.05	10.7	0.404	0.43	1.4
NBL6	137	0.002	0.63	1.52	2	3.1	347	0.98	0.06	9.3	0.383	0.79	4.3
NBL7	137	0.003	0.27	1.76	2	2.6	374	1	0.09	7.1	0.394	0.87	6.6
NBL8	141	<0.002	0.01	0.68	2	4.1	270	1.4	<0.05	9	0.444	0.76	1.6
NBL9	142	<0.002	0.02	1.01	1	4.5	149	1.15	<0.05	5.2	0.446	0.81	1
NBL10	140	<0.002	0.01	0.12	2	2.7	687	0.96	0.05	10	0.393	0.37	1.3
NBL11	140	<0.002	0.23	3.02	1	4.6	157	1.33	<0.05	6.5	0.502	1.28	1.7
NBL12	142	<0.002	0.01	0.92	1	3.9	227	1.22	<0.05	12.4	0.422	0.72	1.1
NBL13	141	<0.002	0.03	1.02	1	3.9	211	1.27	0.05	9.7	0.494	0.8	1.4
NBL14	24	<0.002	0.08	0.69	1	3.2	186	1.05	0.06	9.5	0.454	0.96	1
NBL15	24	<0.002	0.01	0.97	1	3.4	253	1.03	<0.05	10.2	0.426	1.05	1.1
NBL16	28	0.003	1.05	0.78	2	2.8	358	0.94	0.05	5.7	0.366	0.97	4.4
NBL17	25	<0.002	0.02	0.29	2	3.4	189	1.1	<0.05	7.5	0.383	0.85	1.1
NBL18	24	<0.002	0.03	0.75	2	3.7	196	1.15	<0.05	6.7	0.463	1.07	1
NBL19	28	<0.002	0.59	0.72	2	3	190.5	1.2	0.05	11	0.48	0.29	4.6
NBL20	25	0.01	0.52	0.55	2	2.8	490	0.94	<0.05	10.6	0.336	0.37	6.8

SAMPLE ID	Core Box	V ppm	W ppm	Y ppm	Zn ppm	Zr ppm	SiO2 %	Al2O3 %	Fe2O3 %	CaO %	MgO %	Na2O %
NBL1	299	127	1.9	51.1	171	75.9	49.6	13.75	5.22	7.27	3.25	5.37
NBL2	299	128	3.4	13.1	33	89.1	56.1	18.65	8.27	0.7	1.22	5.71
NBL3	299	133	1.8	19.2	89	69	44.2	14.75	7.48	5.86	4.49	4.16
NBL4	298	127	3.7	12.5	36	90.7	56.7	18.8	8.02	0.3	1.14	4.76
NBL5	298	91	2.7	25.2	35	86.5	56.6	15.95	6.55	3.33	2.26	6.05
NBL6	137	136	1.3	19.7	107	82.6	46.6	15.35	7.47	4.76	5.26	3.8
NBL7	137	152	1.1	18.1	102	87.5	45.8	14.55	7.09	5.08	5.93	4.15
NBL8	141	96	2.4	15	85	62.8	47.3	18.4	9.1	2.79	3.61	6.32
NBL9	142	99	2.4	12.9	145	86	49	19.05	9.37	1.42	3.58	6.26
NBL10	140	172	1.1	26.2	67	110	41.8	14.45	6.67	8.95	5.4	5.86
NBL11	140	121	2.3	13	139	69.4	47.2	19.65	10.15	1.51	3.04	6.42
NBL12	142	86	2.9	15.5	118	59.6	48.4	18.55	8.64	2.14	3.53	6.5
NBL13	141	100	3.1	15.8	160	80.5	48.5	19	9.1	1.57	3.05	6.73
NBL14	24	201	1.4	14.8	116	108.5	50.5	18.35	8.64	1.99	3.77	6.68
NBL15	24	112	2.3	19.2	112	69.8	46.6	18.4	8.93	2.81	4.06	5.94
NBL16	28	150	1.4	17.3	98	81.9	48.1	15.45	8.1	4.41	5.6	4.4
NBL17	25	150	1.8	16.8	132	78.5	52	17.65	8.05	2.19	3.88	5.62
NBL18	24	132	2	14	110	78.5	47.4	18.75	8.9	2.04	3.85	6.33
NBL19	28	142	2.2	29.2	102	133.5	56.4	18.2	6.54	1.66	2.39	7.41
NBL20	25	102	1.5	26.7	93	75.1	43.4	14.8	6.73	6.92	5.33	4.58

SAMPLE ID	Core Box	K2O %	Cr2O3 %	TiO2 %	MnO %	P2O5 %	SrO %	BaO %	LOI %	Total %	B ppm	C %
NBL1	299	2.41	0.01	0.69	0.15	0.28	0.04	0.05	11.6	99.7	<20	3.07
NBL2	299	4.85	0.01	0.89	0.03	0.07	0.01	0.05	2.39	99	30	0.26
NBL3	299	4.46	0.01	0.64	0.11	0.11	0.04	0.04	13.3	99.7	<20	4.02
NBL4	298	6.12	0.01	0.91	0.02	0.08	0.01	0.05	1.96	98.9	40	0.09
NBL5	298	2.76	0.01	0.86	0.18	0.11	0.02	0.04	5.74	100.5	40	1.42
NBL6	137	5.28	0.01	0.67	0.11	0.1	0.04	0.05	9.13	98.6	<20	2.64
NBL7	137	4.83	0.01	0.66	0.12	0.13	0.04	0.04	9.83	98.3	30	3.12
NBL8	141	3.52	0.01	0.79	0.14	0.13	0.03	0.07	8.24	100.5	120	1.12
NBL9	142	3.75	0.01	0.85	0.04	0.14	0.02	0.06	6.71	100.5	120	0.35
NBL10	140	2.29	0.01	0.71	0.16	0.12	0.08	0.07	13.2	99.8	40	3.22
NBL11	140	3.45	0.01	0.9	0.06	0.13	0.02	0.07	7.22	99.8	90	0.39
NBL12	142	3.77	0.01	0.81	0.11	0.12	0.03	0.07	7.41	100	120	0.84
NBL13	141	3.52	0.01	0.9	0.09	0.11	0.02	0.07	6.68	99.4	130	0.62
NBL14	24	3.09	0.01	0.87	0.11	0.07	0.02	0.05	5.98	100	30	0.76
NBL15	24	3.7	0.01	0.78	0.14	0.11	0.03	0.07	8.63	100	190	1.16
NBL16	28	4.69	0.01	0.65	0.1	0.03	0.04	0.04	9.04	100.5	30	2.72
NBL17	25	3.86	0.02	0.68	0.08	0.08	0.02	0.05	5.58	99.8	30	1.01
NBL18	24	3.62	0.01	0.84	0.11	0.09	0.02	0.07	8.4	100.5	120	0.88
NBL19	28	2.05	0.01	0.9	0.05	0.19	0.02	0.12	2.92	98.9	<20	0.4
NBL20	25	3.56	0.01	0.59	0.14	0.07	0.06	0.06	12.55	98.8	<20	3.78

SAMPLE ID	Core Box	C organic %	Ce ppm	Dy ppm	Er ppm	Eu ppm	Gd ppm	Ho ppm	La ppm	Lu ppm	Nd ppm	Pr ppm
NBL1	299	0.2	141	11.7	6.2	2.3	11.8	2.5	56.9	0.7	57	15.4
NBL2	299	0.11	79.8	4	2.3	1.4	6.4	0.9	38.8	0.4	35.8	9.9
NBL3	299	0.75	69.2	3.7	2.3	1.2	5.3	0.9	34.2	0.3	30.1	8.3
NBL4	298	0.01	77.1	4	2.2	1.4	6.2	0.8	38.3	0.3	35.9	9.8
NBL5	298	0.03	116.5	8.5	4.5	2.4	11	1.7	58.5	0.6	53	14.4
NBL6	137	0.63	56.9	3.6	2.1	1.2	4.8	0.8	27.8	0.4	26	7
NBL7	137	0.9	56.9	3.3	2	1.1	4.4	0.7	28.1	0.3	24.1	6.7
NBL8	141	0.01	74.5	3.7	1.6	1.4	6.4	0.7	42.5	0.3	37.5	10.2
NBL9	142	0.01	70.1	3	1.8	1	4.3	0.6	25.6	0.4	24.6	6.5
NBL10	140	0.16	76.3	5.4	2.7	1.7	7.7	1	35	0.4	40.3	10.2
NBL11	140	0.01	50.5	2.8	1.5	1	4.4	0.6	30.1	0.3	25.4	7
NBL12	142	0.06	51.6	4.2	1.8	1.3	6.6	0.7	32.3	0.2	32.9	8.5
NBL13	141	0.12	49.1	3.3	1.6	1.2	4.5	0.6	30.3	0.3	26.5	7.3
NBL14	24	0.03	60.3	3.4	1.8	1.2	5.2	0.7	34.7	0.4	30.1	8.2
NBL15	24	0.01	52.4	4.2	2.2	1.4	5.5	0.8	29.7	0.3	30.7	8.1
NBL16	28	0.77	61	3.2	1.8	1	4.4	0.7	30.1	0.3	26.1	7.2
NBL17	25	0.14	77.9	3.3	1.8	1	4.9	0.7	30.9	0.3	28.7	7.8
NBL18	24	0.02	63.9	3.2	1.9	1.1	4.6	0.7	31.3	0.4	27.3	7.5
NBL19	28	0.09	91.4	6	2.8	2	8.3	1.1	43.5	0.5	44.2	11.5
NBL20	25	0.77	70.3	5.4	2.9	1.5	6.6	1.1	33.4	0.4	32.3	8.6

SAMPLE ID	Core Box	Sm ppm	Tb ppm	Th ppm	Tm ppm	U ppm	Y ppm	Yb ppm
NBL1	299	12.2	2	35	0.8	7.7	57.6	4.4
NBL2	299	6.9	0.8	10	0.3	1.9	19.6	2.2
NBL3	299	5.6	0.7	10	0.4	7.3	18.8	2.2
NBL4	298	6.9	0.9	10	0.3	1.9	18.4	2.2
NBL5	298	10.8	1.6	12	0.7	1.8	39.8	3.8
NBL6	137	4.8	0.7	9	0.3	5.4	18	2
NBL7	137	4.9	0.6	7	0.3	7.1	15.8	2
NBL8	141	7.1	0.9	11	0.2	2.1	15.6	1.6
NBL9	142	4.8	0.6	7	0.3	1.4	15.4	1.8
NBL10	140	8.6	1.1	10	0.4	1.5	24.2	2.5
NBL11	140	4.8	0.6	8	0.2	2.1	13.4	1.6
NBL12	142	6.4	0.9	12	0.2	1.1	16.8	1.5
NBL13	141	5.1	0.7	9	0.2	1.7	15	1.7
NBL14	24	5.6	0.7	10	0.3	1.3	15.7	1.9
NBL15	24	6.4	0.8	12	0.3	1.4	19.7	2.1
NBL16	28	4.9	0.6	5	0.3	5	15.8	1.7
NBL17	25	5.4	0.7	9	0.3	1.3	16.5	1.9
NBL18	24	4.8	0.6	9	0.3	1.4	15.1	1.8
NBL19	28	9.2	1.2	11	0.4	5.2	26.6	2.6
NBL20	25	6.7	1	10	0.4	7.4	24.8	2.4

SAMPLE ID	Core Box	Pyritic S ppm	AVS ppm
NBL1	299	227	44.1
NBL2	299	11.4	36
NBL3	299	346	56.2
NBL4	298		
NBL5	298		
NBL6	137	3584	45.9
NBL7	137	1498	293.2
NBL8	141	3.8	5
NBL9	142		
NBL10	140	17	33.6
NBL11	140	1562	6.6
NBL12	142		
NBL13	141		
NBL14	24	411	51.9
NBL15	24		
NBL16	28	6290	11.4
NBL17	25	73	31.7
NBL18	24		
NBL19	28	4089	16.1
NBL20	25	4332	13.6

APPENDIX II

Free energies of formation ($\Delta G°_{298}$) of various solids and aqueous species used in thermodynamic calculations. In situ free energies of reaction were calculated assuming pH = 8, $[HS^-] = 10^{-5}$ M, $[O_2] = 10^{-3.9}$ M, $[NO_3^-] = 10^{-4}$ M, $[Fe^{2+}] = [Mn^{2+}] = [NO_2^-] = [As(OH)_3] = 10^{-6}$ M.

Compound		$\Delta G°_{298}$ (kJ/mol)	Source
$FeAsS_{(s)}$	arsenopyrite	-136.45	[1]
$As(OH)_{3(aq)}$	arsenite	-639.8	[2]
FeS_2	pyrite	-160.2	[3]
FeS	mackinawite	-93.3	[4]
MnO_2	birnessite	-453.1	[4]
Mn^{2+}	aqueous	-228	[4]
Fe^{2+}	aqueous	-85.56	[5]
O_2	aqueous	+16.64	[5]
H_2O		-237.2	[5]
HS^-	bisulfide	12	[6]
NO_3^-	nitrate	-111.3	[7]
NO_2^-	nitrite	-37.2	[7]

1. Perfetti, E., et al. (2008) Densities and heat capacities of aqueous arsenious and arsenic acid solutions to 350°C and 300 bar, and revised thermodynamic properties of $As(OH)_3^o(aq)$, $AsO(OH)_3^o(aq)$ and iron sulfarsenide minerals. *Geochim. Cosmochim. Acta*, **72**: 713-731.

2. Pokrovski, G., et al. (1996) Thermodynamic properties and stoichiometry of As(III) hydroxide complexes at hydrothermal conditions. *Geochim. Cosmochim. Acta*, **60**: 737-749.

3. Robie, R. A., Hemingway, B. S., and Fisher, J. R. (1978) Thermodynamic properties of minerals and related substances at 298.15K and 1bar (105 pascals) pressure and at higher temperatures. *U.S. Geological Survey Bulletin*, **1452**: 1–456.

4. Drever, J. I. (1997) *The Geochemistry of Natural Waters: Surface and Groundwater Environments*. 3rd ed, Englewood Cliffs: Prentice Hall.

5. Woods, T. L. and Garrels, R. M. (1987) *Thermodynamic Values at Low Temperature for Natural Inorganic Materials: An Uncritical Summary*, New York: Oxford University Press.

6. Shock, E. L. and Helgeson, H. C. (1988) Calculation of the Thermodynamic and Transport-Properties of Aqueous Species at High-Pressures and Temperatures - Correlation Algorithms for Ionic Species and Equation of State Predictions to 5-Kb and 1000-Degrees-C. *Geochim. Cosmochim. Acta*, **52**: 2009-2036.

7. Stumm, W. and Morgan, J. J. (1993) *Aquatic Chemistry*. 3rd ed: Wiley.

APPENDIX III

BT medium composition

10X BT SALTS	**CON. (g/L)**
Na2HPO4*7H2O	79
KH2PO4	15
NH4Cl	3
PS-1	
MgSO4*7H2O	20
VS Minerals	
EDTA(acid form)	50
ZnSO4*7H2O	22
CaCl2*7H2O	7.4
MnCl2*4H2O	8
FeSO4*7H2O	5
(NH4)2Mo7O24*4H2O	1.1
CuSO4*5H2O	1.6
CoCl2*6H2O	1.6
S8 Vitamins	
Biotin	0.002
Folic Acid	0.002
Pyridoxine HCl	0.01
Riboflavin	0.005
Nicotinic acid	0.005
Pantothenic acid	0.005
Vitamin B12	0.0001
P-amino benzoic acid	0.005
Thiocetic acid	0.005
To make a 1 Liter BT medium mix	
100 mL 10xBT salts	
5mL PS-1	
5mL Minerals	
1mL vitamins	
900mL sterile H2O	

WENYI ZHU

Department of Environmental Sciences
Rutgers University, the State University of New Jersey
14 College Farm Road, New Brunswick, NJ, 08854
wenyizhu@eden.rutgers.edu

EDUCATION

Ph.D. **Rutgers University-New Brunswick, NJ.**
Environmental Sciences (Option: Environmental chemistry), 2010
Adviser: John R. Reinfelder

B.S. **Nanjing University, Nanjing, China.**
Environmental Sciences (Option: Environmental Biology), 2003

PROFESSIONAL EXPERIENCE

Research assistant **2005-present**
Department of Environmental Sciences, Rutgers University-New Brunswick, NJ

Teaching Assistant **2004-2005**
Department of Environmental Sciences, Rutgers University-New Brunswick, NJ

Research Assistant **2002-2003**
School of Environmental Science, Nanjing University, Nanjing, P.R.China.

Lab assistant **2002**
Environmental Monitoring Center, Nanjing, China

PUBLICATIONS

Zhu, W., E.D. Rhine, L.Y. Young, and J.R. Reinfelder (2008), Sulfide-driven arsenic solubilization from arsenopyrite and pyritic black shale. ***Geochim. Cosmochim. Acta***. 72(21): 5243-5250.